ASSOCIATIONS OF STIM1 DURING STORE-OPERATED CALCIUM ENTRY
AND
DEVELOPMENT OF A NOVEL METHOD FOR MULTI-BIOMOLECULE PATTERNING

A Dissertation

Presented to the Faculty of the Graduate School

of Cornell University

In Partial Fulfillment of the Requirements for the Degree of

Doctor of Philosophy

by

Kari Marie Midthun

January 2013

ASSOCIATIONS OF STIM1 IN STORE-OPERATED CALCIUM ENTRY AND DEVELOPMENT OF A NOVEL METHOD FOR MULTI-BIOMOLECULE PATTERNING

Kari Marie Midthun, Ph. D.

Cornell University 2013

To understand immune responses, such as asthma and allergies, we must first understand the inter- and intramolecular regulation of the signaling pathways responsible for these complex biological processes. Of particular importance in immune cell signaling is understanding Ca^{2+} mobilization and the pathway of store-operated Ca^{2+} entry (SOCE), wherein Ca^{2+} released from the endoplasmic reticulum (ER) stores leads to an influx of Ca^{2+} from the extracellular environment via Ca^{2+} release-activated Ca^{2+} (CRAC) channels. Activation of SOCE is accomplished by coupling of Ca^{2+} sensing stromal interaction molecule 1 (STIM1), an ER transmembrane protein, to Orai1 proteins located at the plasma membrane (PM). While numerous research efforts have focused on understanding the STIM1-Orai1 interactions required to elicit SOCE, much uncertainty remains about the associations that regulate STIM1 before and during SOCE. This dissertation provides new insights into the inter- and intramolecular interactions regulating STIM1, both at rest and following activation.

Using immunoprecipitation (IP) assays, we provide evidence that STIM1 exists in multiple low-order oligomer states at rest, including a 110 kDa hetero-dimer with a 20-25 kDa unidentified protein (possibly a proteolytic fragment) and a 260 kDa homo-dimer complex. We further establish that non-covalent interactions are sufficient to maintain these oligomers in resting cells. However, following cell lysis, disulfide bonds form to stabilize the protein

complexes. Following activation of STIM1 by thapsigargin, the presence and appearance of these oligomers is not detectably altered. Although we made multiple attempts to identify components of the 110 kDa and 260 kDa STIM1 complexes, we are unable to identify any components of the oligomeric species aside from STIM1.

Following the discovery of the CRAC activation domain (CAD), which is the minimal region of STIM1 required to bind Orai1 and activate CRAC channels, much research has focused on understanding the exact interactions required to facilitate this process. Mutational analysis reveals that Cys-437 in the CAD region of STIM1 participates in the stabilization of the 110 kDa hetero-dimer protein complex. Using confocal microscopy and FRET analysis, we find that C437A mutant STIM1 translocates to the PM following store depletion and associates with Orai1 at a rate similar to that of wildtype STIM1. However, this same mutant STIM1 form exhibits a significant delay in SOCE as compared to wildtype, suggesting an important gating role for the Cys-437 residue in regulating SOCE.

In a separate set of studies, we have collaborated in the development of a novel multi-biomolecule patterning technique that utilizes fluorinated resist and developers, low-temperature and pressure conditions, and imprint lithography. We show that both the resist and developers are largely benign to biomolecules, including proteins and DNA, and are suitable for use in cell studies. We further demonstrate capacity of this method for multi-biomolecule patterning by fabricating multi-protein arrays and provide evidence that surface-immobilized biomolecules can undergo at least 10 cycles of lithographic processing with negligible deleterious effects. Importantly, the success of this patterning method demonstrates a new model for multi-biomolecule patterning that avoids many of the problems associated with more traditional lithographic techniques.

BIOGRAPHICAL SKETCH

Kari was born on August 2, 1984 to Douglas and Leona Midthun in Madison, Wisconsin. The youngest of three children, Kari spent her early years tagging along behind her siblings, Laurie and Darrell, and cousins in work and in play on the family farm. Her formative years were spent learning animal husbandry and agronomy from the seats of tractors on the back forty. While her parents argue that she would try anything to avoid work in the tobacco fields, even extra homework, the truth is that Kari fell in love with school, especially math and science. As a child, she often dreamed of becoming a medical doctor; though an ill-fated softball game in 1997 convinced her to pursue a different form of doctoral degree. In 2002, she graduated from DeForest Area High School and made the lengthy 25 minute drive around Lake Mendota to attend the University of Wisconsin-Madison. Here, Kari developed a passion for combining scientific analysis with a career in public service, earning degrees in chemistry, biochemistry, and criminal justice. Her varied interests have allowed for numerous laboratory experiences over the years, from mass spectrometry and forensic science to paper fiber and food product analyses. However, one research experience eluded her – live, biological specimens. To fulfill this dream, Kari left the land of cows, corn, and cheesecurds to pursue a graduate degree from Cornell University. Under the guidance of Drs. Barbara Baird and David Holowka, she studied associations of STIM1 protein in living mast cells. She plans to continue her scientific career as a civilian employee in the government.

DEDICATION

To Grandma Carol and Great, Great Aunt Arlette –

the matriarchs who challenged me to achieve academic success and to dream beyond the cornfields of Norway Grove. May this work honor your memories and serve as a reminder of how much one can achieve with the love and support of family.

And to Mom & Dad –

for continuing this legacy…

Some dei gamle sungo, so kveda dei unge

(As the old birds sing, so does the young ones tweet.)

~ Norwegian Proverb

ACKNOWLEDGEMENTS

I would like to thank Dave and Barbara for all of the support that they have given me during my time at Cornell. In addition, I would like to thank my committee members, Dr. Christopher Ober and Dr. Brian Crane, for their time and words of wisdom. From 2009 to 2010, my work was funded by the NSF FlexEBio IGERT Fellowship (Grant 0654112). While this experience was challenging, it also rewarded me with lasting friendships and memories, both at Cornell and abroad.

To my parents, family, and friends back home in Wisconsin, I am eternally grateful for the love and encouragement you have provided me throughout my education. In times of cheers and tears, you were never more than a phone call away to celebrate my victories or to pick me up when I was blue. Mom and Dad, I cannot thank you enough for all of the sacrifices that you have made for your children. With your guidance, we have each achieved greatness. Please know that you were instrumental in our successes and we will always strive to make you proud. Special thanks must also be made to my brother, Darrell, whose constant presence at home has made it possible for me to continue my education on the East Coast. Knowing that you were always there watching over everything when I could not be has been an immense comfort. And to my extended family, thank you so much for believing in me and for the constant support via phone calls, emails, refrigerator art, and care packages.

Of course, I also need to thank my Cornell family. The Baird-Holowka lab members of past and present provided countless hours of entertainment, both inside the laboratory and out: Sil, Stephanie, Lavanya, Sarah V., Ethan, Alexis, Roy, Nat, Norah, Marcela, Deepti, Jinmin, Amit, Kirsten, Alice, Kate, Josh, Sarah S., Devin, Lily, Marek, and Marcus. I will absolutely

miss our vast array of homemade baked goods that seemed to arrive almost daily and cannot wait to see how long the B exam cake legacy will continue. Stephanie, thank you for your patience in answering countless biology questions – and for teaching me the foundations of Western blotting and the joys of the dark room. Alice, Norah, and Marcela, workouts and aerobics classes will never be the same without you. Baking adventures, holidays, and movies with Kate provided much needed stress relief. Alexis, thank you for instilling your patterning wisdom on me and for providing countless laughs. Nat taught me the basics of FRET and MatLab, and always left me wondering who had used the last of my buffer solutions. Extra special thanks must be given to Amit, who has become like a brother to me. Your help and advice in the laboratory has been invaluable, though I will treasure our times spent outside of the lab even more. Throughout the past five years, we have had quite the adventures: vegetarian cooking & eggless baking lessons, moving apartments in subzero temperatures, getting lost on countless hikes and drives, and attending your wedding in India to name a few. Thank you so much for being such a great friend. I wish you and Shruti only the best in your future endeavors!

My extended Cornell family has truly made Ithaca feel like my home away from home. I shall miss my Flora Rose House family members, both staff and residents. Dela, Rosa, Sidra, Trent, and Rae, our late night chats and planning sessions were always full of laughs, even when interrupted by lock-outs and on-call emergencies. To my EYH family, I am so proud of how our hard work and dedication has improved the conference year after year. Sarah and Maureen, it was a pleasure to chair the conference with you both for the past two years – I knew I could always count on you whenever I needed help. To JD and Matt, the original members of the Three Musketeers, I sincerely miss our Trillium lunches and escapes to the movie theater. While I wish you were both still in Ithaca, you are on to bigger and better careers! Paul, Karen,

Pendo and Amani shared their love of Fall Creek and IthacaFest with me and served as avid baked good consumers whenever I wanted to test a recipe. I have also enjoyed several dinner and board game nights with Lou, Erin, Amy, and Daniel. To all of these dear friends, you have filled my time here in Ithaca with such great memories and enriched my life with lasting friendships – thank you!

Lastly, I must give my utmost thanks and appreciation to Mike. From our hiking and kayaking expeditions to taking India by storm, the last several years have been unforgettable with you by my side. Thank you for all the wonderful little things that you have done to put a smile on my face and to get me through the tough times. To my budding photographer, Trivial Pursuit rival, novice carpenter, and gourmet griller, thank you so much for the grand adventures thus far and for the promise of more to come.

TABLE OF CONTENTS

LIST OF FIGURES

LIST OF TABLES

LIST OF ABBREVIATIONS

A488	AlexaFluor 488
A546	AlexaFluor 546
A568	AlexaFluor 568
ABTS	2,2'-azino-bis(3-ethylbenzthiazoline-6-sulfonic acid)
αCP	affinity contact printing
AcGFP	*Aequorea coerulescens* derived green fluorescent protein
AFM	atomic force microscopy
AIBN	azobisisobutyronitrile
APTMS	3-aminopropyl (trimethoxysilane)
βME	β-mercaptoethanol
BiFC	bimolecular fluorescent complementation
BMH	bismaleimideohexane
BSA	bovine serum albumen
BSS	buffered saline solution
CAD	CRAC activation domain
CC	coiled coil (domain)
CCE	capacitative Ca^{2+} entry
CDI	Ca^{2+}-dependent inactivation
CFP	cyan fluorescent protein
CMD	CRAC modulatory domain
Cos7	monkey kidney cell line
CRAC	Ca^{2+} release-activated Ca^{2+}

Cys	Cysteine residue
DAG	diacylglyerol
DDM	dodecylmaltoside
DMSO	dimethyl sulfoxide
DNP	2,4-dinitrophenyl
DPN	dip-pen nanolithography
DTT	dithiothreitol
EB1	end binding 1
ER	endoplasmic reticulum
FcεRI	high affinity receptor for IgE
FLAG	a polypeptide protein tag encoded by the sequence N'-DYKDDDDK-C'
FM	fluorescein-5-maleimide
FRET	Förster resonance energy transfer
GFP	green fluorescent protein
GSH	glutathione
GOK	former name of STIM1 protein ("God Only Knows" protein)
HFE	hydrofluoroether
HRP	horseradish peroxidase
IgE	Immunoglobulin E
ImR	imprint resist
IP	immunoprecipitation
IP_3	inositol-1,4,5-trisphosphate
IP_3R	IP_3 receptor

ITAM	immunoreceptor tyrosine-based activation motif
LAT	linker for the activation of T-cells
μCP	microcontact printing
μFN	microfluidic networks
mRFP	monomeric red fluorescent protein
MS	mass spectrometry
NEM	N-ethylmaleimide
OASF	Orai1-activating small fragment
OD	optical density
PAGE	polyacrylamide gel electrophoresis
PDB	phorbol-12,13-dibutyrate
PDMS	polydimethylsiloxane
PIP_2	phosphatidylinositol-4,5-bisphosphate
PLCγ	phospholipase Cγ
PKC	protein kinase C
PM	plasma membrane
PSA	prostate specific antigen
PVDF	polyvinylidene fluoride
RBL-2H3	rat basophilic leukemia 2H3 cell line
RT	room temperature
S/P rich	Serine/Proline rich region
SAM	sterile-α-motif
SCID	severe combined immunodeficiency

SDS	sodium dodecyl sulfate
SEM	standard error of the mean
SERCA	sarco/endoplasmic reticulum Ca^{2+} ATPase
SH2	Src homology 2 (domain)
SHD	STIM1 homomerization domain
SOAR	STIM Orai1-activating region
SOCE	store-operated Ca^{2+} entry
STIM1	stromal interaction molecule 1
TBST	Tris-buffered saline Tween-20
TFT	benzotrifluoride
Tg	glass transition temperature
TG	thapsigargin
TM	transmembrane domain
TRP	transient receptor potential (channel)
TX-100	Triton X-100
UV	ultraviolet
wt	wildtype

CHAPTER ONE

Introduction

Mast Cells & the FcεRI Signaling Pathway:

It is well established that mast cells are key effectors in the allergic response and also play significant roles in the innate immune response. Immunoglobulin E (IgE), an antibody that binds with high-affinity to its receptor, FcεRI, at the plasma membrane (PM) of mast cells, recognizes foreign particles, also known as antigens, and elicits an intracellular signaling cascade as a result. Most commonly, this response involves mast cell degranulation to release pre-formed allergic mediators, such as histamine and proteases (Metcalfe et al. 1997; Church & Levi-Schaffer 1997; Platts-Mills 2001). Within minutes of their release, these mediators can elicit an immediate hypersensitivity response, presenting classic allergy and asthma symptoms, including watery eyes, sneezing, runny noses, and constricted airways (Galli & Tsai 2012). The most dangerous mediator effect, however, is the systemic response of anaphylaxis which can result in death if not treated promptly and/or properly (Ring et al. 2010). With allergies and asthma affecting as many as 30-40 % of the population, research has and will continue to focus on understanding the vast complexities of immune response in the hope of identifying new protein targets and drug therapies (Pawankar 2012).

To understand this complex process, we must first understand the underlying mechanisms of the IgE-mediated signaling pathways (Figure 1.1). The process begins when a multivalent antigen, specific to certain IgE, crosslinks IgE-bound FcεRI receptor complexes simultaneously

Figure 1.1: Signal transduction pathway for FcεRI in mast cells. Upon binding to multivalent antigen, IgE bound FcεRI crosslinks and clusters. This clustering leads to phosphorylation of the receptor by Lyn kinase, initiating a signal cascade that includes Ca^{2+} mobilization. As a result of this cascade, secretory granules undergo degranulation – the release of allergic mediators.

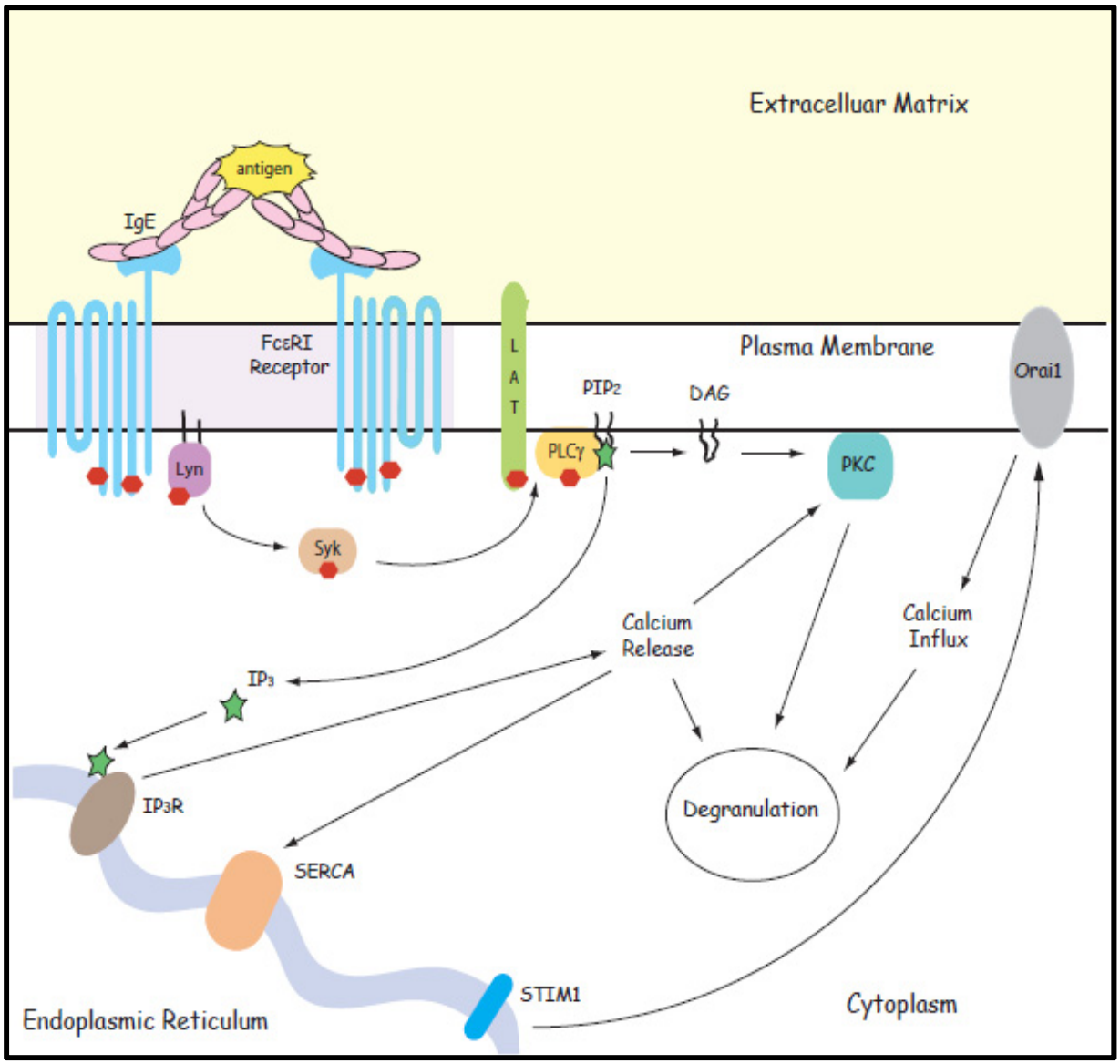
Extracelluar Matrix
antigen
IgE
FcεRI
Receptor
Plasma Membrane
L
A
T
PIP2
DAG
Orai1
Lyn
PLCγ
PKC
Syk
Calcium
Release
Calcium
Influx
IP3
IP3R
Degranulation
SERCA
STIM1
Endoplasmic Reticulum
Cytoplasm

on the exterior of the cell. This action causes the receptors to cluster (Holowka & Baird 1996). Aside from the extracellular IgE binding α-subunit, FcεRI receptors also contain intracellular subunits important to both signal transduction (γ subunits) and signal amplification (β subunit), each of which contains an immunoreceptor tyrosine-based activation motif (ITAM) (Rivera & Gilfillan 2006, Turner & Kinet 1999). Upon antigen binding and receptor crosslinking, aggregated receptors localize to more ordered lipid domain regions within the PM, also known as lipid rafts (Holowka et al. 2005). Inside the ordered domains, Lyn kinase, a Src family kinase associated with lipid rafts, phosphorylates tyrosine residues within receptor ITAMs, enabling further recruitment of Lyn and other tyrosine kinases (Kinet 1999, Young et al. 2003, Holowka et al. 2005, Powell & Hogarth 2008, Hammond et al. 2009).

Phosphorylation and activation of the receptor is the first detectable step in FcεRI signaling and initiates the remaining downstream cascade. Next, phosphorylated FcεRI recruits Syk kinase to lipid raft domains via interaction between the phosphorylated ITAMs and tandem Src homology 2 (SH2) domains present on Syk (Kinet 1999). Once present in lipid rafts, Syk kinase is phosphorylated and activated by Lyn kinase (Scharenberg et al. 1995). Activated Syk, in turn, phosphorylates a number of downstream target proteins, including tyrosine residues within the linker for the activation of T-cells (LAT), a PM bound adaptor protein (Rivera & Gilfillan 2006). When phosphorylated, LAT recruits SH2 domain-containing proteins, such as phospholipase Cγ (PLCγ), to the PM (Turner & Kinet 1999). Following its phosphorylation by Syk, activated PLCγ hydrolyzes membrane phosphosphatidylinositol-4,5-bisphosphate (PIP_2) into soluble inositol-1,4,5-trisphosphate (IP_3), which initiates intracellular Ca^{2+} mobilization, and membrane-bound diacylglycerol (DAG) needed for protein kinase C (PKC) activation (Gilfillan & Tkaczyk 2006). Both the elevation of intracellular Ca^{2+} and activation of PKC are required

for mast cell degranulation (Rivera & Gilfillan 2006, Hammond et al. 2009). Recent research, including our own, has focused on better understanding the proteins and mechanisms responsible for intracellular Ca^{2+} mobilization because of the crucial role Ca^{2+} plays in various cellular processes, including degranulation.

Intracellular Ca^{2+} & Store-Operated Ca^{2+} Entry (SOCE):

Understanding the process of intracellular Ca^{2+} trafficking is critical to the regulation of many processes, including gene expression, protein folding, cell signaling, degranulation, and cell death (Berridge et al. 2003, Baba & Kurosaki 2009, Fahrner et al. 2009). At any moment in time, intracellular Ca^{2+} levels are determined by a delicate balance between 'on' reactions that import Ca^{2+} into the cytoplasm and 'off' reactions that export cytoplasmic Ca^{2+} into various organelles and/or the surrounding extracellular space (Berridge et al. 2003). This constant flux of Ca^{2+} into the cell activates effector proteins and elicits a variety of Ca^{2+}-signaling pathways. Of particular importance in immune cell research is the pathway of Ca^{2+} release-activated Ca^{2+} (CRAC) entry, wherein Ca^{2+} released from the endoplasmic reticulum (ER) stores leads to an influx of Ca^{2+} from the extracellular environment (Baba & Kurosaki 2009).

When at rest, mast cell cytoplasmic Ca^{2+} levels remain relatively low, ~ 100 nM; however, upon stimulation, the intracellular Ca^{2+} concentration rapidly increases to more than 10x this value and in a biphasic manner (Beaven et al. 1984). In the first phase, soluble IP_3, formed from the hydrolysis of PIP_2, binds to IP_3 receptor (IP_3R) channels on the ER and stimulates a transient release of Ca^{2+} from ER stores into the cytoplasm (Streb et al. 1983, Taylor et al. 2004). This depletion of intracellular Ca^{2+} stores then leads to a second, sustained phase of

Ca^{2+} entry which involves the activation of Ca^{2+}-permeable CRAC channels within the PM, a process originally known as capacitative Ca^{2+} entry (CCE) (Putney 1986) and later termed store-operated Ca^{2+} entry (SOCE) (Parekh & Putney 2005). Though other plasma membrane proteins, such as transient receptor potential (TRP) channels and IP_3R channels, can also contribute to Ca^{2+} entry (Bird et al. 2004), SOCE was found to be the main mechanism for Ca^{2+} influx in lymphocytes and other immune cells (Feske 2007).

While originally proposed by Putney more than 25 years ago (Putney 1986), the molecular basis for SOCE was not well understood until 2005 with the discoveries of stromal interaction molecule 1 (STIM1) (Roos et al. 2005, Liou et al. 2005) and Orai1 (Yeromin et al. 2006, Vig et al. 2006a, Vig et al. 2006b, Prakriya et al. 2006). As shown in Figure 1.2A, at rest, STIM1 is a Ca^{2+} sensing, ER transmembrane, protein while Orai1, the pore-forming subunit of CRAC channels, resides in the PM. Following release of Ca^{2+} from ER stores, due to the interaction of IP_3 with IP_3R, STIM1 oligomerizes (Figure 1.2B) and accumulates in regions known as puncta juxtaposed to the plasma membrane (Liou et al. 2005, Zhang et al. 2005, Wu et al. 2006). At the ER-PM junctions, oligomerized STIM1 recruits Orai1 proteins, forming the complete CRAC channel, and activates SOCE (Vig et al. 2006a) as depicted in Figure 1.2C. While inactivation of SOCE is not entirely understood, most agree that refilling the stores via the ER Ca^{2+} pump, sarco/endoplasmic reticulum Ca^{2+} ATPase (SERCA), is required (Taylor 2006).

The importance of SOCE in the immune system cannot be overstated. Since the discovery of STIM1 and Orai1, research has focused on understanding how SOCE activity regulates a variety of immune cell functions including T cells, B cells, mast cells, neutrophils, and macrophages (Shaw & Feske 2012). These findings suggest important roles for SOCE in the regulation of: gene expression by activating Ca^{2+}-dependent transcription factors, such as the

Figure 1.2: Ca^{2+} mobilization and store-operated calcium entry (SOCE). (A) Soluble IP_3 messenger molecule activates its ER receptor (IP_3R) causing the release of Ca^{2+} from ER stores. **(B)** No longer sensing the presence of Ca^{2+} in the ER, STIM1 proteins oligomerize and redistribute into puncta near the plasma membrane. **(C)** Orai1 proteins cluster with oligomerized STIM1 at ER-PM junctions, forming Ca^{2+} release-activated Ca^{2+} (CRAC) channels, which activate and allow for Ca^{2+} influx in a process termed SOCE.

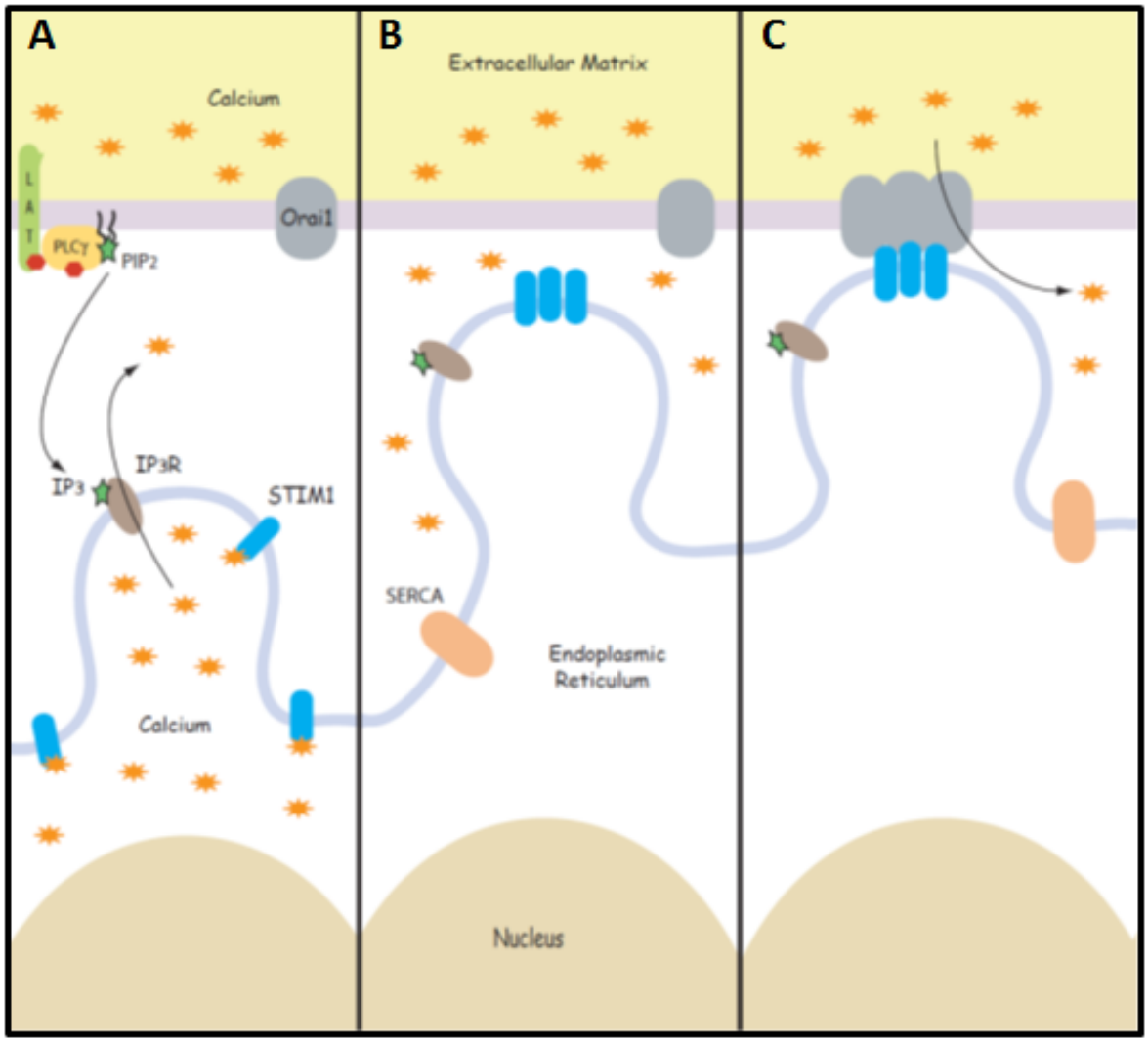
A
B
C
Calcium
Extracellular Matrix
L
A
T
PLCγ
PIP2
Orai1
IP3
IP3R
STIM1
SERCA
Endoplasmic
Reticulum
Calcium
Nucleus

nuclear factor of activated T cells (NFAT) (Hogan et al. 2003) and activating transcription factor 2 (ATF-2) (Enslen et al. 1996); cytokine production (Matsumoto et al. 2011, Maul-Pavicic et al. 2011); release of cytolytic granules in $CD8^+$ T cells (Maul-Pavicic et al. 2011); and release of histamine containing granules in mast cells (Vig et al. 2008). Most importantly, defects in SOCE and CRAC channel activity have been found in some patients suffering from severe combined immunodeficiency (SCID) syndrome and were found to be caused by rare mutations in Orai1 (Feske et al. 2006, Feske 2011). While just as rare, mutations in STIM1 leading to impaired SOCE and immunodeficiency have also been described (Feske 2011).

Stromal Interaction Molecule 1 (STIM1):

I. Structure

Originally identified as a tumor suppressor protein, GOK, in humans (Parker et al. 1996, Sabbioni et al. 1997) and a cell adhesion molecule, Stim, in *Drosophila* (Oritani & Kincade 1996), the role of STIM1 in SOCE was not discovered until 2005 (Roos et al. 2005, Liou et al. 2005). Using STIM1 knockdowns, these studies showed dramatic reductions in SOCE, whereas overexpression of STIM1 increased the rate and magnitude of SOCE. In addition, both studies established STIM1 as being mainly an ER-membrane protein, countering previous studies which placed the location of STIM1 at the PM (Manji et al. 2000).

As shown in Figure 1.3, STIM1 is a type-I transmembrane protein. The luminal, N-terminus of STIM1 contains a canonical EF-hand domain, a hidden EF-hand domain, and a sterile-α-motif (SAM). The canonical EF-hand domain performs the role of sensing luminal Ca^{2+} levels via interaction between Ca^{2+} and the aspartic acid-76 residue. Using the point

Figure 1.3: Stromal interaction molecule 1 (STIM1). Putative domains are shown. EF (EF-hand domain), SAM (sterile α-motif), TM (transmembrane domain), CC (coiled coil), CMD (CRAC modulatory domain), S/P (Serine/Proline rich region), K (Lysine-rich region), ERM (Ezrin Radixin Moesin-like domain), OASF (Orai activating small fragment), CAD (CRAC activation domain), SOAR (STIM Orai1-activating region), CCb9 (CC domain containing region b9), SHD (STIM1 homomerization domain). [Figure from Derler et al. 2012]

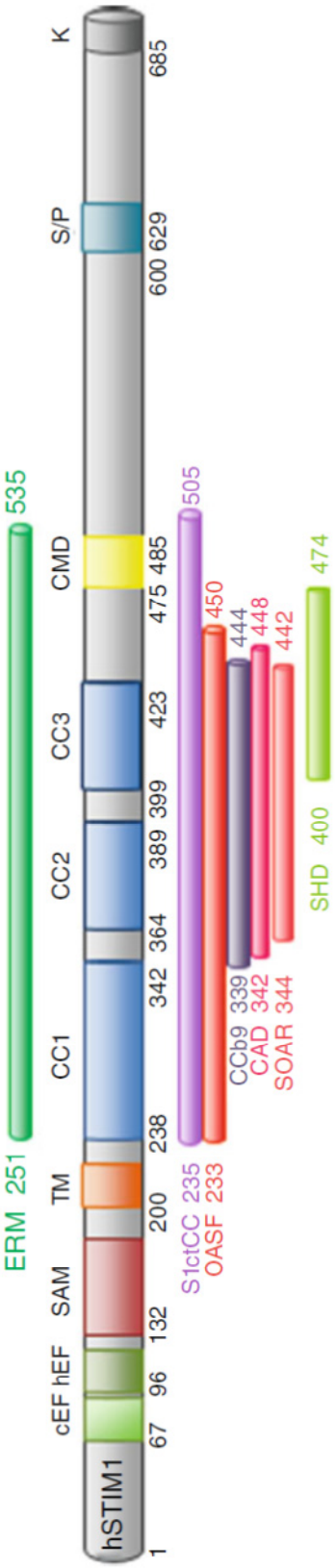
hSTIM1
1
cEF 67
hEF 96
SAM 132
TM 200
CC1 238
CC2 342
CC3 364
CMD 389
S/P 399
K 423
475
485
600
629
685
ERM 251
535
S1ctCC 235
OASF 233
505
CCb9 339
CAD 342
SOAR 344
450
444
448
442
SHD 400
474

mutation D76A, Liou et al. (2005) showed that STIM1 is no longer able to bind Ca^{2+}, causing the protein to become constitutively active, even when ER stores are replete with Ca^{2+}. While the role of the SAM domain in STIM1 activity remains unclear, deletion of the SAM domain prevents STIM1 from forming inducible puncta (Baba et al. 2006). In addition, N-linked glycosylations are found to occur at two separate asparagine residues located within the SAM region (Williams et al. 2002). The cytoplasmic portion of STIM1 is found to contain three putative coiled-coil (CC) regions near the transmembrane domain as well as a Serine/Proline (S/P) rich region and a Lysine-rich polybasic domain nearer the C-terminal tail (Dziadek & Johnstone 2007). Ultimately, the cytosolic region serves as the critical link for coupling ER Ca^{2+} depletion events, sensed in the lumen, to SOCE at the PM.

II. Essential domains that mediate interaction with and activation of Orai1

In addition to these putative motifs, researchers have identified several important residues and regions within STIM1 based on their functional roles in the activation of STIM1 and SOCE activity (Figure 1.3). Arguably, the most important region discovered is known as the CRAC activation domain (CAD, residues 342-448) – also called the STIM1 Orai1-activating region (SOAR, residues 344-442), the Orai1-activating small fragment (OASF, residues 233-450) and/or the CC domain containing region b9 (CCb9, residues 339-444). Simultaneously in 2009, several research groups identified the approximately 100 amino acid residue sequence containing CC2 and CC3 as being the minimal region of STIM1 required for both interaction with Orai1 and activation of the CRAC channel (Park et al. 2009, Yuan et al. 2009, Muik et al. 2009, Kawasaki et al. 2009). Soon after, CAD was found to directly interact with Orai1 (Zhou et al.

2010) via interactions between a short basic residue sequence within CAD (residues 382-387) and several acidic residues located on the C-terminus of Orai1 (Calloway et al. 2010). An additional region containing the latter half of CAD and several residues C-terminal to it, the STIM1 homomerization domain (SHD, approximately residues 400-474), was identified as being important to STIM1 oligomerization (Muik et al. 2009). Muik et al. (2009) found that the SHD was necessary for the formation of at least low-order STIM1 oligomers, which are required for activation of CRAC channels and SOCE. However, using C-terminal truncations, Park et al. (2009) also found that deletion of residues immediately after the CAD region, including part of the SHD, did not affect the ability of STIM1 to form puncta and interact with Orai1 though CRAC channel activity was impaired (Schindl et al. 2012). Together these results implicate the importance of the C-terminal residues of CAD, approximately residues 400-440, in regulating at least some oligomeric states of STIM1.

While it is clear that CAD directly binds Orai1 and activates SOCE, researchers were surprised to find that expression of the entire cytosolic portion of STIM1 failed to interact with Orai1 or constitutively activate CRAC channel current (Park et al. 2009). These findings suggested the existence of an internal region within the cytosolic domain of STIM1 that regulates the active state of the protein. In support of this idea, Korzeniowski et al. (2010) identified a series of acidic residues within the CC1 domain important to the inactivity of STIM1 at rest, though the exact mechanism remains unclear. They proposed that these residues serve as an autoinhibitory switch for the STIM1 protein by electrostatically interacting with basic STIM1 residues also in the cytoplasm (Korzeniowski et al. 2010), such as the basic residue sequence located inside CAD (Calloway et al. 2010). A schematic of this hypothesis is shown in Figure 1.4 (Wang et al. 2010). In the inactive state, the acidic residues of CC1 are electrostatically

Figure 1.4: STIM1 activates via an intramolecular switching mechanism. At rest (left), electrostatic interactions between acidic residues in CC1 and basic residues in the CAD region mask CAD and maintain STIM1 in an inactive state. Following Ca^{2+} depletion from the ER lumen, the EF-hand domain releases Ca^{2+} and initiates conformational changes throughout the STIM1 protein (right), removing intramolecular inactivation. Once unmasked, the basic residues within CAD interact with acidic residues in Orai1 (marked by 'A') to activate the CRAC channel and initiate SOCE. Electrostatic interaction between the polybasic tail of STIM1and phosphoinositides within the plasma membrane help to stabilize STIM1 at the plasma membrane (marked by 'C'). [Figure from Wang et al. 2010]

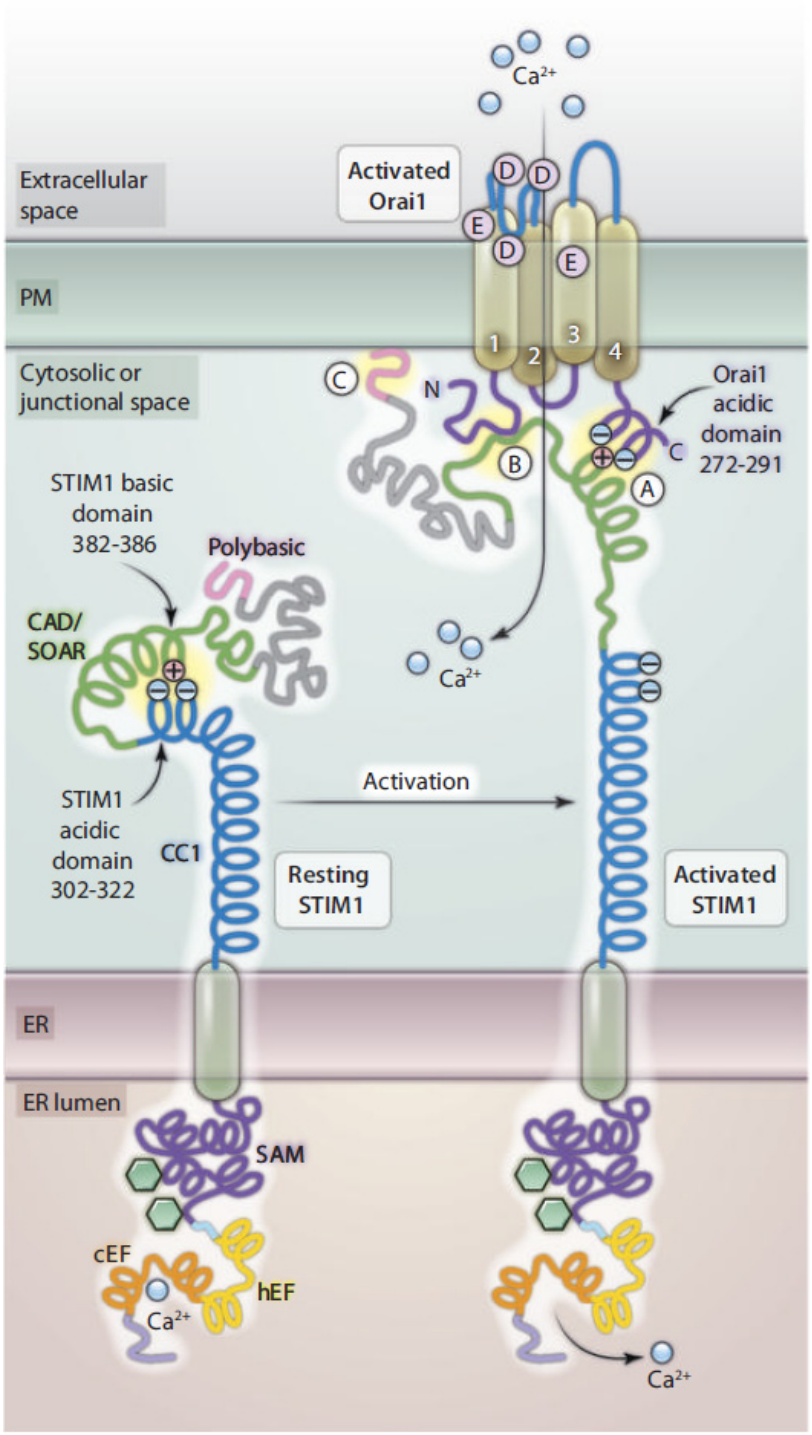
Ca2+
Extracellular space
Activated Orai1
D
D
E
D
E
PM
1
2
3
4
Cytosolic or junctional space
C
N
B
A
C
Orai1 acidic domain 272-291
STIM1 basic domain 382-386
Polybasic
CAD/ SOAR
Ca2+
Activation
STIM1 acidic domain 302-322
CC1
Resting STIM1
Activated STIM1
ER
ER lumen
SAM
cEF
hEF
Ca2+
Ca2+

bound to the CAD region, preventing CAD from interacting with Orai1. Following conformational changes throughout the protein, initiated by dissociation of Ca^{2+} from the luminal EF-hand domain (Stathopulos et al. 2006), interactions between CC1 and CAD are broken. The basic residues of CAD then bind to the acidic residues within the C-terminus of Orai1 (Calloway et al. 2010). Figure 1.4 also highlights the functional role of the polybasic, Lysine-rich tail of STIM1. Containing a series of positively charged residues, the polybasic tail targets STIM1 to ER-PM junctions and helps to stabilize STIM1-PM interactions (Liou et al. 2007, Korzeniowski et al. 2009, Walsch et al. 2010). More recent work by Calloway et al. (2011) suggests that, following sustained store depletion by thapsigargin, STIM1-Orai1 coupling is positively regulated by PIP_2 in ordered lipid regions of the plasma membrane.

In addition to intramolecular regulation of STIM1, researchers have uncovered a C-terminal region within the protein that may be important to intermolecular regulation of SOCE. Called the CRAC modulatory domain (CMD, approximately residues 475-490), this region C-terminal to the SHD comprises several acidic amino acids that regulate the extent of coupling between STIM1 and Orai1 and has been shown to be crucial to fast Ca^{2+}-dependent inactivation (CDI) of the CRAC channel (Derler et al. 2009, Fahrner et al. 2009, Lee et al. 2009, Mullins et al. 2009). These studies reveal that neutralization of the acidic residues within the CMD prevents inactivation of CRAC channel activity, thus sustaining SOCE. Working in concert with Orai1, researchers believe that acidic clusters within both proteins may serve as Ca^{2+} sensors to mediate CDI (Lee et al. 2009).

III. STIM1 oligomerization

At rest, STIM1 is distributed throughout the ER membrane (Roos et al. 2005, Zhang et al. 2005). Upon store depletion, STIM1 undergoes conformational changes, oligomerizes, and translocates to ER-PM junctions, where the creation of puncta facilitates CRAC channel formation and activation (Zhang et al. 2005, Baba et al. 2006, Luik et al. 2006, Xu et al. 2006, Liou et al. 2007). While it is known that the oligomerization of STIM1 is the key step required to tie store depletion to SOCE activation (Liou et al. 2007, Luik et al. 2008, Muik et al. 2008), debate remains as to the resting state and/or stoichiometry of STIM1.

Both the luminal and cytoplasmic portions of STIM1 have been shown to contribute to STIM1 oligomerization. Using luminal fragments of STIM1 containing the EF-hand and SAM domains, Stathopulous et al. (2006, 2008) showed that these fragments are monomeric when bound to Ca^{2+}. However, upon store depletion, the loss of Ca^{2+} from the canonical EF-hand leads to conformational changes and oligomerization of the fragments. Evidence for STIM1 self-association at rest was first noted via co-immunoprecipitation assays by Williams et al. in 2002, though the exact stoichiometry remained unknown. Since that time, numerous laboratories have confirmed the self-association of STIM1 in store-replete cells (Baba et al. 2006, Liou et al. 2007, Penna et al. 2008), and further determined that interactions of the cytosolic CC domains and CAD were important to the formation and stabilization of these oligomers (Baba et al. 2006, Muik et al. 2009, Covington et al. 2010). Visualization of resting STIM1 using bimolecular fluorescence complementation (BiFC) confirms that STIM1 forms self-assembled structures at rest, which could be as small as dimers, though the exact stoichiometry was not determined (He et al. 2012). Recent elucidation of the CAD crystal structure by Yang et al. (2012) suggests that CAD is present as a dimer in its inactive state and undergoes conformational changes following

store depletion to extend the region and render the CAD dimer into its active state. However, their structural model is at odds with the previous electrostatic inactivation mechanism described in Figure 1.4 (Korzeniowski et al. 2010, Wang et al. 2010) and proposes that an inhibitory helix within CAD provides the interactions required to maintain the CAD dimer in an inactive state at rest (Yang et al. 2012). It is important to note that, to date, no crystal structure has been determined for full-length STIM1 or the entire cytosolic fragment. Thus, while many agree that STIM1 exists in an oligomeric, autoinhibited state at rest, the exact interactions required to maintain this state and the exact stoichiometry of the STIM1 species remain unclear. For these reasons, it is important to determine both the structural basis and stoichiometry of full-length STIM1 oligomers in resting cells.

Nanobiotechnology & the Fabrication of Patterned Biomolecule Arrays:

Recent interest has focused on understanding both spatial and temporal regulation of receptor signal transduction pathways. Using new fabrication techniques made possible by the emerging field of nanobiotechnology, researchers have developed a large toolkit for immobilizing biomolecules, such as proteins and DNA, onto spatially defined regions of silicon surfaces (Torres et al. 2008b). The biomolecules provide a rigidly defined ligand area for cell membrane receptors and other signaling proteins to associate, which can then be monitored both spatially and temporally via fluorescence microscopy. By designing both the size and shape of the biomolecule region patterned and the distance between features, researchers can spatially regulate stimuli. This ability to adhere biomolecules to defined regions within a surface is integral to the development of biochemical and biomedical devices, such as for microarray

analysis, tissue engineering, and fundamental cell studies (Blawas & Reichert 1998, Kane et al. 1999, Voldman et al. 1999, Orth et al. 2003, Torres et al. 2008b).

In more recent years, multi-component biomolecule patterning has become an active research field, as the needs for more complex bio-devices arise. While single component patterning methods have been extensively developed (Blawas & Reichert 1998, Christman et al. 2006), multi-component patterning is riddled with challenges. For example, fabrication of multi-protein patterns requires the ability to adhere biomolecules onto discrete regions of a substrate while retaining the functionality of the proteins and avoiding non-specific interactions and degradation of previously patterned regions (Taylor 2011). While several techniques have been explored, each fabrication method brings its own unique set of challenges that must be addressed before high-resolution, high-throughput, multi-component patterning can be achieved.

I. Photolithography

Traditional photolithography generates patterns onto a surface by first coating the surface with photoresist and selectively irradiating the surface with ultraviolet (UV) light through a designed template, or mask. Depending on the properties of the photoresist, either positive tone or negative tone, exposure to UV light through the patterned mask serves to polymerize or depolymerize the resist and thus makes the photoresist more/less soluble. These more soluble regions of resist are then removed using chemical developers, exposing bare substrate surface for further chemical modifications and/or biomolecule adherence (Campbell 1996), as shown in Figure 1.5A (Torres et al. 2008b).

Figure 1.5: Diagram of traditional microfabrication methods. (A) Conventional lithography using positive tone or negative tone photoresist. **(B)** Polymer lift-off method. **(C)** Microcontact printing (μCP), a soft lithography technique. [Figure from Torres et al. 2008b]

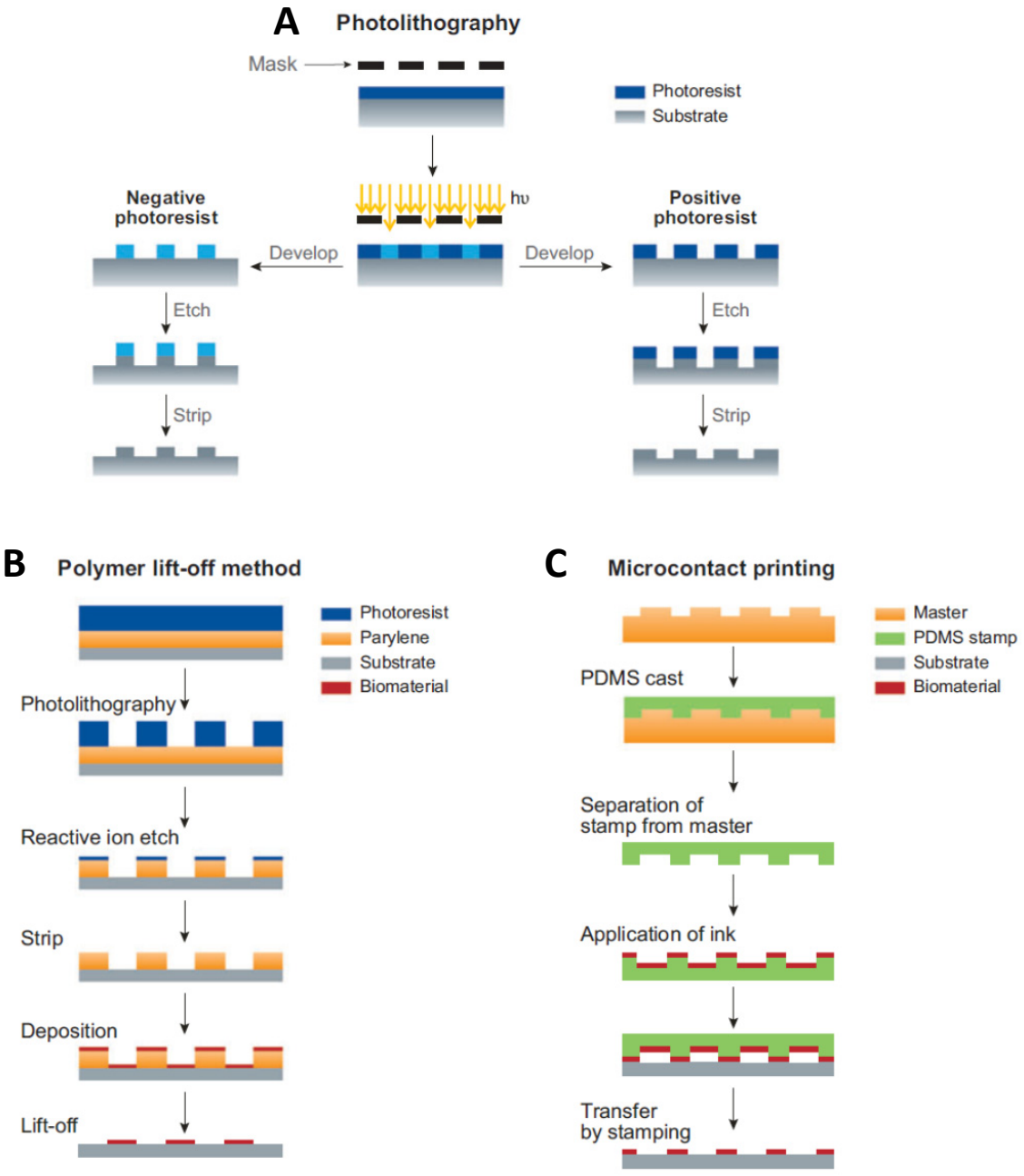
A
Photolithography
Mask
Photoresist
Substrate
hυ
Negative photoresist
Positive photoresist
Develop
Develop
Etch
Etch
Strip
Strip
B
Polymer lift-off method
Photoresist
Parylene
Substrate
Biomaterial
Photolithography
Reactive ion etch
Strip
Deposition
Lift-off
C
Microcontact printing
Master
PDMS stamp
Substrate
Biomaterial
PDMS cast
Separation of stamp from master
Application of ink
Transfer by stamping

One of the greatest advantages of photolithography is its capacity for high-resolution patterning. While patterned feature dimensions range greatly depending on the scientific field, biological assays typically require features based at the cellular scale, tens of micrometers, or smaller, tens or hundreds of nanometers. (Torres et al. 2008b). At the present, photolithographic techniques have been optimized to achieve features < 50 nm in size and with high-throughput capacity (Gates et al. 2005, Pimpin & Srituravanich 2011). While photolithography provides for excellent spatial control, the mechanical details of the technique make it ill-suited for multi-component biomolecule patterning. From the use of harsh chemical photoresists and developers to steps involving high temperature 'baking' and UV exposure, photolithography provides numerous opportunities for biomolecule degradation (Taylor 2011).

Even with these obstacles, several laboratories have attempted multi-protein patterning using photolithographic techniques. In one of the first examples, Pritchard et al. (1995) devised a scheme wherein biotin, conjugated to a photactivatable probe, was bound to an avidin-adsorbed surface. Addition of a protein layer and subsequent UV exposure to activate the probe allowed for covalent binding of the protein to the biotin-avidin complexes. A similar technique developed by Sundberg et al. (1995) required UV exposure to deprotect adsorbed biotin on the substrate surface and allow for subsequent protein binding. However, in this example, the proteins were not exposed to irradiation, as protein addition occurred after UV exposure. Other more recent techniques have also exploited the use of protective layers (Sorribas et al. 2002) and selective photo-activation/bleaching to pattern biomolecules (Holden & Cremer 2003).

Other groups have identified more biocompatible ways of applying and removing photoresist. Citing their chemically amplified resist (CAR) system, Douvas et al. (2001, 2002) generated two-protein patterned arrays using relatively low bake temperatures (~ 50 ^{o}C) and

aqueous weak base developers. Similarly, Doh and Irvine (2004) developed a pH-dependent photoresist that allowed for the generation of two-protein patterned arrays in aqueous solutions. In both cases, the photoresist was patterned using UV exposure and proteins were adsorbed to the exposed regions of substrate. Following resist removal, the second protein was then deposited as a 'backfill' into the background areas between the initial protein features. Hence, the second protein is not deposited in a spatially defined manner, nor is there the capacity to adhere additional layers of proteins in a spatially defined manner.

II. Parylene Lift-Off Method

An alternative method used in multi-component patterning that merits further review is the parylene lift-off method. Developed by Ilic and Craighead in 2000, a thin layer of parylene C polymer is first deposited over a substrate, as shown in Figure 1.5B (Torres et al. 2008b). A layer of photoresist is then added on top of the parylene layer and both are patterned using photolithography irradiation techniques. Biomolecules, present in an aqueous solution, are then incubated atop the entire surface and adhere. Following adsorption, the parylene-photoresist layer is mechanically peeled off the substrate, leaving patterned protein features behind (Ilic & Craighead 2000).

As a further extension of this technique, Orth et al. (2003) showed the capacity to pattern lipid bilayers and Torres et al. (2008a) patterned proteins. In collaboration with our laboratory, these patterned biomolecules have seen extensive use in fundamental cell studies with rat basophilic leukemia (RBL)-2H3 mast cells (Orth et al. 2003, Wu et al. 2004, Torres et al. 2008a, Torres et al. 2008b) and more recently with NIH-3T3 fibroblasts (Singhai 2012). For example,

using a combination of fluorescently labeled lipids and phospholipids conjugated to dinitrophenyl (DNP), patterned lipid bilayers are fabricated using the parylene lift-off method. Next, RBL cells, sensitized with (anti-DNP)-IgE, are allowed to settle on the patterned surface. Within minutes, IgE-bound FcεRI can be seen clustering above the DNP-containing lipid patterns (Wu et al. 2004). By monitoring the localization of proteins important to the IgE-receptor signaling cascade at varying incubation times, Wu et al. (2004) determined both spatial and temporal regulation of the FcεRI signaling pathway.

More recently, Craighead and colleagues have demonstrated the ability to fabricate multi-protein patterns using a combination of parylene lift-off and ink-jet printing (Tan et al. 2010). This 'peel and print' process allows for generation of sub-micrometer patterns and combinatorial patterning, wherein the substrate was run through the ink-jet printer more than once. While this method shows immense promise for the fabrication of complex nanoarrays, the technique is still constrained by the fact that once the parylene layer is removed, no additional proteins can be deposited in a spatially defined manner. At most, a final protein layer can be 'backfilled' into the surrounding space.

III. Soft Lithography

A low cost set of fabrication techniques, termed soft lithography, has also demonstrated the capacity to pattern biomolecules. Using a template made of soft, elastomeric polymers, such as polydimethylsiloxane (PDMS), a wide variety of techniques involving molding, imprinting, and embossing can be employed to form the patterns (Torres et al. 2008b). The overall process

is inexpensive and has the ability to pattern feature sizes as small as tens of nanometers (Pimpin & Srituravanich 2011).

One form of soft lithography, microcontact printing (μCP) is used extensively in biological applications (Figure 1.5C, Torres et al. 2008b). Here, an elastomeric stamp is fabricated and followed by addition of the biomolecules to the stamp. The stamp is then used to transfer the biomolecules to the appropriate substrate in geometries defined by the relief structure of the stamp. As an added benefit of this technique, the soft, pliable stamp allows for transfer of biomolecules onto flexed and/or curved substrates (Pimpin & Srituravanich 2011). The capacity for multi-protein patterning has been demonstrated with μCP through sequential printing of patterns and also through single step transfers of multiple biomolecules (Bernard et al. 2000).

Similar soft lithography techniques including patterning through microfluidic networks (μFN) and affinity contact printing (αCP) have also been developed for multi-protein patterning (Delamarche et al. 1997, Kaji et al. 2006, Bernard et al. 2001, Renault et al. 2002). Both techniques take advantage of selective and specific binding interactions between proteins and the elastomeric stamp and/or the functionalized substrate surfaces for successful deposition. In addition, Whitesides and colleagues have shown the ability to pattern both cells and proteins using elastomeric lift-off membranes (Otsuni et al. 2000).

While soft lithography has demonstrated its viability in multi-component biomolecule patterning, it too contains challenges. Due to the elastomeric and pliable nature of the stamps, mechanical deformation of the stamp can occur, resulting in deformation of pattern feature geometry. Furthermore, soft lithography is limited by an overall lack of registration and

alignment capabilities, making it difficult to attempt multiple layers of deposition with spatial precision (Taylor 2011).

IV. Additional patterning techniques

In an attempt to provide more controlled patterning with high-resolution, Mirkin and colleagues developed dip-pen nanolithography (DPN) (Piner et al. 1999). Using a sharp probe and atomic force microscope (AFM), they demonstrated the ability to transfer molecules selectively onto a substrate with nanoscale feature dimensions. Moreover, this technique can be performed without the use of large electromagnetic fields or shear forces (Pimpin & Srituravanich 2011), suggesting its use in biomolecule patterning. As proof of this concept, Mirkin and colleagues have shown the ability to fabricate multi-protein arrays using DPN (Lee et al. 2003, Lim et al. 2003). While this technique does afford impressive resolution and patterning control, it is extremely time consuming and difficult to scale up (Taylor 2011, Pimpin & Srituravanich 2011), making it ill-suited for most research applications.

As an alternative to DPN, spot-arraying techniques, including ink-jet printing, have garnered wide attention for their ability to fabricate low cost and high-throughput arrays (Barbulovic-Nad et al. 2006). Using modified commercial printers, biomolecule solutions replace ink cartridges and allow for the fabrication of multi-protein arrays with micrometer dimensions (Pardo et al. 2002). Soon after, Bruckbauer et al. (2003) developed a nanopipet dispensing system to allow for fabrication of sub-micrometer multi-protein arrays. While an attractive technique based on its low cost and high reproducibility, spot-arraying methods are riddled with challenges. Some of the largest drawbacks include that spot-arraying can only be

performed with flexible substrates and fall victim to traditional printing issues, such as clogged printing nozzles and the formation of satellite droplets, which can contaminate neighboring features (Barbulovic-Nad et al. 2006). In addition, the high temperatures and shear forces required for some spot-array techniques risk denaturing the biomolecules (Okamoto et al. 2000).

V. Outlook on biomolecule patterning

Recent advances in micro- and nano-fabrication techniques have presented vast opportunities for applications in biology and medicine. As techniques have been refined, the capacity to create multi-component biomolecule patterns has also improved. While each of the patterning methods presented thus far offers certain advantages for fabricating multi-component arrays, each is plagued by certain disadvantages as well. To overcome these shortfalls, new patterning methods must be able to simultaneously address several key issues in multi-biomolecule patterning including, but not limited to: (1) retaining biomolecule structure and function, (2) avoiding cross-contamination, (3) providing high resolution and pattern fidelity, (4) utilizing biocompatible temperatures and solvents, (5) maintaining low cost and high-throughput capacity, (6) and overall reproducibility of results. In addition, the ability to pattern more complex and multi-layered arrays, such as three-, four-, or even five-protein patterned arrays, and with spatial precision remains an obstacle that has not been satisfactorily addressed. Thus, the goal of providing a universal, high-throughput patterning method that is able to achieve high-resolution nanoscale multi-biomolecule patterns has remained elusive.

Scope of Thesis:

Understanding the mechanisms by which processes occur at the cellular and molecular level is critical to determining the regulation of biological pathways. In the case of mast cells, a better understanding of the proteins and pathways involved in degranulation and the immune response is vital to identifying new protein targets and developing drug therapies to alleviate allergy symptoms. Particular attention has also focused on the role of Ca^{2+} mobilization, whose regulation remains vital to a number of cellular processes, including degranulation and the immune response. Indeed, misregulation of Ca^{2+} mobilization, such as impaired SOCE, has been shown to have severe and detrimental effects. While much is known about the overall process of SOCE, specific details about the proteins and interactions required to facilitate this process remain elusive. Taken together, these issues reinforce the need to investigate the mechanisms by which signaling pathways and individual proteins control intracellular Ca^{2+} responses.

This dissertation provides new insights and details into the role of STIM1 and its activation of SOCE and describes a new patterning fabrication technique which can be used for future biological applications, such as fundamental cell studies. In Chapter Two, biochemical experiments are used to determine the oligomeric state and stoichiometry of STIM1 in living cells. We demonstrate that STIM1 exists in multiple low-order oligomeric states in resting cells, which can be retained as disulfide-bonded products when cells are lysed. We further elucidate the stoichiometry of the largest oligomer observed and identify the presence of a previously unknown 110 kDa STIM1-containing product. Continued investigation of the 110 kDa STIM1 product is discussed in Chapter Three, wherein we explore the role of this complex in the steps leading to SOCE activation. As discussed in Chapter Four, we have developed a new method for fabricating multi-protein patterned arrays using imprint lithography and highly fluorinated

photoresist and developers. This method was also found to be compatible with DNA patterning and fundamental cell studies. In Chapter Five, a summary of concluding remarks is provided along with future directions for projects presented in this thesis.

REFERENCES

Baba Y, Hayashi K, Fujii Y, Mizushima A, Watarai H, Wakamori M, Numaga T, Mori Y, Iino M, Hikida M, and Kurosaki T (2006). Coupling of STIM1 to store-operated Ca^{2+} entry through its constitutive and inducible movement in the endoplasmic reticulum. Proc Natl Acad Sci USA, 103: 16704-16709.

Baba Y and Kurosaki T (2009). Physiological function and molecular basis of STIM1-mediated calcium entry in immune cells. Immunol Rev, 231: 174-188.

Barbulovic-Nad I, Lucente M, Sun Y, Zhang M, Wheeler AR, and Bussmann M (2006). Bio-microarray fabrication techniques – A review. Crit Rev Biotechnol, 26: 237-259.

Beaven MA, Moore JP, Smith GA, Hesketh TR, and Metcalfe JC (1984). The calcium signal and phosphatidylinositol breakdown in 2H3 cells. J Biol Chem, 259: 7137-7142.

Bernard A, Renault JP, Michel B, Bosshard HR, and Delamarche E (2000). Microcontact printing of proteins. Adv Mater, 12: 1067-1070.

Bernard A, Fitzli D, Sonderegger P, Delamarche E, Michel B, Bosshard HR, and Biebuyck H (2001). Affinity capture of proteins from solution and their dissociation by contact printing. Nat Biotechnol, 19: 866-869.

Berridge MJ, Bootman MD, and Roderick HL (2003). Calcium signalling: Dynamics, homeostasis and remodelling. Nat Rev Mol Cell Biol, 4: 517-529.

Bird GS, Aziz O, Lievremont JP, Wedel BJ, Trebak M, Vazquez G, and Putney JW, Jr. (2004). Mechanisms of phospholipase C-regulated calcium entry. Curr Molec Med, 4: 291-301.

Blawas AS and Reichert WM (1998). Protein patterning. Biomaterials, 19: 595-609.

Bruckbauer A, Zhou DJ, Ying LM, Korchev YE, Abell C, and Klenerman DJ (2003). Multicomponent submicron features of biomolecules created by voltage controlled deposition from a nanopipet. J Am Chem Soc, 125: 9834-9839.

Calloway N, Holowka D, and Baird B (2010). A basic sequence in STIM1 promotes Ca^{2+} influx by interacting with the C-terminal acidic coiled coil of Orai1. Biochemistry, 49: 1067-1071.

Calloway N, Owens T, Corwith K, Rodgers W, Holowka D, and Baird B (2011). Stimulated association of STIM1 and Orai1 is regulated by the balance of PtdIns(4,5)P2 between distinct membrane pools. J Cell Sci, 124: 2602-2610.

Campbell SA (1996). The science and engineering of microelectronic fabrication. New York: Oxford University Press.

Christman KL, Enriquez-Rios VD, and Maynard HD (2006). Nanopatterning proteins and peptides. Soft Matter, 2: 928-939.

Church MK and Levi-Schaffer F (1997). The human mast cell. J Allergy Clin Immunol, 99: 155-160.

Covington E, Wu MM, and Lewis RS (2010). Essential role for the CRAC activation domain in store-dependent oligomerization of STIM1. Molec Biol Cell, 21: 1897-1907.

Delamarche E, Bernard A, Schmid H, Michel B, and Biebuyck H (1997). Patterned delivery of immunoglobulins to surfaces using microfluidic networks. Science, 276: 779-781.

Derler I, Fahrner M, Muik M, Lackner B, Schindl R, Groschner K, and Romanin C (2009). A Ca^{2+} release-activated Ca^{2+} (CRAC) modulatory domain (CMD) within STIM1 mediates fast Ca^{2+}-dependent inactivation of Orai1 channels. J Biol Chem, 284: 24933-24938.

Derler I, Madl J, Schütz, and Romanin C (2012). Structure, regulation, and biophysics of I_{CRAC}, STIM/Orai1. In "Calcium Signalling" (Ed. MS Islam). Adv Exp Med Biol, 740: 383-410.

Doh J and Irvine DJ (2004). Photogenerated polyelectrolyte bilayers from an aqueous-processible photoresist for multicomponent protein patterning. J Am Chem Soc, 126: 9170-9171.

Douvas AM, Argitis P, Diakoumakos CD, Misiakos K, Dimotikali D, and Kakabakos SE (2001). Photolithographic patterning of proteins with photoresists processable under biocompatible conditions. J Vac Sci Technol B, 19: 2820-2824.

Douvas AM, Argitis P, Misiakos K, Dimotikali D, Petrou PS, and Kakabakos SE (2002). Biocompatible photolithographic process for the patterning of biomolecules. Biosens Bioelectron, 17: 269-278.

Dziadek MA and Johnstone LS (2007). Biochemical properties and cellular localization of STIM proteins. Cell Calcium, 42: 123-132.

Enslen H, Tokumitsu, Stork PJ, Davis RJ, and Soderling TR (1996). Regulation of mitogen-activated protein kinases by a calcium/calmodulin-dependent protein kinase cascade. Proc Natl Acad Sci USA, 93: 10803-10808.

Fahrner M, Muik M, Derler I, Schindl R, Fritsch R, Frischauf I, and Romanin C (2009). Mechanistic view on domains mediating STIM1-Orai coupling. Immunol Rev, 231: 99-112.

Feske S, Gwack Y, Prakriya M, Srikanth S, Puppel SH, Tanasa B, Hogan PG, Lewis RS, Daly M, and Rao A (2006). A mutation in Orai1 causes immune deficiency by abrogating CRAC channel function. Nature, 441: 179-185.

Feske S (2007). Calcium signalling in lymphocyte activation and disease. Nat Rev Immunol, 7: 690-702.

Feske S (2011). Immunodeficiency due to defects in store-operated calcium entry. Ann NY Acad Sci, 1238: 74-90.

Galli SJ and Tsai M (2012). IgE and mast cells in allergic disease. Nat Med, 18: 693-704.

Gates BD, Xu Q, Stewart M, Ryan D, Willson CG, and Whitesides GM (2005). New approaches to nanofabrication: Molding, printing, and other techniques. Chem Rev, 105: 1171-1196.

Gilfillan AM and Tkaczyk C (2006). Integrated signalling pathways for mast-cell activation. Nat Rev Immunol, 6: 218-230.

Hammond S, Holowka D, and Baird B (2009). Membrane compartments in immune cell signaling and trafficking. In Wiley Encyclopedia of Chemical Biology, 4 Volume Set (Ed. TP Begley). Wiley InterSci, 2: 718-728.

He J, Yu T, Pan J, and Li H (2012). Visualization and identification of the interaction between STIM1s in resting cells. PLoS One, 7: e33377.

Hogan PG, Chen L, Nardone J, and Rao A (2003). Transcriptional regulation by calcium, calcineurin, and NFAT. Genes Dev, 17: 2205-2232.

Holden MA and Cremer PS (2003). Light activated patterning of dye-labeled molecules on surfaces. J Am Chem Soc, 125: 8074-8075.

Holowka D and Baird B (1996). Antigen-mediated IgE receptor aggregation and signaling: A window on cell surface structure and dynamics. Annu Rev Biophys Biomol Struct, 25: 79-112.

Holowka D, Gosse JA, Hammond AT, Han X, Sengupta P, Smith NL, Wagenknecht-Wiesner A, Wu M, Young RM, and Baird B (2005). Lipid segregation and IgE receptor signaling: A decade of progress. Biochim Biophys Acta, 1746: 252-259.

Ilic B and Craighead HG (2000). Topographical patterning of chemically sensitive biological materials using a polymer-based dry lift off. Biomed Microdevices, 2: 317-322.

Kaji H, Hashimoto M, and Nishizawa M (2006). On-demand patterning of protein matrixes inside a microfluidic device. Anal Chem, 78: 5469-5473.

Kane RS, Takayama S, Ostuni E, Ingber DE, and Whitesides GM (1999). Patterning proteins and cells using soft lithography. Biomaterials, 20: 2363-2376.

Kawasaki T, Lange I, and Feske S (2009). A minimal regulatory domain in the C terminus of STIM1 binds to and activates Orai1 CRAC channels. Biochem Biophys Res Commun, 385: 49-54.

Kinet JP (1999). The high-affinity IgE receptor (FcεRI): From physiology to pathology. Annu Rev Immunol, 17, 931-972.

Korzeniowski MK, Popovic MA, Szentpetery Z, Varnai P, Stojilkovic SS, and Balla T (2009). Dependence of STIM1/Orai1-mediated calcium entry on plasma membrane phosphoinositides. J Biol Chem, 284: 21027-21035.

Korzeniowski MK, Manjarrés IM, Varnai P, and Balla T (2010). Activation of STIM1-Orai1 involves an intramolecular switching mechanism. Sci Signal, 3: ra 82.

Lee KB, Lim JH, and Mirkin CA (2003). Protein nanostructures formed via direct-write dip-pen nanolithography. J Am Chem Soc, 125: 5588-5589.

Lee KP, Yuan JP, Zeng W, So I, Worley PF, and Muallem S (2009). Molecular determinants of fast Ca^{2+}-dependent inactivation and gating of the Orai channels. Proc Natl Acad Sci USA, 106: 14687-14692.

Lim JH, Ginger DS, Lee KB, Heo J, Nam JM, and Mirkin CA (2003). Direct-write dip-pen nanolithography of proteins on modified silicon oxide surfaces. Angew Chem Int Ed, 42: 2309-2312.

Liou J, Kim ML, Heo WD, Jones JT, Myers JW, Ferrell JE, Jr., and Meyer T (2005). STIM is a Ca^{2+} sensor essential for Ca^{2+}-store-depletion-triggered Ca^{2+} influx. Curr Biol, 15: 1235-1241.

Liou J, Fivaz M, Inoue T, and Meyer T (2007). Live-cell imaging reveals sequential oligomerization and local plasma membrane targeting of stromal interaction molecule 1 after Ca^{2+} store depletion. Proc Natl Acad Sci USA, 104: 9301-9306.

Luik RM, Wu MM, Buchanan J, and Lewis RS (2006). The elementary unit of store-operated Ca^{2+} entry: Local activation of CRAC channels by STIM1 at ER-plasma membrane junctions. J Cell Biol, 174: 815-825.

Luik RM, Wang B, Prakriya M, Wu MM, and Lewis RS (2008). Oligomerization of STIM1 couples ER calcium depletion to CRAC channel activation. Nature, 454: 538-542.

Manji SS, Parker NJ, Williams RT, van Stekelenburg L, Pearson RB, Dziadek M, and Smith PJ (2000). STIM1: A novel phosphoprotein located at the cell surface. Biochim Biophys Acta, 1481: 147-151.

Matsumoto M, Fujii Y, Baba A, Hikida M, Kurosaki T, and Baba Y (2011). The calcium sensors STIM1 and STIM2 control B cell regulatory function through interleukin-10 production. Immunity, 34: 703-714.

Maul-Pavicic A, Chiang SCC, Rensing-Ehl A, Jessen B, Fauriat C, Wood SM, Sjöqvist S, Hufnagel M, Schulze I, Bass T, Schamel WW, Fuchs S, Pircher H, McCarl C-A, Mikoshiba K, Schwarz K, Feske S, Bryceson YT, and Ehl S (2011). Orai1-mediated calcium influx is required for human cytotoxic lymphocyte degranulation and target cell lysis. Proc Natl Acad Sci USA, 108: 3324-3329.

Metcalfe DD, Baram D, and Mekori YA (1997). Mast cells. Physiol Rev, 77: 1033-1079.

Muik M, Frischauf I, Derler I, Fahrner M, Bergsmann J, Eder P, Schindl R, Hesch C, Polzinger B, Fritsch R, Kahr H, Madl J, Gruber H, Groschner K, and Romanin C (2008). Dynamic coupling of the putative coiled-coil domain of Orai1 with STIM1 mediates Orai1 channel activation. J Biol Chem, 283: 8014-8022.

Muik M, Fahrner M, Derler I, Schindl R, Bergsmann J, Frischauf I, Groschner K, and Romanin C (2009). A cytosolic homomerization and a modulatory domain within STIM1 C terminus determine coupling to Orai1 channels. J Biol Chem, 284: 8421-8426.

Mullins FM, Park CY, Dolmetsch RE, and Lewis RS (2009). STIM1 and calmodulin interact with Orai1 to induce Ca^{2+}-dependent inactivation of CRAC channels. Proc Natl Acad Sci USA, 106: 15495-15500.

Okamoto T, Suzuki T, and Yamamoto N (2000). Microarray fabrication with covalent attachment of DNA using bubble jet technology. Nat Biotechnol, 18: 438-441.

Oritani K and Kincade PW (1996). Identification of stromal cell products that interact with pre-B cells. J Cell Biol, 134: 771-782.

Orth RN, Wu M, Holowka DA, Craighead HG, and Baird BA (2003). Mast cell activation on patterned lipid bilayers of subcellular dimensions. Langmuir, 19: 1599-1605.

Otsuni E, Kane R, Chen CS, Ingber DE, and Whitesides GM (2000). Patterning mammalian cells using elastomeric membranes. Langmuir, 16: 7811-7819.

Pardo L, Wilson WC, and Boland TG (2002). Characterization of patterned self-assembled monolayers and protein arrays generated by the ink-jet method. Langmuir, 19: 1462-1466.

Parekh AB and Putney JW, Jr. (2005). Store-operated calcium channels. Physiol Rev, 85: 757-810.

Park CY, Hoover PJ, Mullins FM, Bachhawat P, Covington ED, Raunser S, Walz T, Garcia KC, Dolmetsch RE, and Lewis RS (2009). STIM1 clusters and activates CRAC channels via direct binding of a cytosolic domain to Orai1. Cell, 136: 876-890.

Parker NJ, Begley CG, Smith PJ, and Fox RM (1996). Molecular cloning of a novel human gene (D11S4896E) at chromosomal region 11p15.5. Genomics, 37: 253-256.

Pawankar R (2012). The unmet global health need of severe and complex allergies: Meeting the challenge. World Allergy Org J, 5: 20-21.

Penna A, Demuro A, Yeromin AV, Zhang SL, Safrina O, Parker I, and Cahalan MD (2008). The CRAC channel consists of a tetramer formed by STIM-induced dimerization of Orai dimers. Nature, 456: 116-120.

Pimpin A and Srituravanich W (2011). Review on micro- and nano-lithography techniques and their applications. Engineering J, 16: 37-55.

Piner RD, Zhu J, Xu F, Hong SH, and Mirkin CA (1999). "Dip-pen" nanolithography. Science, 283: 661-663.

Platts-Mills TA (2001). The role of Immunoglobulin E in allergy and asthma. Am J Respir Crit Care Med, 164: S1-S5.

Powell MS and Hogarth PM (2008). Chapter 3: Fc receptors. In "Multichain Immune Recognition Receptor Signaling" (Ed. A Sigalov). New York: Springer.

Prakriya M, Feske S, Gwack Y, Srikanth S, Rao A, and Hogan PG (2006). Orai1 is an essential pore subunit of the CRAC channel. Nature, 443: 230-233.

Pritchard DJ, Morgan H, and Cooper JM (1995). Micron-scale patterning of biological molecules. Angew Chem Int Ed, 34: 91-93.

Putney JW, Jr. (1986). A model for receptor-regulated calcium entry. Cell Calcium, 7: 1-12.

Renault JP, Bernard A, Juncker D, Michel B, Bosshard HR, and Delamarche E (2002). Fabricating microarrays of functional proteins using affinity contact printing. Agnew Chem-Int Ed, 41: 2320-2323.

Ring J, Grosber M, Möhrenschlager M, and Brockow K (2010). Anaphylaxis: Acute treatment and management. Chem Immunol Allergy, 95: 201-210.

Roos, J, DiGregorio PJ, Yeromin AV, Ohlsen K, Lioudyno M, Zhang S, Safrina O, Kozak JA, Wagner SL, Cahalan MD, Veliçelebi G, and Stauderman KA (2005). STIM1, an essential and conserved component of store-operated Ca^{2+} channel function. J Cell Biol, 169: 435-445.

Rivera J and Gilfillan AM (2006). Molecular regulation of mast cell activation. J Allergy Clin Immunol, 117: 1214-1225.

Sabbioni S, Barbanti-Brodano G, Croce CM, and Negrini M (1997). GOK: A gene at 11p15 involved in rhabdomyosarcoma and rhabdoid tumor development. Cancer Res, 57: 4493-4497.

Scharenberg AM, Lin S, Cuenod B, Yamamura H, and Kinet JP (1995). Reconstitution of interactions between tyrosine kinases and the high affinity IgE receptor which are controlled by receptor clustering. EMBO J, 14: 3385-3394.

Schindl R, Fahrner M, Muik M, and Romanin C (2012). The STIM1-Orai pathway. In "Store-operated Ca^{2+} entry (SOCE) pathways" (Eds. K Groschner, WF Graier, and C Romanin). Pg. 45-56.

Shaw PJ and Feske S (2012). Physiological and pathophysiological functions of SOCE in the immune system. Front Biosci, 4: 2253-2268.

Singhai A (2012). Micro-patterned ligand surfaces provide new insights into spatial regulation of EGF receptor signaling and IgE receptor endocytosis. PhD thesis. Cornell University, Ithaca, New York.

Sorribas H, Padeste C, and Tiefenauer L (2002). Photolithographic generation of protein micropatterns for neuron culture applications. Biomaterials, 23: 893-900.

Stathopulos PB, Li GY, Plevin MJ, Ames JF, and Ikura M (2006). Stored Ca^{2+} depletion-induced oligomerization of stromal interaction molecule 1 (STIM1) via the EF-SAM region: An initiation mechanism for capacitive Ca^{2+} entry. J Biol Chem, 281: 35855-35862.

Stathopulos PB, Zheng L, Li GY, Plevin MJ, and Ikura M (2008). Structural and mechanistic insights into STIM1-mediated initiation of store-operated calcium entry. Cell, 135: 110-122.

Streb H, Irvine RF, Berridge MJ, and Schulz I (1983). Release of Ca^{2+} from a nonmitochondrial intracellular store in pancreatic acinar cells by inositol-1,4,5-trisphosphate. Nature, 306: 67-69.

Sundberg SA, Barrett RW, Pirrung M, Lu AL, Kiangsoontra B, and Holmes CP (1995). Spatially-addressable immobilization of macromolecules on solid supports. J Am Chem Soc, 117: 12050-12057.

Tan CP, Cipriany BR, Lin DM, and Craighead HG (2010). Nanoscale resolution, multicomponent biomolecular arrays generated by aligned printing with parylene peel-off. Nano Lett, 10: 719-725.

Taylor CW, da Fonseca PCA, and Morris EP (2004). IP3 receptors: The search for structure. Trends Biochem Sci, 29: 210-219.

Taylor CW (2006). Store-operated Ca^{2+} entry: A STIMulating stOrai. Trends Biochem Sci, 31: 597-601.

Taylor PG (2011). Lithographic patterning processes for organic electronics and biomaterials. PhD thesis. Cornell University, Ithaca, New York.

Torres AJ, Vasudevan L, Holowka D, and Baird BA (2008a). Focal adhesion proteins connect IgE receptors to the cytoskeleton as revealed by micropatterned ligand arrays. Proc Natl Acad Sci USA, 105: 17238-17244.

Torres AJ, Wu M, Holowka D, and Baird B (2008b). Nanobiotechnology and cell biology: Micro- and nanofabricated surfaces to investigate receptor-mediated signaling. Annu Rev Biophys, 37: 265-288.

Turner H and Kinet JP (1999). Signalling through the high-affinity IgE receptor FcεRI. Nature, 402: 24-30.

Vig M, Peinelt C, Beck A, Koomoa DL, Rabah D, Koblan-Huberson M, Kraft S, Turner H, Fleig A, Penner R, and Kinet JP (2006a). CRACM1 is a plasma membrane protein essential for store-operated Ca^{2+} entry. Science, 312: 1220-1223.

Vig M, Beck A, Billingsley JM, Lis A, Parvez S, Peinelt C, Koomoa DL, Soboloff J, Gill DL, Fleig A, Kinet JP, and Penner R (2006b). CRACM1 multimers form the ion-selective pore of the CRAC channel. Curr Biol, 16: 2073–2079.

Vig M, DeHaven WI, Bird GS, Billingsley JM, Wang H, Rao PE, Hutchings AB, Jouvin M-H, Putney JW, Jr., and Kinet JP (2008). Defective mast cell effector functions in mice lacking the CRACM1 pore subunit of store-operated calcium release-activated calcium channels. Nat Immunol, 9: 89-96.

Voldman J, Gray ML, and Schmidt MA (1999). Microfabrication in biology and medicine. Ann Rev Biomed Eng, 1: 401-425.

Walsch CM, Chvanov M, Haynes LP, Petersen OH, Tepikin AV, and Burgoyne RD (2010). Role of phosphoinositides in STIM1 dynamics and store-operated calcium entry. Biochem J, 425: 159-168

Wang Y, Deng X, and Gill DL (2010). Calcium signaling by STIM and Orai: Intimate coupling details revealed. Sci Signal, 3: pe42.

Williams RT, Senior PV, van Stekelenburg L, Layton JE, Smith PJ, and Dziadek MA (2002). Stromal interaction molecule 1 (STIM1), a transmembrane protein with growth suppressor activity, contains an extracellular SAM domain modified by N-linked glycosylation. Biochim Biophys Acta, 1596: 131-137.

Wu M, Holowka D, Craighead HG, and Baird B (2004). Visualization of plasma membrane compartmentalization with patterned lipid bilayers. Proc Natl Acad Sci USA, 101: 13798-13803.

Wu MM, Buchanan J, Luik RM, and Lewis RS (2006). Ca^{2+} store depletion causes STIM1 to accumulate in ER regions closely associated with the plasma membrane. J Cell Biol, 174: 803-813.

Xu P, Lu J, Li Z, Yu X, Chen L, and Xu T (2006). Aggregation of STIM1 underneath the plasma membrane induces clustering of Orai1. Biochem Biophys Res Commun, 350: 969-976.

Yang X, Jin H, Cai X, Li S, and Shen Y (2012). Structural and mechanistic insights into the activation of stromal interaction molecule 1 (STIM1). Proc Natl Acad Sci USA, 109: 5657-5662.

Yeromin AV, Zhang SL, Jiang W, Yu Y, Safrina O, and Cahalan MD (2006). Molecular identification of the CRAC channel by altered ion selectivity in a mutant of Orai. Nature, 443: 226-229.

Young RM, Holowka D, and Baird B (2003). A lipid raft environment enhances Lyn kinase activity by protecting the active site tyrosine from dephosphorylation. J Biol Chem, 278: 20746-20752.

Yuan JP, Zeng W, Dorwart MR, Choi Y-J, Worley PF, and Muallem S (2009). SOAR and the polybasic STIM1 domains gate and regulate Orai channels. Nat Cell Biol, 11, 337-343.

Zhang SL, Yu Y, Roos J, Kozak JA, Deerinck TJ, Ellisman MH, Stauderman KA, and Cahalan MD (2005). STIM1 is a Ca^{2+} sensor that activates CRAC channels and migrates from the Ca^{2+} store to the plasma membrane. Nature, 437: 902-905.

Zhou Y, Meraner P, Kwon HT, Machnes D, Oh-hora M, Zimmer J, Huang Y, Stura A, Rao A, and Hogan PG (2010). STIM1 gates the store-operated calcium channel Orai1 in vitro. Nat Struct Mol Biol, 17, 112-116.

CHAPTER TWO

Isolation and Characterization of Oligomeric Forms of STIM1 in Living Cells

Introduction:

Understanding the process of intracellular Ca^{2+} mobilization is critical to the regulation of many processes, including gene expression, protein folding, cell signaling, and cell death (Berridge et al. 2003). Of particular importance in immune cells is the mechanism of store-operated Ca^{2+} entry (SOCE), in which depletion of Ca^{2+} stores from the endoplasmic reticulum (ER) leads to activation of Ca^{2+} influx through Ca^{2+} release-activated Ca^{2+} (CRAC) channels in the plasma membrane (PM). While first proposed as capacitative Ca^{2+} entry (Putney 1986), it took nearly two decades to determine the protein players essential to this process.

In 2005-2006, several laboratories characterized the identities of the two main components of SOCE: the Ca^{2+} sensing, ER transmembrane protein and CRAC channel activator named stromal interaction molecule 1 (STIM1) (Roos et al. 2005, Liou et al. 2005, Zhang et al. 2005) and the PM channel pore protein named Orai1 or CRACM1 (Yeromin et al. 2006, Vig et al. 2006a, Vig et al. 2006b, Prakriya et al. 2006). When cells are at rest, STIM1 is located throughout the membrane of the ER where its EF-hand domain, located inside the lumen, senses Ca^{2+} levels (Dziadek & Johnstone 2007). Upon depletion of Ca^{2+} from ER stores, STIM1 oligomerizes, forming discrete puncta juxtaposed to the PM (Liou et al. 2005, Zhang et al. 2005, Wu et al. 2006). Here, STIM1 aggregates recruit Orai1 proteins, forming the CRAC channel, to initiate SOCE (Vig et al. 2006a). Using rat basophilic leukemia (RBL) mast cells as a model system, previous work in our laboratory has established that the Ca^{2+} gating required for SOCE

involves electrostatic interaction between a basic sequence in the cytoplasmic portion of STIM1 and an acidic sequence in the C-terminus of Orai1 (Calloway et al. 2009, Calloway et al. 2010). We further determined that, following ER store depletion, STIM1-Orai1 association at the PM is positively regulated by the amount of phosophatidylinositol-4,5-bisophosphate (PIP_2) in ordered lipid domain regions of the PM (Calloway et al. 2011).

While numerous research efforts have focused on understanding the intermolecular and intramolecular interactions of STIM1 and Orai1 to elicit SOCE, much remains to be learned about the mechanisms by which STIM1 activates CRAC channels. In fact, the oligomeric state of STIM1 in living cells at rest continues to be a matter of uncertainty. Originally, some argued that STIM1 exists as a monomer in cells at rest, forming higher order states only after ER store depletion produces conformational changes in the protein required for oligomerization (Stathopulos et al. 2006; Liou et al. 2007). This hypothesis was based on experiments by Stathopulos et al. (2006) wherein the luminal region of STIM1 was shown to exist in a monomeric state in its Ca^{2+} bound form, such as when cells are at rest. Others argued that STIM1 maintained an oligomeric form in resting cells, citing co-immunoprecipitation experiments by Williams et al. (2002), which showed isolation of STIM1-STIM1 and STIM1-STIM2 complexes from resting cells via Western blotting of the reduced immunoprecipitates. Their work also showed that the luminal region of STIM1 is not required for homo-typic STIM1 interactions and further pointed to the cytosolic domain as the source of pre-existing oligomeric STIM1 interactions. This self-association of STIM1 in ER Ca^{2+}-replete cells was later confirmed by numerous laboratories (Baba et al. 2006, Penna et al. 2008, Covington et al. 2010). Collectively these data provide evidence for higher oligomeric forms of STIM1 in resting cells. However, previous use of SDS/PAGE of immuno-isolated STIM1 in addition to chimeric and/or

truncated STIM1 proteins prohibited exploration of both the stoichiometry and native interactions involved in the formation of these complexes in living cells at rest.

More recent work has focused on visualizing STIM1 oligomerization via live-cell microscopy. In 2007, Liou et al. showed that depletion of Ca^{2+} in ER stores leads to oligomerization of STIM1 proteins detected via Förster resonance energy transfer (FRET). Their work established that large scale oligomerization of STIM1 is a separate process that occurs prior to the translocation of STIM1 to the PM. However, their method did not explore whether basal oligomeric forms of STIM1 exist prior to stimulation. This question remained unanswered until 2012 when He et al., using bimolecular fluorescence complementation (BiFC), determined that STIM1 exists as an oligomer in living cells at rest. In BiFC, a fluorescent protein is split into two non-fluorescent pairs, which are conjugated separately to a pair of potentially interacting proteins. If the proteins interact with one another, then the non-fluorescent protein halves are brought within close proximity of one another and form the fully fluorescent constituent (Kerppola 2008). By over-expressing STIM1 tagged with separate non-fluorescent protein halves onto their N-termini, He et al. (2012) detected the fluorescence of the fully formed fluorophore in resting cells, providing evidence for oligomeric STIM1 when cells are at rest. Furthermore, the BiFC fluorescence obtained for resting cells revealed the presence of STIM1 oligomers throughout the ER, suggesting that aggregation into even higher order forms of STIM1 is required for puncta formation and SOCE.

With this evidence for oligomeric full-length STIM1 in living cells, we proceeded to investigate the stoichiometry of the oligomers that are present. BiFC results suggest that STIM1 is present in forms as small as dimers in resting cells (He et al. 2012), but the results cannot yield the exact stoichiometry of the STIM1 oligomers formed. In 2008, it was proposed that a dimer

of STIM1 could recruit two Orai1 dimers, leading to the formation of the Orai1 tetrameric channel pore (Penna et al. 2008). Further studies suggest that at least eight STIM1 proteins are required to bind with an Orai1 tetramer to form a fully active CRAC channel, but conflicting data still exist as to the oligomeric state of STIM1 that binds to Orai1 (Li et al. 2011, Hoover & Lewis 2011). Thus, determining the stoichiometry of STIM1 oligomers, both for cells at rest and under store-depleted conditions, will advance our understanding of the mechanisms that regulate SOCE.

In the current study, we provide further biochemical evidence for the existence of full-length STIM1 oligomers present in resting cells, including both a homo-dimeric 260 kDa species and a previously unidentified 110 kDa hetero-dimer. Using immunoprecipitation (IP) and Western blotting analysis of chemically crosslinked cells, we show that these oligomeric species are present prior to cell lysis and can be stabilized with a sulfhydryl-reactive crosslinker. We further show that non-covalent bond interactions are sufficient for forming STIM1 oligomers in native, intact cells and that disulfide bonds form during cell lysis to retain the minimal oligomeric forms observed. Lastly, we determine that the retained 110 kDa species is formed via a disulfide bond between Cys-437 of STIM1 and a 20-25 kDa peptide.

Materials & Methods:

Materials:

Anti-STIM1 (S6197, C-terminal) antibody (rabbit, polyclonal, ~ 1 mg/mL), anti-green fluorescent protein (GFP) antibody (mouse, monoclonal, 1 mg/mL), and N-ethylmaleimide (NEM) were all purchased from Sigma Aldrich (St. Louis, MO). Anti-STIM1 antibody (mouse,

monoclonal, 250 μg/mL) and anti-end binding1 (EB1) antibody (mouse, monoclonal, 250 μg/mL) were from BD Biosciences (San Jose, CA). Both anti-Myc antibody (mouse, monoclonal, 1 mg/mL) and anti-Rac1 antibody (mouse, monoclonal, 1 mg/mL) were from Upstate Biotechnology (Lake Placid, NY). The secondary antibodies of biotin-(SP) conjugated $F(ab')_2$ fragment goat anti-mouse IgG (H + L) and goat anti-rabbit IgG (H + L) were purchased from Jackson Immunoresearch Labs (West Grove, PA), while amplification and detection were provided by NeutrAvidin conjugated with Horseradish Peroxidase (HRP) (1 mg/mL) from Thermo Fisher Scientific (Rockford, IL). Anti-Orai2 (TMEM142B) antibody (rabbit, polyclonal, 0.8 mg/mL) was purchased from Alomone Labs (Jerusalem, Israel) while an alternative anti-Orai2 antibody (rabbit, polyclonal) came from Abcam (Cambridge, MA). Anti-SERCA2 (MA3-919) antibody (mouse, monoclonal, 1 mg/mL) was from Affinity Bioreagents (Golden, CO). Anti-Cdc42 antibody (mouse, monoclonal, 250 μg/mL) was purchased from EMD Millipore (Billerica, MA).

Cell culture:

Rat basophilic leukemia (RBL)-2H3 cells (Barsumian et al. 1981) were maintained in a monolayer culture in Minimum Essential Medium (MEM) from Invitrogen (Carlsbad, CA) supplemented with 20 % (v/v) fetal bovine serum (FBS), purchased from Atlanta Biologicals (Lawrenceville, GA). Similarly, Cos7 cells were maintained in a monolayer culture in Dulbecco's Modified Eagle Medium (DMEM, Invitrogen, Carlsbad, CA), supplemented with 10% (v/v) FBS as described by Felgner et al. (1987). Growth medium for both cell types was further supplemented with 10 μg/mL gentamicin sulfate (Invitrogen, Carlsbad, CA) to prevent

bacterial growth. Cells were harvested with trypsin-ethylenediaminetetraacetic acid (trypsin-EDTA, Invitrogen, Carlsbad, CA) three to five days after passage (Pierini et al. 1996).

For experiments involving transfection of DNA constructs into RBL cells, plasmids containing wildtype (wt)-STIM1 and/or C437A-STIM1 were incorporated by electroporation using 32 μg of plasmid for ~5 x 10^6 cells (Exponential Decay pulse, 280 V, 950 μF). RBL cells were harvested 24-48 hours post-transfection. Similarly, some Cos7 cells were transfected with wt-STIM1 or C437A-STIM1 constructs via electroporation (Exponential Decay pulse, 220 V, 950 μF) using 32 μg of plasmid for ~ 1.5 x 10^6 cells. For other experiments involving co-transfection of DNA into Cos7 cells, plasmids containing wt-STIM1, C437A-STIM1, or CFP-STIM1 were chemically transfected with the indicated constructs (~ 5 μg plasmid for ~ 7 x 10^6 cells) and Lipofectamine 2000 (Invitrogen, Carlsbad, CA) as previously described (Varnai et al. 2007). Cos7 cells were harvested 18-24 hours post-transfection.

DNA constructs:

Wildtype (wt)-STIM1 cDNA with a C-terminal myc tag (STIM1-Myc), encoded in a pcDNA4-myc-his vector, was a gift from Dr. Jean-Pierre Kinet at Harvard University Medical School (Vig et al. 2006a). C437A-STIM1 was generated by the Cys to Ala mutation at residue 437 using the sense primer 5'-GCA ACA GAT CGA GAT CCT CGC TGG CTT CCA GAT TGT CAA CAA CC-3' and the antisense primer 5'-GGT TGT TGA CAA TCT GGA AGC CAG CGA GGA TCT CGA TCT GTT GC -3' (Integrated DNA Technologies, Coralville, IA) in collaboration with Dr. Alice Wagenknecht-Wiesner (Cornell University). CFP-STIM1 cDNA was a gift from Dr. Marek Korzeniowski (Cornell University).

Immunoprecipitations (IPs):

RBL cells were harvested, rinsed, and resuspended at 9-10 x 10^6 cells/mL in Buffered Saline Solution (BSS; 135 mM NaCl, 5 mM KCl, 1.8 mM $CaCl_2$, 1 mM $MgCl_2$, 5.6 mM glucose, 20 mM HEPES, pH 7.4) supplemented with 1 mg/mL bovine serum albumen (BSA). Approximately 900 μL aliquots were chilled for 5-10 min on ice. Cells were lysed by addition of an equal volume addition of cold 2x Lysis Buffer (20 mM Tris, 100 mM NaCl, 2 mM sodium orthovanadate, 60 mM sodium pyrophosphate-$10H_2O$, 20 mM sodium β-glycerophosphate, 0.04 units/mL aprotinin, and 0.02 % sodium azide) with 1 % (v/v) Triton X-100 (TX-100), 4 mM 4-(2-Aminoethyl) benzenesulfonyl fluoride hydrochloride (AEBSF), and a 1/2000 dilution of protease inhibitor cocktail (Sigma Aldrich, St. Louis, MO) for 10 min on ice while rocking continuously. Nuclear debris was removed by centrifugation in a microcentrifuge at 10,000 rpm for 10 min at 4 ^oC. The resulting supernatants were carefully removed and added to 30 μL of Protein A beads (Thermo Fisher Scientific, Rockford, IL) and 5 μg of appropriate primary antibody: anti-STIM1 (C-terminal) or an irrelevant control antibody produced in rabbit. To prevent beads from settling, samples were incubated on a rotator for 2-2.5 hours at 4 ^oC. Following IP, beads were separated from the supernatant via centrifugation at 2000 rpm for 1 min at room temperature (RT). Supernatants were removed and saved at -80 ^oC. To ensure removal of all excess supernatant material, beads were rinsed twice with 2x Lysis Buffer by resuspending and respinning the samples. IP products were detached from the Protein A beads and prepared as Western blotting samples by adding 80 μL of 1x SDS Sample Buffer (10 % (w/v) glycerol, 1 % (w/v) sodium dodecyl sulfate (SDS), 0.02 % (w/v) bromophenol blue in 50 mM Tris, pH 6.8) and boiling for 5 min. Samples were centrifuged at 2000 rpm for 1 min to

pellet the beads. Resulting supernatant solutions containing the IP products were stored at -20 ^{o}C for subsequent immunoblotting.

In some instances, the IP assay included variations. For example, some cells were pre-stimulated with thapsigargin (TG) prior to cell lysis. In these instances, cells were harvested and resuspended at 5-10 x 10^6 cells/mL in BSS, sometimes containing 1 mg/mL BSA. Stimulation was initiated by addition of 0.5 μg/mL TG (Sigma Aldrich, St. Louis, MO), and the cells were rotated for 5-7 min at 37 ^{o}C. Following stimulation, cells were rinsed with BSS, lysed, and immunoprecipitated as described above.

In some experiments, cells were treated with N-ethylmaleimide (NEM), either before or during cell lysis. When cells were pre-treated with NEM, they were harvested and resuspended at ~ 1 x 10^7 cells/mL in BSS, without BSA. 1 mM NEM was added to the appropriate samples and rotated for 20 min at 37 ^{o}C. The cells were then rinsed with BSS and immunoprecipitated as described above. On occasion, NEM was also added during cell lysis. In these cases, 2 mM NEM was pre-mixed with the detergent-containing 2x Lysis Buffer solution to allow for simultaneous cell lysis and alkylation by NEM.

In other experiments, the homo-bifunctional chemical crosslinker bismaleimideohexane (BMH, Thermo Fisher Scientific, Rockford, IL) was added to cells prior to lysis to cause covalent crosslinking between free sulfhydryl groups. Here, cells were harvested and resuspended at ~ 5 x 10^6 cells/mL in BSS, which did not contain BSA so as to avoid its modification by BMH. BMH, in a stock solution of 50 mM in dimethyl sulfoxide (DMSO), was added to cells at a final concentration of 100 μM – 1 mM, and samples were incubated on a plate shaker for 20 min at RT. To quench excess BMH, 5 mM glutathione (GSH, Sigma Aldrich, St.

Louis, MO) in BSS was added, and samples were incubated for an additional 20 min at RT as above. Cells were rinsed twice with BSS, lysed, and immunoprecipitated as described above. Control experiments were also performed wherein BMH was pre-quenched before being added to the cells. In these instances, 500 μM BMH in DMSO and 10 mM GSH in BSS were combined into a single solution and incubated for 5 min at RT. The pre-quenched solution was then added to an equal volume of cell solution, achieving final concentrations of 250 μM BMH and 5 mM GSH, and incubated for 20 min at RT atop a plate shaker. The cells were rinsed twice with BSS and immunoprecipitated as described above.

RBL cells transfected with wt-STIM1 or C437A-STIM1 were harvested 18-24 hours following transfection via electroporation. These cells were less confluent than their untransfected counterparts at the time of harvest and thus afforded starting cells concentrations of ~7 x 10^6 cells/mL. Aside from lower starting cell concentration, the transfected RBL cells were immunoprecipitated identically to untransfected RBL cells as described above. Cos7 cell immunoprecipitates were prepared identically to the RBL cell immunoprecipitates, although starting cell concentrations were only 2-3 x 10^6 cells/mL due to the larger size of Cos7 cells as compared to RBL cells. Single transfection experiments with Cos7 cells using wt-STIM1 or C437A-STIM1 were performed by electroporation, whereas co-transfection experiments with STIM1-Myc and CFP-STIM1 were performed via chemical transfection with Lipofectamine.

Immunoblotting:

Western blotting samples were prepared as described above for the IP assay. In some instances, samples were also prepared under reducing conditions by adding 1 % (v/v) β-

mercaptoethanol (βME) and boiling for 5 min. Approximately 15-20 μL of Western blotting samples were loaded into each gel lane. Samples were SDS/PAGE separated on 10 % or 4-12 % gradient Novex Tris-Glycine mini gels using an Xcell Surelock Mini-Gel Electrophoresis System from Invitrogen (Carlsbad, CA). Samples were transferred onto polyvinylidene fluoride (PVDF) membrane (EMD Millipore, Billerica, MA) using semi-dry conditions and a TE22 Tank Transfer Unit (GE Healthcare, Piscataway, NJ). Membranes were immediately blocked with Tris-buffered saline Tween (TBST: 50 mM Tris, pH 7.6, 150 mM NaCl, and 0.1 % (v/v) Tween 20) supplemented with 10 mg/mL BSA and 1 % (v/v) fish gelatin (Sigma Aldrich, St. Louis, MO). Primary antibodies were used at the following dilutions: anti-STIM1 (mouse, monoclonal) 1:250, anti-Myc 1:1000, anti-GFP 1:500, anti-SERCA2 1:1000, anti-EB1 1:2000, anti-Orai2 (Abcam) 1:2000 or (Alomone) 1:1000, anti-Rac1 1:1000 and anti-Cdc42 1:250 dilution. Secondary antibodies were goat-anti-mouse and goat-anti-rabbit, each conjugated to biotin and used at 1:4000 dilution. NeutrAvidin-HRP was used at 1:1400 dilution. All of these solutions were prepared in TBST supplemented with BSA and fish gelatin. Blots were developed using SuperSignal West Pico Chemiluminescent Substrate (Thermo Fisher Scientific, Rockford, IL).

Samples for mass spectrometry analysis:

Non-reduced IP products were prepared using double to triple the original cell concentrations to improve visibility of protein bands for gel excision. RBL cells were harvested and resuspended in 20-30 x 10^6 cells/mL in BSS supplemented with 1 mg/mL BSA. To ensure lysis of the larger cell population, 2x Lysis Buffer was prepared with double the original concentrations of detergent and additives: 2 % (v/v) TX-100, 8 mM AEBSF, and a 1:1000

dilution of protease inhibitor cocktail. IP was performed as described above, and products were stored at -20 ^{o}C. Thawed samples were loaded into SDS/PAGE gels, electrophoresed, and stained with Sypro Ruby for detection of protein bands as described below. Visualized protein bands of interest were excised from the gels and stored at -20 ^{o}C or -80 ^{o}C until being submitted for mass spectrometric analysis at the Proteomics and Mass Spectrometry Core Facility at Cornell University or the Taplin Mass Spectrometry Facility at Harvard University.

Sypro Ruby staining:

Non-reduced IP products were prepared for Western blotting as described above. Approximately 25 μL of Western blotting samples were loaded into each gel lane. Samples were electrophoresed on 10 % SDS/PAGE gels. Following electrophoresis, the gels were immediately placed into an aqueous fixing solution of 10 % MeOH: 7 % Acetic Acid for 30 min at RT. After rinsing thoroughly with dH_2O, gels were placed into a 1:1 solution of Sypro Ruby Stain (Sigma Aldrich, St. Louis, MO) and dH_2O for 4 hours at RT or overnight at 4 ^{o}C. The excess staining solution was removed and the gels were rinsed with fixing solution again to decrease the overall background fluorescence, followed by several rinses with dH_2O. Gels were viewed under UV light for detection of luminescence from the Sypro Ruby stain. Bands of interest were excised from the gels and stored at -20 ^{o}C or -80 ^{o}C.

Blue NativePAGE assay:

RBL cells were harvested, rinsed, and resuspended at 2 x 10^7 cells/mL in BSS supplemented with 1 mg/mL BSA. 0.5 mL aliquots of cell solution were placed into separate microtubes and placed on ice for 5 min. An equal volume of cold 2x Lysis Buffer, supplemented with 4 mM AEBSF, 1 % (v/v) dodecylmaltoside (DDM), and a 1:2000 dilution of protease cocktail inhibitor, was added to each sample tube. The cells were placed on ice for 10 min atop a plate shaker to lyse. To remove nuclear debris, the cells were spun in a microcentrifuge at 11,000 rpm for 10 min at 4 ^{o}C. Supernatants were carefully removed and added to new tubes, containing 30 μL of Protein A beads and 5 μg of anti-STIM1 (C-terminal) antibody, and rotated for 2-3 hours at 4 ^{o}C. The tubes were centrifuged at 2000 rpm for 1 min to separate the supernatant from the protein-bound beads. The supernatants were removed and stored at -80 ^{o}C. Beads were rinsed twice with 2x Lysis Buffer to ensure that all unbound proteins had been removed. To elute the proteins from the beads, 100 μL of Alkaline Buffer (100 mM Glycine-NaOH, 0.1 % (v/v) DDM, pH 11.5) was added to each sample and incubated for 30 min on ice, with mixing every 10 min. Tubes were centrifuged at 2000 rpm for 1 min to separate the eluted IP products from the beads. To return samples to a more neutral pH for Western blotting analysis, samples were dialyzed (Spectrophore 12 kDa cut-off dialysis tubing, Spectrum Laboratories Inc., Rancho Dominguez, CA) with 1x NativePAGE Sample Buffer (50 mM Bis-Tris, 6 N HCl, 50 mM NaCl, 10 % (w/v) glycerol, 0.001 % (v/v) Ponceau S, pH 7.2) overnight at 4 ^{o}C on a rotator. Following dialysis with sample buffer, the samples were removed and stored at -80 ^{o}C.

Immediately prior to immunoblotting, native samples were thawed and 0.25 % (v/v) Coomassie Blue G250 was added to impart negative charges to the proteins within each sample

without denaturing them and to thus provide them with similar isoelectric points, pH ~ 7.5 (Wittig et al. 2006). In some experiments, addition of Coomassie Blue G250 was preceded by reduction with 1 % (v/v) βME for 10-30 min at RT. Approximately 20 μL of prepared native samples were loaded into each gel lane. Samples were electrophoresed on 4-16 % Novex NativePAGE Bis-Tris gels (Invitrogen, Carlsbad, CA) at 4 ^{o}C to avoid overheating the gels (Schägger 2001). Dark Blue Cathode Buffer (Invitrogen, Carlsbad, CA) was used at the start of electrophoresis and exchanged with Light Blue Cathode Buffer (Invitrogen, Carlsbad, CA) when the dye front reached approximately half-way through the gel, per manufacturer's instructions. Samples were transferred onto PVDF membrane (EMD Millipore, Billerica, MA) using 1x NuPAGE Transfer Buffer (25 mM Bicine, 25 mM Bis-Tris, 1 mM EDTA, pH 7.2). Following transfer, the proteins were fixed to the membranes by washing with an aqueous solution of 8% acetic acid for 10-15 min at RT. The membranes were then rinsed thoroughly with dH_2O and blocked with TBST supplemented with 10 mg/mL BSA and 1 % (v/v) fish gelatin. Antibody and other labeling solutions were used at identical dilutions and developed with pico chemiluminescent substrate as described above.

Results:

STIM1 forms disulfide-bonded oligomeric IP products from cell lysates

To investigate intracellular STIM1 interactions, a series of immunoprecipitation (IP) assays were performed involving the pulldown of STIM1 from RBL-2H3 cell lysates. The products of IP, prepared under reduced or non-reduced conditions, were then separated by electrophoresis and Western blotted to detect for the presence of STIM1. As shown in Figure

2.1A, four distinct bands are present in the STIM1 IP product lane that are not present in the control IP product lane, where an irrelevant antibody was used for pull-down. Protein standards indicate that the lowest of these three bands has a molecular weight of ~ 85 kilodaltons (kDa), consistent with the molecular weight of monomeric STIM1. The second lowest band is ~ 110 kDa, suggesting that it could be a hetero-dimer product formed between STIM1 and a 20-25 kDa protein. While the exact weight of the highest band cannot be calculated with confidence because it exceeds the highest molecular weight standard, an estimate of ~ 260 kDa is assigned for identification purposes. The presence of this high molecular weight band reveals the existence of a higher order STIM1 product, possibly a homo-oligomer or STIM1-containing complex, in unstimulated cells. The relative abundance of the discrete bands at 85 kDa, 110 kDa, and 260 kDa further suggests that these bands contain a substantial percentage of immunoprecipitated STIM1 protein. A fourth, fainter band appears below the 260 kDa major band, near ~220 kDa. This band is more variable in its appearance, suggesting some heterogeneity in this species, perhaps due to proteolytic cleavage. When the same IP products are reduced with β-mercaptoethanol (βME) before electrophoresis and Western blotting, the higher molecular weight bands all disappear, as shown in Figure 2.1B. These results indicate that the high MW STIM1 IP products form as a result of disulfide bonds, from either homo- or hetero-oligomers.

Disulfide bonds in STIM1 complexes form during cell lysis

To determine whether the disulfide-bonded products exist in living cells or form as a result of detergent-mediated cell lysis, IP products were prepared after the addition of N-

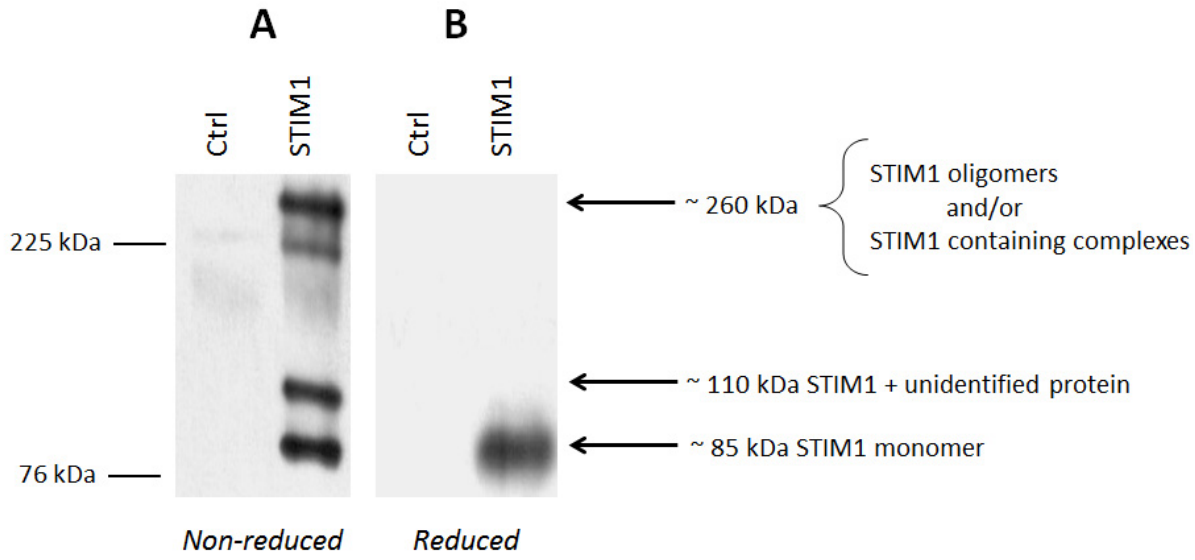

Figure 2.1: STIM1 exists in multiple disulfide-bonded states in resting cells. RBL-2H3 cells were lysed with detergent and immunoprecipitated with anti-STIM1 or an irrelevant control antibody. Samples were prepared under **(A)** non-reduced conditions or **(B)** reduced with 1% (v/v) βME prior to SDS/PAGE and Western blotting. Blots are representative of more than 20 individual experiments.

ethylmaleimide (NEM), a sulfhydryl reactive reagent. When free sulfhydryl groups are present, such as the –SH group of cysteine residues, NEM alkylates and blocks the thiol group from further chemical reaction, including the formation of a disulfide bond (Figure 2.2A). In this experiment, whole cells were treated with 1 mM NEM either before or during TX-100 detergent based cell lysis. The cell lysates were then immunoprecipitated and analyzed via Western blotting, as shown in Figure 2.2B-C. Under non-reducing conditions (Figure 2.2B), addition of NEM before or during cell lysis inhibits a significant amount of the high molecular weight (110 kDa and 260 kDa) STIM1 IP products from forming as compared to the STIM1 IP lane devoid of NEM, and the 85 kDa monomeric band becomes the most prominent band present in the lane. While inhibition is more extensive when NEM is added during cell lysis, the inhibition of high molecular weight STIM1 IP products in both cases indicates that NEM alkylation of free sulfhydryl groups interferes with covalent bonding of larger STIM1 species. To verify that NEM alkylation inhibited disulfide bond formation, the STIM1 IP samples were reduced with βME prior to electrophoresis and Western Blotting. As shown in Figure 2.2C, all three lanes confirm complete reduction of the high molecular weight STIM1 species to the 85 kDa monomeric component. Thus, treatment with βME does not significantly alter the banding patterns seen in either NEM-containing lane as compared to the dramatic reduction of bands in the control lane, further indicating that the disulfide bonds in STIM1 complexes do not exist prior to cell lysis. Rather, the high molecular weight STIM1 IP products form during cell lysis, likely due to pre-existing non-covalent complexes present within cells. The high reproducibility and high abundance of the three major bands suggests that STIM1 exists in multiple structures in intact cells at rest and that disulfide bond formation during cell lysis is necessary for retention of the higher molecular species under denaturing conditions.

Figure 2.2: N-ethylmaleimide (NEM) alkylates free sulfhydryls and prevents formation of disulfide-bonded STIM1 complexes. (A) Alkylation reaction of NEM with the free sulfhydryl group of a cysteine residue. STIM1 IP products were prepared from RBL-2H3 cell lysates treated in the absence (control) or presence of 1 mM NEM under **(B)** non-reduced and **(C)** reduced conditions. NEM addition was performed either concurrently with the addition of detergent lysis buffer (+ NEM During) or prior to cell lysis but after rinsing with BSS buffer (+ NEM Before). Blots are representative of 5-7 individual experiments.

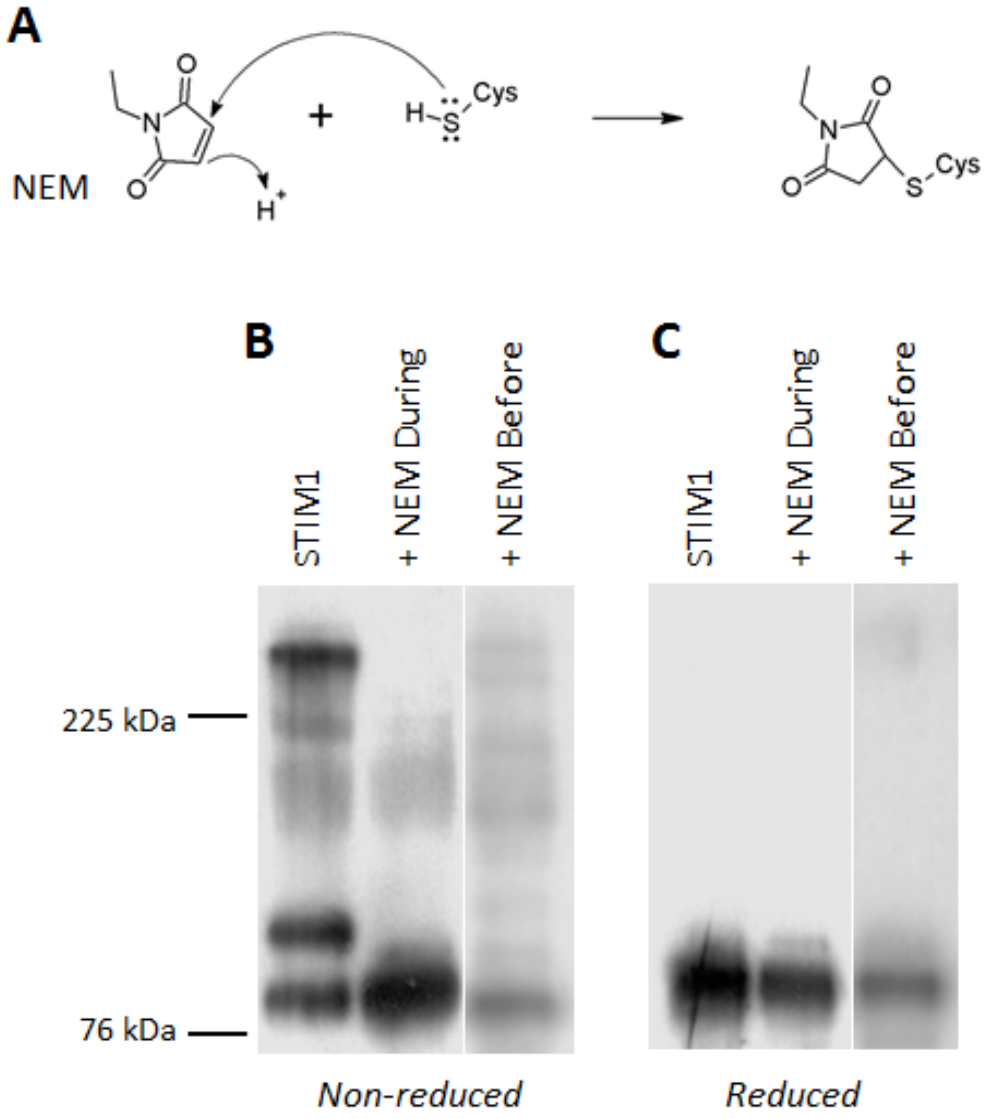
A
NEM
Cys
Cys
B
STIM1
+ NEM During
+ NEM Before
225 kDa
76 kDa
Non-reduced
C
STIM1
+ NEM During
+ NEM Before
Reduced

Thapsigargin stimulation does not alter disulfide-bonded STIM1 complexes

To assess whether activation of SOCE alters STIM IP products, cells were stimulated with the sarco/endoplasmic reticulum Ca^{2+} ATPase (SERCA) pump inhibitor, thapsigargin (TG). In mast cells, TG bypasses the early signaling steps stimulated by antigen crosslinking of IgE bound to receptors on the cell surface. TG causes Ca^{2+} release from endoplasmic reticulum (ER) stores in an IP_3-independent manner (Thastrup et al. 1990), to initiate the aggregation and translocation of STIM1 proteins to the PM (Liou et al. 2005, Luik et al. 2008). There, further association with and activation of Orai1 completes SOCE by facilitating influx of Ca^{2+} from the extracellular environment. As shown by Western blot analysis in Figure 2.3, treatment of cells with TG does not alter the presence or appearance of STIM1 IP products as compared to resting cells. Under non-reducing conditions (Figure 2.3A), both the STIM1 IP lane and STIM1+TG IP lane show identical band patterns and similar abundances for each band present at 85 kDa, 110 kDa, and 260 kDa respectively. Control IP lanes indicate the presence of non-specific binding interactions that occur during the IP process. Addition of βME to the samples prior to electrophoresis eliminates all non-specific interactions and all high molecular weight STIM1 species, leaving only the 85 kDa monomer of STIM1 (Figure 2.3B). Thus, TG does not cause further disulfide-bonded oligomerization relative to that in unstimulated cells. Furthermore, retention of the same IP products, in the absence or presence of TG, suggests that these STIM1 species may serve as the basic building blocks of higher order STIM1 oligomers required for SOCE.

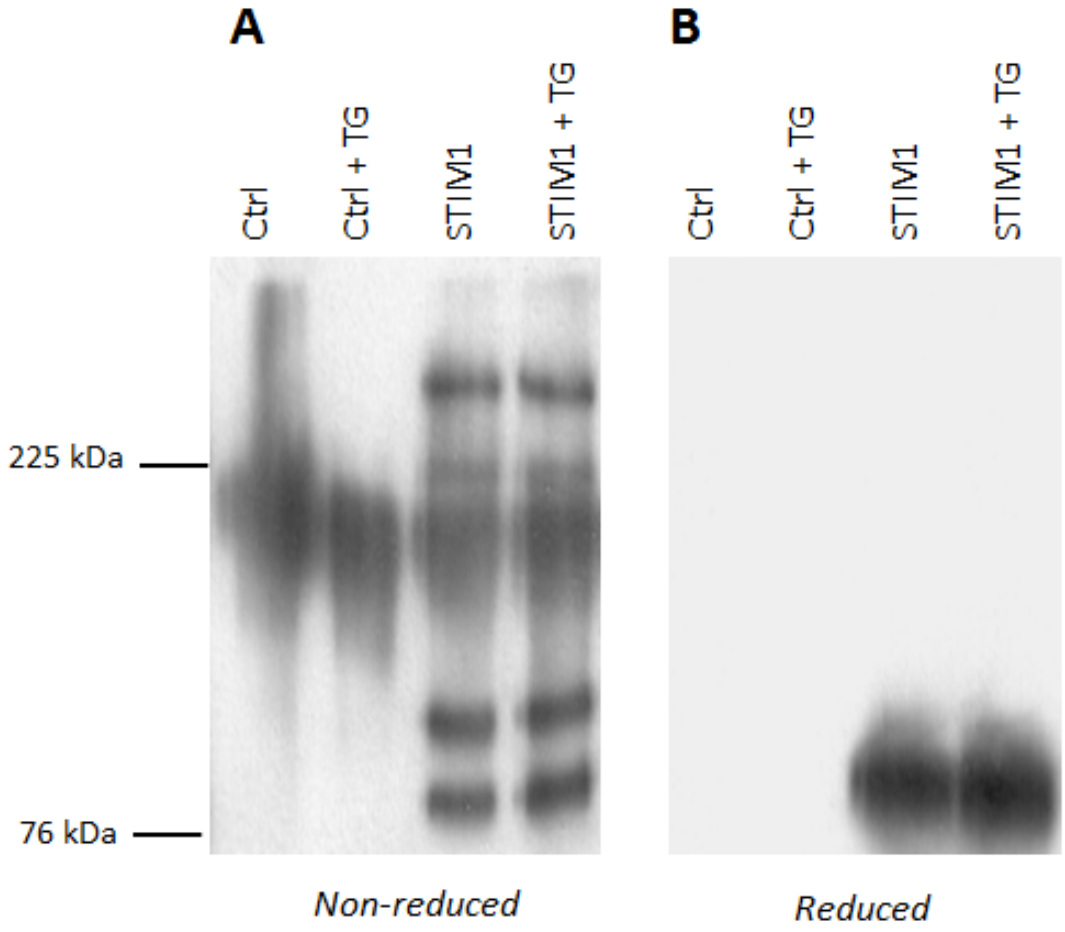

Figure 2.3: Thapsigargin (TG) stimulation does not alter STIM1 disulfide-bonded complexes. Unstimulated and TG (~ 0.5 μg/mL) stimulated RBL-2H3 cells were lysed and immunoprecipitated with anti-STIM1 or an irrelevant control antibody. Samples were prepared under **(A)** non-reduced and **(B)** reduced conditions. Blots are representative of 3 individual experiments.

BMH crosslinker stabilizes formation of high molecular weight STIM1 species in intact cells

Figure 2.2 showed that disulfide bonds formed during detergent-mediated cell lysis are necessary for stabilization of the 110 kDa and 260 kDa STIM1 IP species observed. To determine whether these protein complexes exist in their larger forms due to non-covalent associations within intact cells, a chemical crosslinker was added to cells prior to lysis and IP. Bismaleimidohexane (BMH), a sulfhydryl reactive homo-bifunctional crosslinker, irreversibly reacts with sulfhydryl groups via maleimide groups on either side of the linker. In addition to withstanding reduction via βME, excess BMH can be quenched in solution via the addition of glutathione (GSH) prior to cell lysis. To determine an optimal concentration of BMH to use in these experiments, cells were treated with doses varying over 0.1-1.0 mM BMH for 20 min at RT. After quenching and washing, cells were lysed and immunoprecipitated with anti-STIM1 (C-terminal) antibody, and samples were reduced with βME prior to Western blot analysis. As shown in Figure 2.4, the addition of BMH crosslinker ($\geq$ 100 μM) resulted in retention of high molecular weight STIM1 species compared to the control lane without BMH. A 260 kDa STIM1 species is evident in all BMH-containing lanes, and the 100 μM and 250 μM BMH lanes also show the retention of the 110 kDa STIM1 species, though faintly. At higher concentrations, the 110 kDa STIM1 band is difficult to detect, possibly due to monovalent binding of the crosslinker at high concentrations, indicating that the lower doses of BMH are better suited for use in this IP assay. Repetition of the experiment reveals that 250 μM provides more reproducible results (data not shown) and thus was found to be the optimal concentration for use in all future crosslinking experiments with this method. Here, retention of the same three IP products found in the non-reduced samples of Figure 2.1 suggests that intact cells contain higher

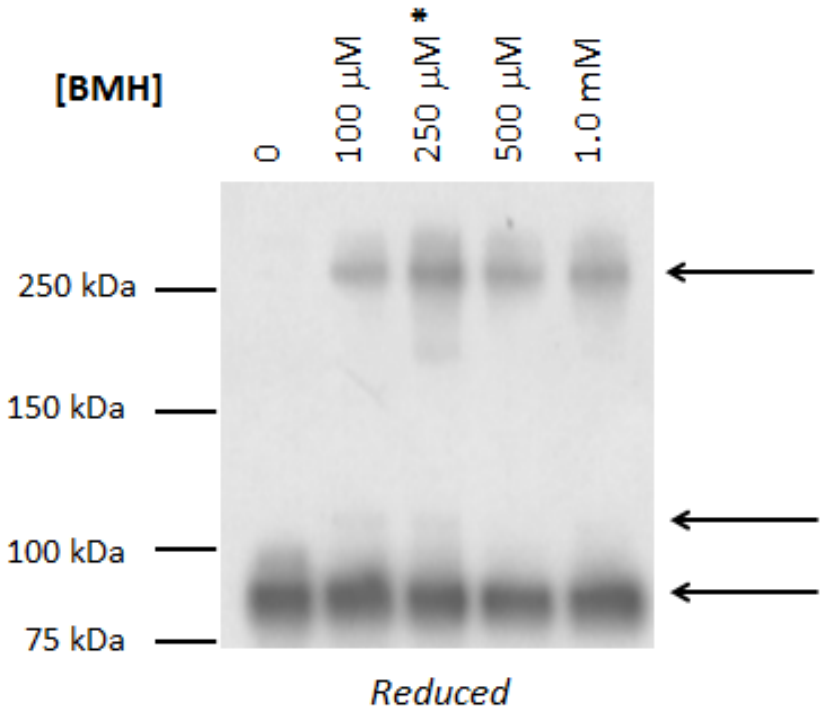

Figure 2.4: Sulfhydryl reactive BMH crosslinker stabilizes STIM1 IP complexes under reduced conditions. RBL-2H3 cells were incubated with 0 – 1.0 mM BMH crosslinker. Following treatment, excess BMH was quenched with 5 mM GSH. Cells were lysed, immunoprecipitated, and reduced prior to electrophoresis and Western blotting analysis. (*) denotes optimal BMH concentration used for all subsequent crosslinking experiments. Blots are representative of more than 10 individual experiments.

order forms of STIM1 in unstimulated cells, and that stabilization of these high molecular weight forms can be accomplished using a sulfhydryl reactive crosslinker.

To evaluate the specificity of retention of higher MW bands using BMH, IPs with crosslinker were also prepared in parallel with control samples. Cells were immunoprecipitated with anti-STIM1(C-terminal) or a control antibody, and Western blotted, as shown in Figure 2.5. Under non-reduced conditions, the control IP lane lacks any and all discrete bands present in the STIM1 IP lane. The smear visible at ~150 kDa is due to non-specific interactions between immunoglobulin proteins in the cell lysate and the antibodies added during the IP process. Under reducing conditions, the non-specific interactions disappear from both lanes while several distinct bands remain in the STIM1 IP lane. Thus, the specificity of BMH-STIM1interaction is confirmed by the retention of the three STIM1-containing bands at 85 kDa, 110 kDa, and 260 kDa respectively and at similar abundances to those in Figure 2.4. Together, these results suggest that the crosslinking of STIM1 by BMH yields high MW products via reaction of key cysteine residues on STIM1 proteins in intact cells.

With a method to stabilize non-covalent interactions of STIM1 in intact cells, it was then possible to re-examine whether stimulation by TG induces new forms of STIM1 species. RBL-2H3 cells were stimulated with TG and treated with BMH prior to quenching. Lysed cells were immunoprecipitated with anti-STIM1(C-terminal) antibody and reduced with βME before undergoing Western blot analysis. Controls were also performed in parallel to compare results in the absence or presence of TG and BMH. As shown in Figure 2.6, in the absence of TG (Lanes 1 & 2), high molecular weight STIM1 IP product bands are only retained in the presence of BMH (Lane 2), which is consistent with results from Figures 2.3-2.5. Upon stimulation with TG (Lanes 3 & 4), no significant differences are detected compared to unstimulated counterparts

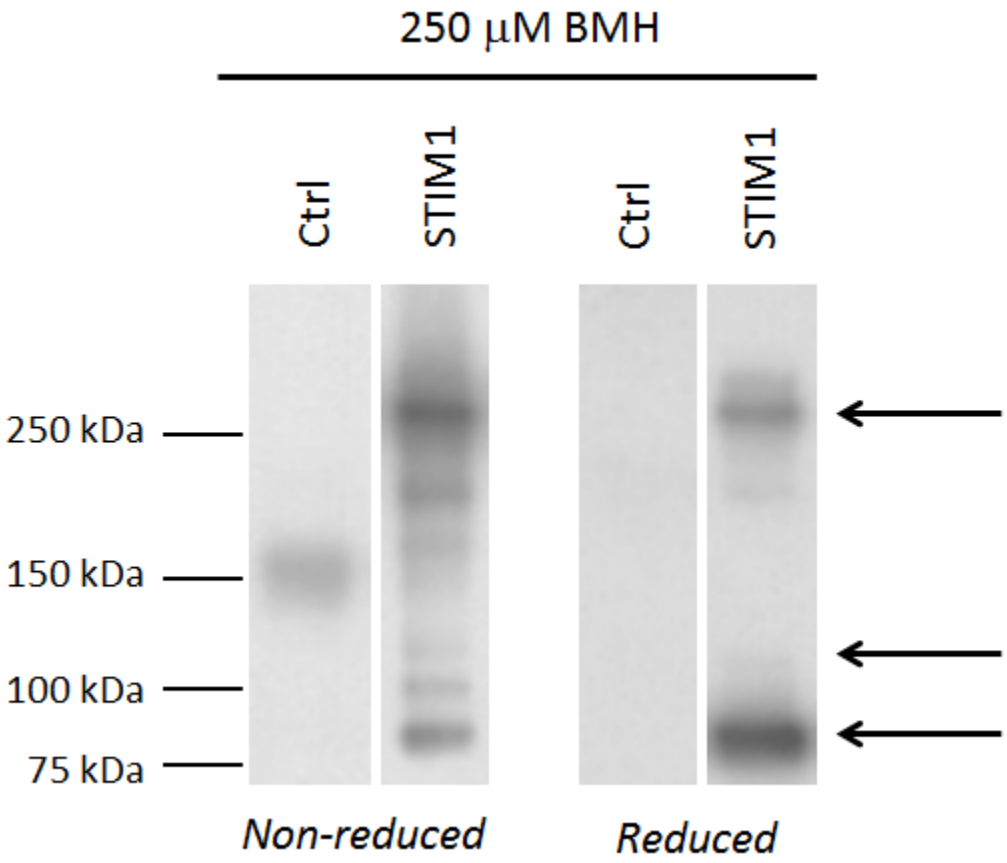

Figure 2.5: BMH crosslinkage is specific to the sites of disulfide bond formation in STIM1 IP complexes. RBL-2H3 cells pre-treated with 250 μM BMH and quenched with 5 mM GSH were lysed and immunoprecipitated using either anti-STIM1 or an irrelevant control antibody. Samples were prepared under **(A)** non-reduced and **(B)** reduced conditions. Blots are representative of 3-5 individual experiments.

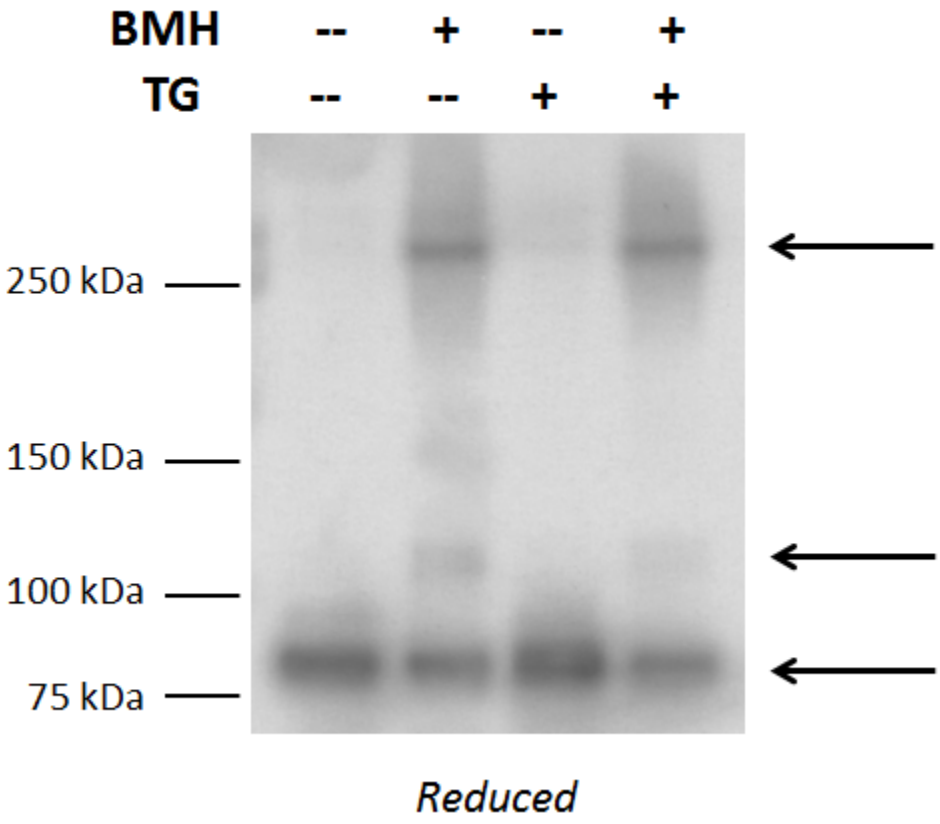

Figure 2.6: BMH crosslinker does not stabilize new and/or different STIM1 IP complexes following TG stimulation. RBL-2H3 cells were stimulated with 0.5 μg/mL TG and treated with 250 μM BMH prior to quenching with 5 mM GSH. Following treatment, cells were lysed, immunoprecipitated with anti-STIM1 antibody, and reduced before electrophoresis and Western blotting analysis. Blots are representative of 6 individual experiments.

(Lanes 1 & 2). In the absence of BMH but presence of TG (Lane 3), STIM1 runs as the 85 kDa monomeric species, consistent with the reduced condition results from Figure 2.3B. In the presence of both BMH and TG (Lane 4), the same three major STIM1 IP products are present and in similar abundance to those in the unstimulated lane (Lane 2). These results confirm the existence of high molecular weight STIM1 species in intact cells at rest (Lane 2), and they further implicate the presence of these same products in cells that have been stimulated with TG (Lane 4). The absence of any new bands in the lane containing both BMH treatment and TG stimulation (Lane 4) further suggests that no new BMH-dependent crosslinking has occurred. Retention of the same IP products, both in unstimulated and TG stimulated cells, supports the view that the identified STIM1 oligomers/complexes serve as the basic building blocks of higher order STIM1 oligomers required for SOCE.

In previous experiments, NEM alkylation of free sulfhydryl groups was shown to prevent formation of the disulfide bonds required to retain the high molecular weight STIM1 species at 110 kDa and 260 kDa respectively (Figure 2.2). However, stabilization of these products using BMH crosslinker resulted in retention of the larger STIM1 IP species (Figures 2.4-2.5), confirming proximity of cysteine residues within oligomeric STIM1 structures in intact cells. To verify the irreversibility of BMH crosslinking, IP products were prepared from RBL-2H3 cells by stimulating cells with TG and treating with BMH. Following quenching and washing, the cells were lysed in the absence or presence of NEM and immunoprecipitated with anti-STIM1 (C-terminal) antibody under reducing conditions. As shown in Figure 2.7, the addition of NEM to the lysis buffer, used to rupture cells pre-treated with BMH crosslinker, did not alter the STIM1 IP products observed (Lanes 3 & 4) as compared to cells that received regular lysis buffer (Lanes 1 & 2). Pre-stimulation with TG, in addition to treatment with BMH and lysis

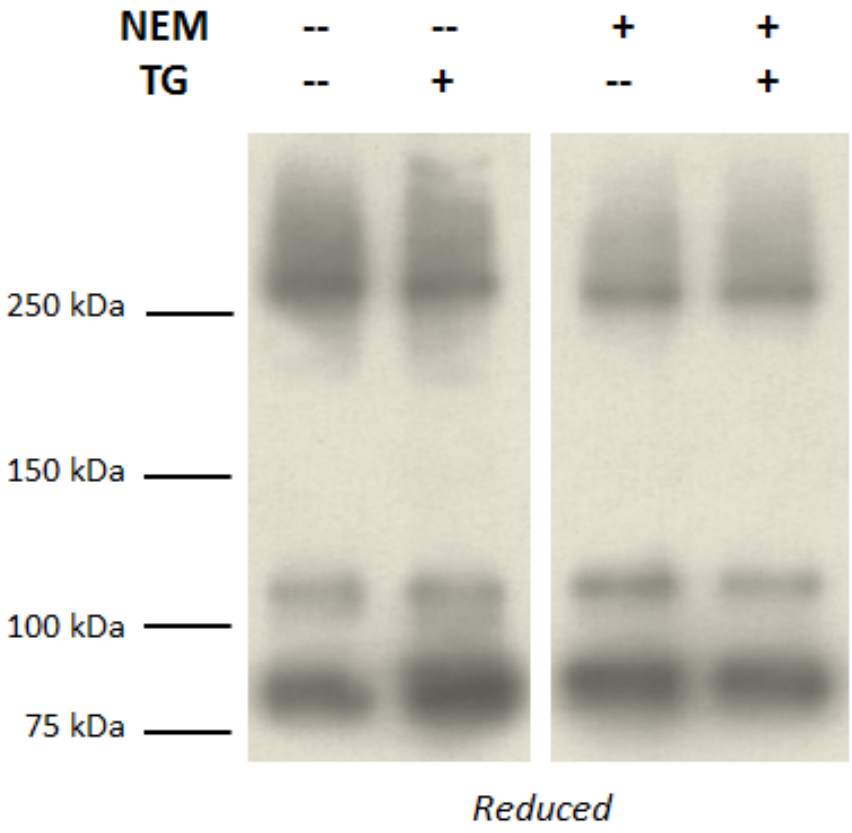

Figure 2.7: Addition of NEM during lysis does not alter BMH crosslinked STIM1 IP complexes. Unstimulated and TG (0.5 μg/mL) stimulated RBL-2H3 cells were treated with 250 μM BMH and quenched with 5 mM GSH. Samples were lysed with detergent in the absence or presence of 1 mM NEM prior to IP with anti-STIM1 antibody and reduction with βME. Western blots shown are representative of 3 individual experiments.

containing NEM, also causes no significant changes to the STIM1 IP products (Lane 4). Results indicate that the BMH crosslinking results in stable, irreversible bonds – able to withstand reduction by βME and the strong alkylating reagent NEM. Retention of identical STIM1 IP products under these varying conditions further confirms that retention of the high molecular weight complexes reflects structures that exist prior to cell lysis. A significant portion of STIM1 detectably exists in complexes, either with itself and/or other proteins, in cells at rest.

To further verify that BMH reacts with the sulfhydryl groups of STIM1, a separate control experiment was performed using BMH that had been pre-quenched with GSH prior to treatment with cells. Here, RBL-2H3 cells were treated with BMH and quenched with GSH prior to lysis and IP under reducing conditions. Addition of BMH and GSH was performed either in separate steps for control samples or added as a single pre-mixed solution for pre-quenched instances (Figure 2.8). Additional samples were prepared using cells that had been pre-stimulated with TG. As shown by the two left lanes of Figure 2.8, when BMH and GSH are added in separate, sequential steps to cells before IP, the high molecular weight forms of STIM1 at 110 kDa and 260 kDa withstand reducing conditions, duplicating the results of Figure 2.6. However, if BMH crosslinker has been pre-quenched with GSH prior to its addition to the cells, the high molecular weight STIM1 IP products are absent from the blot (Lanes 3 & 4). These results resemble those of the STIM1 IP products obtained in the absence of crosslinker but presence of sulfhydryl reactive βME and NEM (Figures 2.1 & 2.2), indicating that the formation of BMH-dependent STIM1 oligomers rely on specific interactions between sulfhydryl groups and the maleimides of BMH. Furthermore, the results confirm that 5 mM GSH is sufficient to quench excess BMH from the cell solution. Pre-stimulation of cells with TG caused no significant changes to the IP products formed, regardless of the BMH treatment condition used,

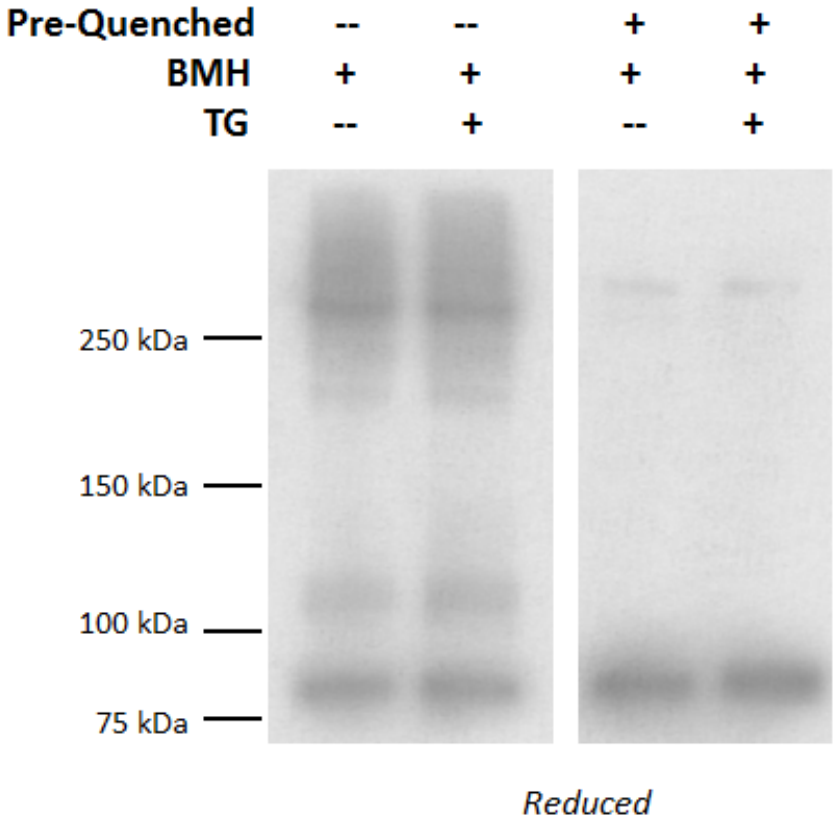

Figure 2.8: Addition of pre-mixed BMH and GSH prevents stabilization of STIM1 complexes. RBL-2H3 cells were treated with 250 μM BMH and quenched with 5 mM GSH, either as separate additions or as a single dose of pre-mixed (Pre-Quenched) solution. Prior to treatment, some cells were also stimulated with 0.5 μg/mL TG. Following treatment, cells were rinsed, lysed, immunoprecipitated with anti-STIM1 antibody, and reduced before electrophoresis and Western blotting. Blots are representative of 3 individual experiments.

further supporting the interpretation that oligomers formed via cell stimulation do not depend on disulfide bond interactions.

Non-covalent interactions are sufficient for forming oligomeric STIM1 species in native cells at rest

Thus far, all blotting that has been described was performed under denaturing conditions using SDS buffer and SDS/PAGE equipment. Preparation with SDS denatures the secondary and tertiary structure of proteins, linearizing the proteins, and imparting negative charge onto the protein directly proportional to its mass. Thus, multi-protein complexes disassemble under denaturing conditions, as proteins are no longer in their native conformations. To establish whether native multi-protein STIM1 complexes from resting cells can be isolated under non-denaturing conditions, a Blue NativePAGE assay was performed on STIM1 immunoprecipitates. RBL-2H3 cells were first lysed with buffer containing dodecylmaltoside (DDM) and immunoprecipitated using anti-STIM1 (C-terminal) antibody. To avoid boiling and denaturation, proteins were eluted from the agarose beads by adding Alkaline Buffer (pH 11.5) and returned to pH 7.2 via dialysis. Immediately prior to electrophoresis, Coomassie Blue G250 was added to each sample to impart an overall negative charge onto the proteins and allow for separation via electrophoresis. A sample Blue NativePAGE blot of STIM1 IP products under non-reducing conditions is shown in Figure 2.9A. IP samples were prepared from RBL-2H3 cells at rest or pre-stimulated with TG. Under both treatments, STIM1 containing complexes are found in highly abundant bands at or below 480 kDa and above 720 kDa, verifying the existence of native multi-protein STIM1 complexes in cells at rest. Pre-stimulation of the cells with TG

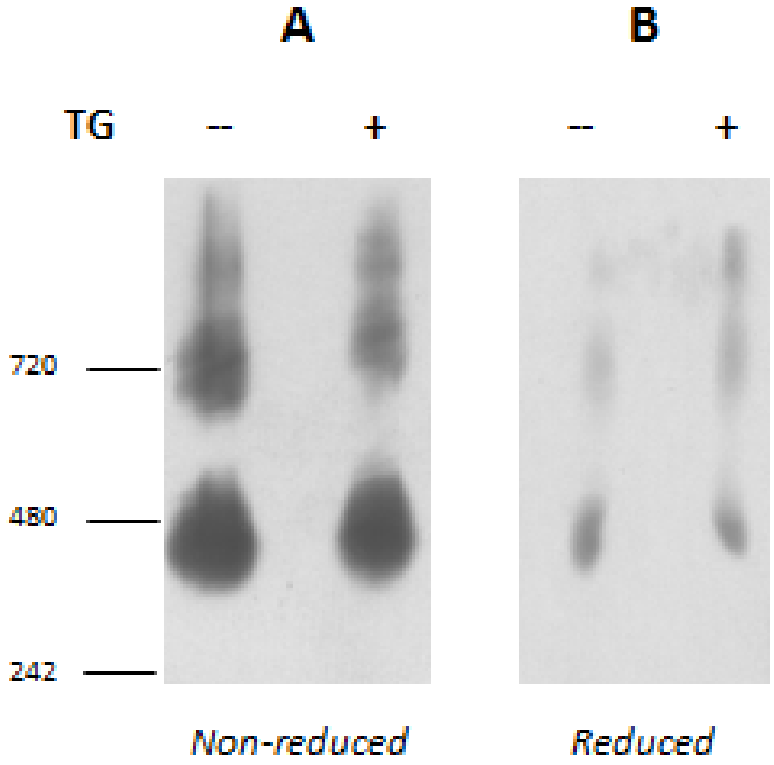

Figure 2.9: Blue NativePAGE blots reveal the existence of non-covalently bound STIM1 complexes in resting cells. RBL-2H3 cells, either unstimulated or TG (0.5 μg/mL) stimulated, were lysed with 1% (v/v) DDM and immunoprecipitated with anti-STIM1 antibody under non-denaturing conditions. To avoid boiling, proteins were eluted with Alkaline Buffer (pH 11.5) and dialyzed overnight into pH 7.2 buffer. Immediately prior to electrophoresis, Coomassie Blue G250 (0.25 %, v/v) was added. Samples were prepared under **(A)** non-reduced and **(B)** βME reduced conditions. Blots are representative of 3 individual experiments.

evokes a slight, yet reproducible, increase in molecular weight to each of the bands present in the native gel, suggesting that conformational changes within the complexes occur as a result of stimulation. Additionally, native samples were reduced with βME immediately prior to Coomassie Blue G250 addition to determine the extent of disulfide bonding present in the STIM1 complexes (Figure 2.9B). The overall yield is greatly reduced in both lanes; however, the overall presence and position of bands in both reduced lanes remains similar to the non-reduced lanes and suggests that disulfide bonds are not necessary for formation of all native STIM1 complexes in cells. Furthermore, these results suggest that non-covalent interactions are sufficient for stabilizing oligomeric STIM1 complexes in intact cells. While the exact stoichiometry of STIM1 in the 480 kDa and 720 kDa complexes is unclear, the apparent molecular weights of the bands suggest that the > 720 kDa complex is approximately twice that of the smaller ~ 480 kDa STIM1 species. We further note that cells lysed with these non-denaturing detergents dissolve the lipid membranes and produce detergent micelles, which average ~ 50 kDa. Membrane-bound proteins are retained within the micelle structure, adding both size and shape to the protein complexes present in the sample. Together with the stabilization of larger complexes under non-denaturing conditions, retention of detergent micelles can explain the large variation in STIM1 complex molecular weight values from NativePAGE gels as compared to SDS/PAGE gels.

Attempts to identify STIM1 binding partners

After establishing the existence of oligomeric STIM1 species in living cells at rest, key questions involving both the stoichiometry and composition of these protein complexes

remained. To address this, we submitted the 110 kDa and 260 kDa STIM1 IP product bands from SDS/PAGE results for tandem mass spectrometry (MS) analysis on several different occasions. Untreated, unstimulated STIM1 IP products from RBL-2H3 cells were first prepared under non-reducing conditions similar to Figure 2.1. Following electrophoresis on an SDS/PAGE gel, the entire gel was fixed and stained with Sypro Ruby. Labeled protein bands were visualized under UV light, as represented in Figure 2.10A. Bands of interest, marked by boxes in Figure 2.10A, were excised from the gel and submitted for MS analysis protein identification either at the Proteomics and Mass Spectrometry Core Facility at Cornell University or the Taplin Mass Spectrometry Facility at Harvard University. There, the proteins present in the sample undergo tryptic digestion before entering the mass spectrometer. The molecular weight of the peptide fragments are detected by the mass spectrometer and compared to those weights listed in a fragment database. Identified proteins are then scored based both on number of times a fragment is identified and the number of fragments identified from within a single protein (James et al. 1993). The top results from each sample submission are listed in Figure 2.10B. In all submissions, STIM1 was identified as the primary protein present in each sample with more than 40 % of the full length protein recognized, which confirms the specificity of the IP pulldown. Additional proteins, such as keratin, Ig heavy chain, and actin, were not considered as valid binding partners, as they are commonly found contaminants of mass spectrometry samples due to human handling of the samples and the high abundance of the proteins within cells. Of the remaining proteins that were identified, none were known to be important modulators of Ca^{2+} signaling and/or known to interact with SOCE proteins. We note that one particular identification – rCG23732, a peptide predicted to exist based on genomic sequencing – was estimated to be ~ 25 kDa in size. While we cannot exclude the possibility that rCG23732

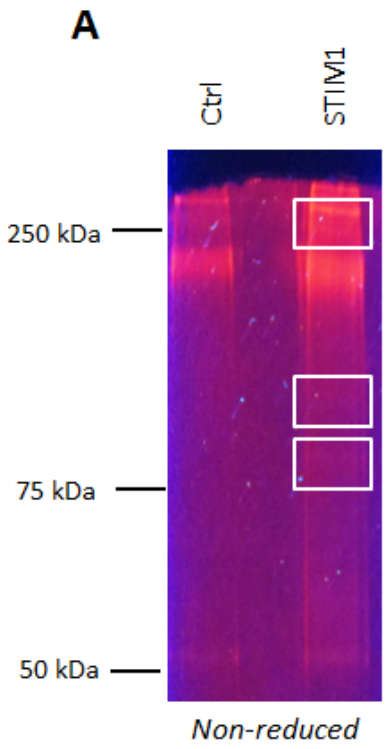

B

260 kDa band (Sept 2009 – Cornell)
STIM1
Keratin
rCG23732 (rat)
α–fetoprotein
Ig heavy chain

85 & 110 kDa combined (June 2009 – Cornell)	110 kDa band (Sept 2009 – Cornell)	110 kDa band (June 2010 – Harvard)
STIM1	STIM1	STIM1
Keratin	Keratin	Actin
Ig heavy chain	α–fetoprotein	Endoplasmin
		HSP-90α

Figure 2.10: MS analysis of STIM1 disulfide-bonded IP complexes. Untreated, unstimulated RBL-2H3 cells were lysed and immunoprecipitated with anti-STIM1 or an irrelevant control antibody under non-reduced conditions. Following SDS/PAGE separation, gels were fixed and protein bands were labeled with Sypro Ruby stain. **(A)** Detection of Sypro Ruby stained STIM1 complexes under UV light. White boxes indicate the location of labeled protein bands, which were excised and submitted for MS protein identification. **(B)** The top proteins identified from each individual MS submission.

may be the binding partner of STIM1 at 110 kDa, we also cannot confirm its existence as a real protein in live rat cells at this time.

In addition to mass spectrometry, we attempted co-IPs to identify the protein binding partners of STIM1 in resting cells. Particular attention was given to proteins that were previously shown to interact with STIM1, such as SERCA2 (Sampieri et al. 2009, Manjarrés et al. 2010) and EB1 (Grigoriev et al. 2008, Jermy 2008). Additional attempts were made with proteins shown to be a component of the pore-forming subunit of SOCE, such as Orai2 (Mercer et al. 2006, Lis et al. 2007), and 20-30 kDa proteins known to be important to Ca^{2+} signaling, such as the Rho-family GTPases Rac1 and Cdc42 (Bishop & Hall 2000, Hong-Geller & Cerione 2000, Rosado & Sage 2000, Price et al. 2003). In each case, immunoblotting using appropriate antibodies were performed on STIM1 IP samples. And in each case, we failed to see evidence for co-localization between STIM1 and the protein being tested (data not shown).

The 110 kDa product occurs as a disulfide bond between STIM1 Cys-437 and a 20-25 kDa peptide

With the identity of STIM1 binding partners unknown, we attempted to identify the disulfide bond site(s) along the STIM1 protein required for retention of these higher oligomeric structures. Our results with βME, NEM, and BMH highlight the essential role of cysteine residues and disulfide bonds in the stabilization of the 110 kDa and 260 kDa products following cell lysis (Figures 2.1, 2.2, & 2.5). As shown by Figure 2.11, STIM1 contains only five cysteine residues – three positioned in the lumen, one inside the transmembrane domain, and one present in the cytoplasm. We chose to investigate the sole cytosolic cysteine residue, Cys-437, which is

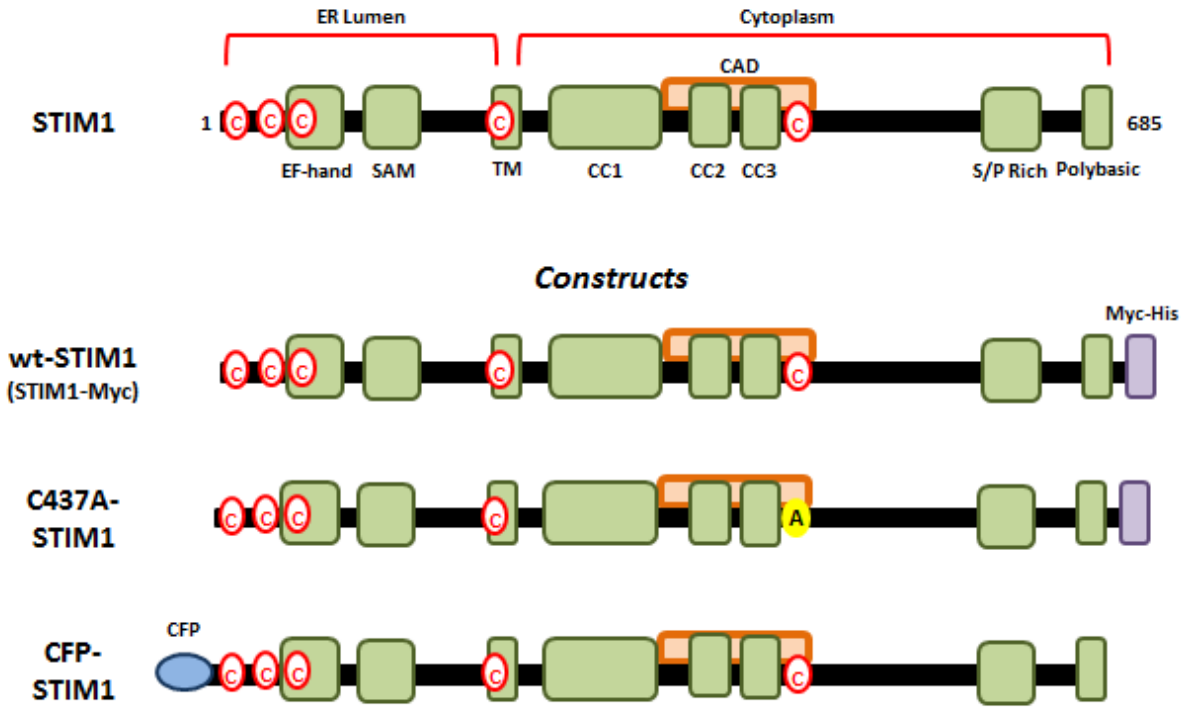

Figure 2.11: Full-length STIM1 and generated STIM1 DNA constructs. (Top) Full-length STIM1 denoting its putative functional domains and the location of all cysteine residues. **(Bottom)** Generated constructs of STIM1, including the addition of reporter labels and/or point mutations. SAM (sterile α-motif), TM (transmembrane domain), CC (coiled-coil region), CAD (CRAC activation domain), S/P Rich (Serine/Proline rich region).

located near the C-terminus of the Ca^{2+} release-activated Ca^{2+} (CRAC) activation domain (CAD). The CAD region was identified as being the minimal fragment of STIM1 required for binding to Orai1 and activating CRAC channels (Park et al. 2009) and was later shown to be important for STIM1 oligomerization following store depletion (Covington et al. 2010). Research by Park et al. (2009) further showed that mutation of Cys-437 within the CAD region to C437G results in a substantial decrease in the Ca^{2+} influx rate (> 70 %), suggesting a functional regulatory role for this residue. To identify whether Cys-437 serves as an important residue in the stabilization of the oligomeric STIM1 species we observe, we generated a set of STIM1 constructs as shown in Figure 2.11.

To test whether Cys-437 is an important binding site for the stabilization of oligomeric STIM1 species after lysis, RBL-2H3 cells were transfected with either wt-STIM1 or C437A-STIM1 and immunoprecipitated with anti-STIM1(C-terminal) or an irrelevant control antibody. Samples were then immunoblotted with either anti-Myc or anti-STIM1 antibody (Figure 2.12). Since both DNA constructs contain a Myc-His tag, use of the anti-Myc antibody allowed for subsequent isolation and identification of the transiently transfected STIM1. As noted by the red arrow in Figure 2.12, cells transfected with C437A-STIM1 and blotted with anti-Myc antibody do not contain a protein band at 110 kDa as compared to their endogenous wt-STIM1 counterpart under non-reducing conditions. These results provide clear evidence that the disulfide bond between STIM1 and the 20-25 kDa protein depends on the Cys-437 residue. Blotting the C437A-STIM1 IP products with anti-STIM1 antibody reveals that non-mutated, endogenous STIM1 continues to form the 110 kDa band, further confirming the significance of the C437A mutation. Interestingly, the C437A mutation does not eliminate the 260 kDa disulfide-bonded STIM1 complex, as shown by the anti-Myc antibody blot. While Cys-437 is

Figure 2.12: The 110 kDa disulfide-bonded STIM1 complex is absent in C437A-STIM1 mutant expressing RBL cells. RBL-2H3 cells were transiently transfected with wt-STIM1 or C437A-STIM1 mutant DNA constructs 24 hours prior to harvest. Both DNA constructs contain a Myc-His tag, which allows for subsequent isolation and identification of transiently transfected STIM1. Cells were lysed and immunoprecipitated with anti-STIM1 antibody under non-reducing conditions. Following SDS/PAGE separation, samples were blotted with anti-Myc antibody, to detect for transiently transfected STIM1 expression, or anti-STIM1 antibody, to detect for total transient and endogenous STIM1 expression. Blots are representative of 4 individual experiments.

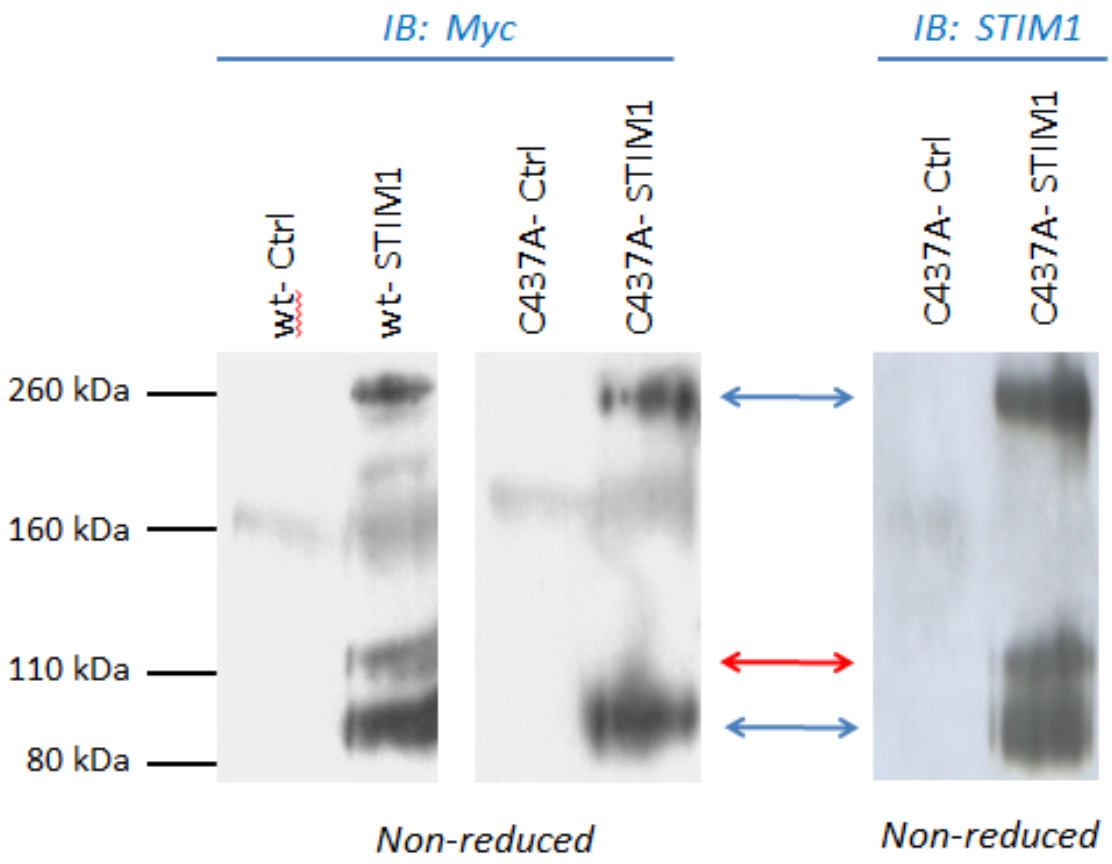
IB: Myc
IB: STIM1
wt- Ctrl
wt- STIM1
C437A- Ctrl
C437A- STIM1
C437A- Ctrl
C437A- STIM1
260 kDa
160 kDa
110 kDa
80 kDa
Non-reduced
Non-reduced

required for stabilization of the 110 kDa product, it is not necessary for retention of the larger 260 kDa product, which implies that the luminal and/or transmembrane cysteine residues stabilize this larger species. C437A-STIM1 transfected cells were also evaluated using BMH crosslinker and with TG stimulation. Our previous findings revealed that BMH crosslinker is sufficient to retain the endogenous 110 kDa and 260 kDa STIM1 bands under reducing conditions in untransfected, TG-stimulated cells (Figure 2.6). In contrast, when TG-stimulated cells are transfected with C437A-STIM1 and immunoblotted with anti-Myc antibody following treatment with BMH, the 110 kDa band is not observed under reducing conditions; yet, the 260 kDa STIM1 IP product remains (Figure 2.13). Together these results confirm that the disulfide bond, formed by the Cys-437 residue of STIM1, is responsible for stabilization of the 110 kDa IP product, but does not play a significant role, if any, in the stabilization of the 260 kDa STIM1 IP product. Rather, this larger IP product is the result of disulfide bond interactions with the luminal and transmembrane cysteine residues present on STIM1 to form homo- or hetero-oligomers.

To verify that endogenous STIM1 was not skewing results observed from the C437A-STIM1 mutation experiments in RBL cells, we repeated this series of experiments in Cos7 cells, which contain extremely low concentrations of endogenous STIM1. When untransfected Cos7 cells are immunoprecipitated with anti-STIM1 (C-terminal) antibody under identical conditions to the RBL cells, faint STIM1 IP product bands are seen, consistent with a limited endogenous pool of STIM1 in Cos7 cells (Figure 2.14A). If the untransfected samples are treated with βME, we see that the oligomeric species are reduced to the 85 kDa species, which suggests that the association and stabilization of STIM1 multi-protein complexes is similar for RBL and Cos7 cells. These untransfected Cos7 cell IP products were immunoblotted with anti-STIM1 antibody

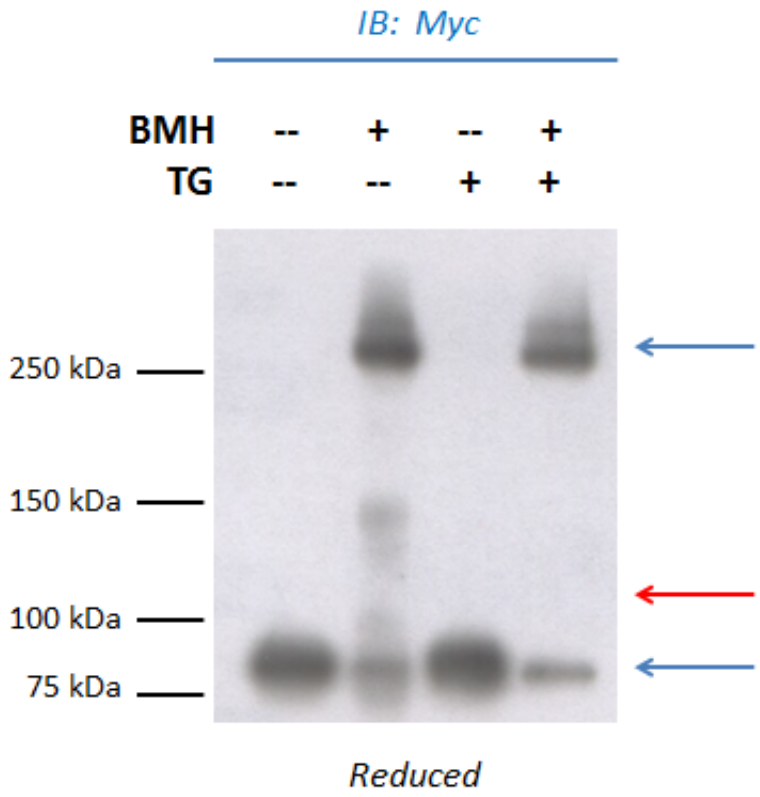

Figure 2.13: BMH treatment and TG stimulation do not alter the disulfide-bonded STIM1 products of RBL cells expressing C437A mutant STIM1. RBL-2H3 were transiently transfected with C437A mutant STIM1 construct one day before harvest. Prior to lysis and IP with anti-STIM1 antibody, some cells were stimulated with 0.5 μg/mL TG and/or treated with 250 μM BMH and quenched with 5 mM GSH. The resulting samples were reduced with βME, SDS/PAGE separated, and Western blotted with anti-Myc antibody to detect for transiently transfected STIM1. Blots are representative of 3 individual experiments.

Figure 2.14: The 110 kDa disulfide-bonded STIM1 complex is also absent from Cos7 cells expressing C437A-STIM1. (A) Untransfected Cos7 cells were immunoprecipitated with anti-STIM1 antibody under non-reduced and reduced conditions and blotted to confirm the presence of low endogenous pools of STIM1. **(B)** Cos7 cells were transfected with wt-STIM1 or C437A-STIM1 one day before harvest. Cells were immunoprecipitated with anti-STIM1 or an irrelevant control antibody under non-reduced conditions. Following SDS/PAGE separation, samples were Western blotted with anti-STIM1 antibody to detect for total STIM1. Blots are representative of 5-6 individual experiments.

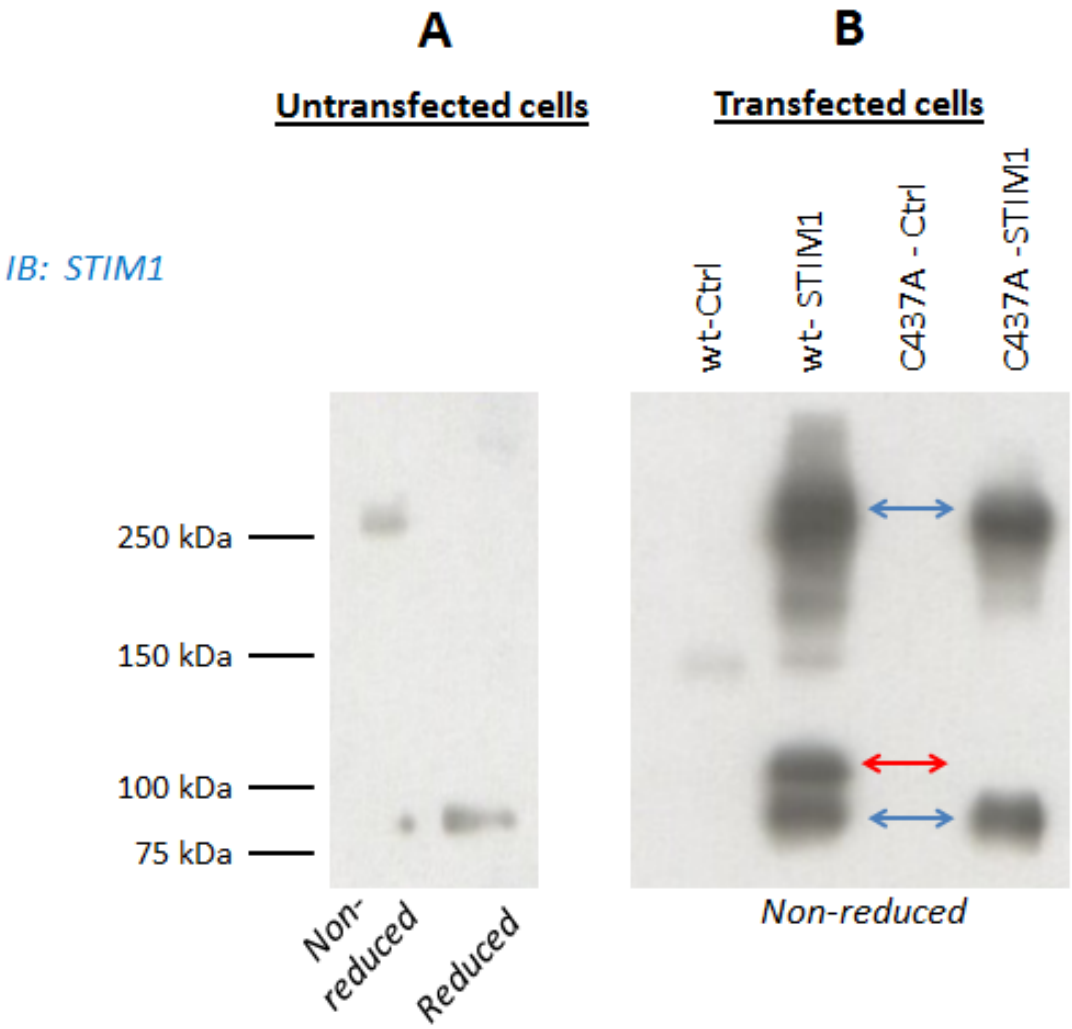
A
B
Untransfected cells
Transfected cells
IB: STIM1
wt-Ctrl
wt- STIM1
C437A - Ctrl
C437A -STIM1
250 kDa
150 kDa
100 kDa
75 kDa
Non-reduced
Reduced
Non-reduced

in parallel with Cos7 cells transfected with wt-STIM1 or C437A-STIM1 constructs, and immunoprecipitated with anti-STIM1 or an irrelevant control antibody, as shown in Figure 2.14B. Similar to RBL cells, Cos7 cells transfected with C437A mutant construct and immunoprecipitated for STIM1 do not contain a protein band at 110 kDa under non-reducing conditions as compared to the abundant band visible at 110 kDa in the wt-STIM1 lane. These results provide additional evidence that stabilization of the 110 kDa product occurs as a disulfide bond at the Cys-437 residue of STIM1 formed between either a proteolytic fragment of STIM1 or an unidentified protein. Both the 85 kDa monomer and 260 kDa oligomeric STIM1 bands are present in both STIM1 IP lanes and with similar abundance to one another, verifying that the endogenous STIM1 present in RBL-2H3 cells did not skew results shown in Figures 2.12-2.13. Moreover, the Cos7 cell STIM1 IP results echo the results of RBL-2H3 cells and further imply that the presence of the 110 kDa and 260 kDa STIM1 oligomers are found in other cell types.

The 260 kDa products is a result of STIM1 dimers isolated from resting cells

A key question that remained was whether we could determine the stoichiometry of the 260 kDa STIM1 oligomer band. Recently, He et al. (2012) provided evidence for full-length STIM1 oligomers in living cells at rest. Using bimolecular fluorescence complementation (BiFC) and live-cell imaging, their method established that STIM1 exists as an oligomer in intact cells at rest, but they did not determine the stoichiometry of these oligomers. Current hypotheses propose that STIM1 exists mainly as a dimer at rest and aggregates into high-order oligomers and puncta following release of Ca^{2+} from ER stores (Penna et al. 2008, Covington et al. 2010). To address this issue, we developed an IP assay that would allow us to determine the

stoichiometry of STIM1 in the 260 kDa band. Briefly, cells were transfected with two separate STIM1 constructs, each with a unique and isolatable tag that varied in size by molecular weight. Following IP, the samples were then immunoblotted using antibodies against STIM1 or one of the reporter tags. As depicted by the schematic in Figure 2.15, the resulting number of bands present near 260 kDa should elucidate the stoichiometry of STIM1 in the protein complex formed. For example, if STIM1 is present as a dimer at 260 kDa, one would expect to see three distinct bands present near 260 kDa – equating to dimer interactions of A-A, A-B, and B-B reporter tags. Likewise, a trimer orientation would be expected to present as four separate bands – AAA, AAB, ABB, and BBB respectively.

To determine the stoichiometry of STIM1 in the 260 kDa IP product, we performed a co-transfection IP experiment using CFP-STIM1 and STIM1-Myc constructs in Cos7 cells to minimize the endogenous STIM1 present. To retain the high molecular weight species, cells were pre-treated with BMH and quenched with GSH prior to lysis. The lysates were immunoprecipitated using anti-STIM1 (C-terminal) antibody and reduced with βME. Samples were then immunoblotted using the appropriate antibodies: anti-Myc, anti-GFP, and anti-STIM1. These samples were also prepared in parallel with control cells that received transfection with only one of the constructs. As shown by Figure 2.16, cells co-transfected with both CFP-STIM1 and STIM1-Myc and immunoblotted with anti-STIM1 antibody form three separate and distinct bands near 260 kDa, indicating the existence of a STIM1 dimer. Of the three bands present, the highest molecular weight band coincides with the most abundant band in that region of the control CFP-STIM1 lane, presumably a CFP-CFP homo-dimer. Likewise, the lowest 260 kDa band present in the co-transfected lane matches closely with an abundant band in the STIM1-Myc control lane, suggesting the presence of a Myc-Myc homo-dimer. As further

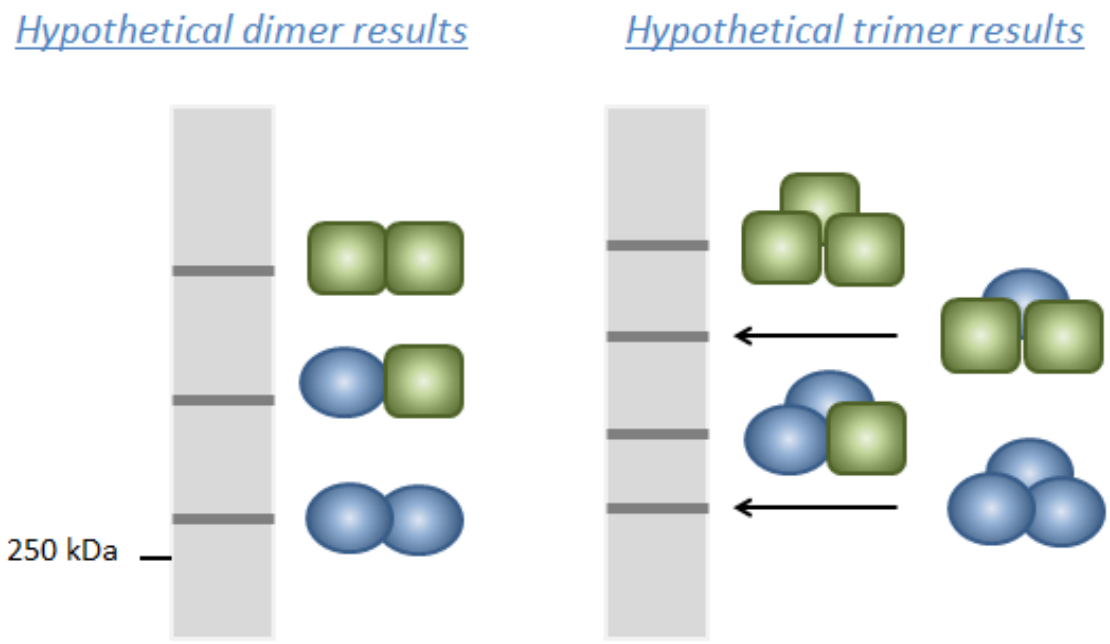

Figure 2.15: Co-transfection of STIM1 constructs can determine the stoichiometry of the 260 kDa STIM1 complex. When co-transfected with two different STIM1 constructs, each with a distinct reporter tag, the resulting number of discrete STIM1 IP product bands near 260 kDa can determine the stoichiometry of the 260 kDa complex. Schematics represent anticipated results from co-transfection experiments in the presence of a **(A)** dimer and **(B)** trimer.

Figure 2.16: The 260 kDa STIM1 species represents a homo-dimer or STIM1 dimer containing complex. Cos7 cells were transfected individually (controls) or co-transfected with CFP-STIM1 and STIM1-Myc constructs one day before harvest. Prior to lysis, cells were treated with 250 μM BMH and quenched with 5 mM GSH to retain STIM1 complexes under reducing conditions. The lysates were immunoprecipitated with anti-STIM1 antibody and immunoblotted with appropriate antibody: anti-STIM1, anti-GFP, or anti-Myc. Blots are representative of 3-5 individual experiments.

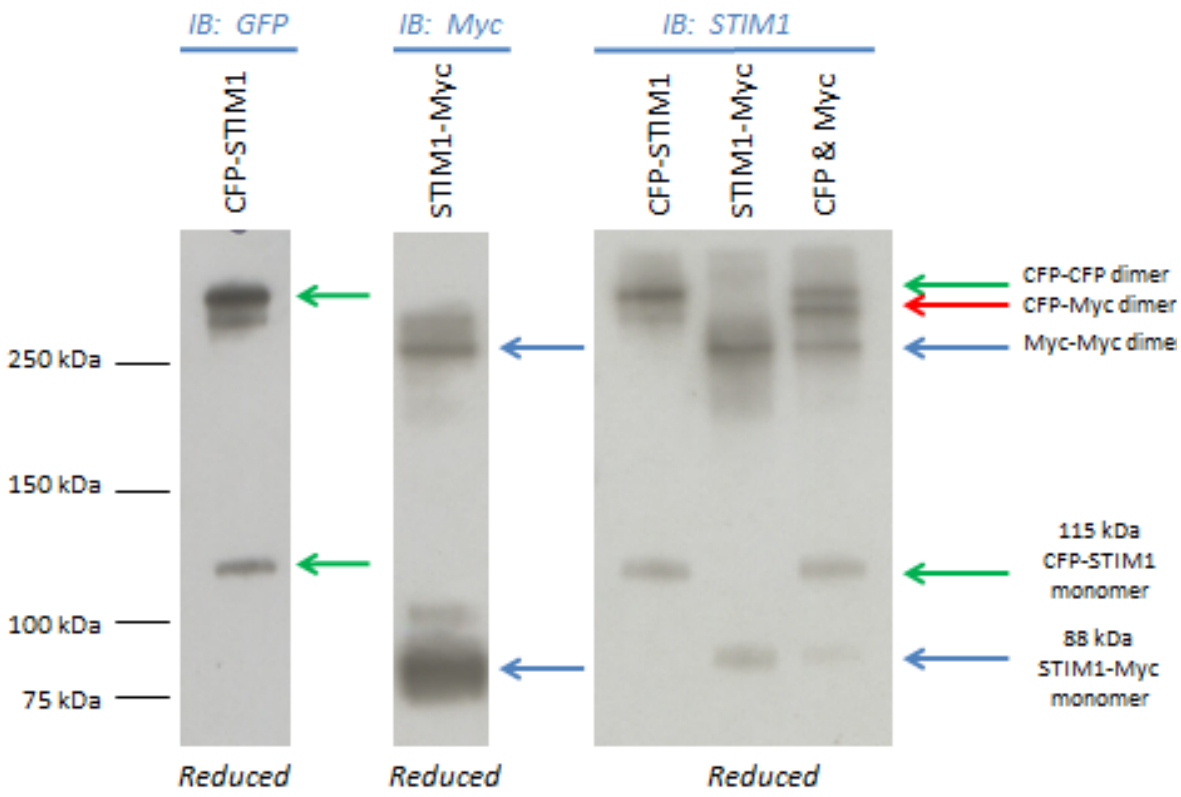
IB: GFP
IB: Myc
IB: STIM1
CFP-STIM1
STIM1-Myc
CFP-STIM1
STIM1-Myc
CFP & Myc
250 kDa
150 kDa
100 kDa
75 kDa
CFP-CFP dimer
CFP-Myc dimer
Myc-Myc dime
115 kDa
CFP-STIM1
monomer
88 kDa
STIM1-Myc
monomer
Reduced
Reduced
Reduced

evidence of a dimer conformation, the third and final protein band present near 260 kDa in the co-transfected lane falls between the two other bands in size, as would be expected of a hetero-dimer formed from CFP-STIM1 and STIM1-Myc. In addition to STIM1 dimer bands, the co-transfected lane contains the monomeric forms of CFP-STIM1 (115 kDa) and STIM1-Myc (88 kDa), which agrees with the monomeric bands present in the control, single-transfection lanes. The banding patterns of the single-transfection IP samples were also immunoblotted for their reporter tags using anti-GFP or anti-Myc antibodies respectively (Figure 2.16) to serve as controls. As shown, the banding patterns present in the anti-GFP blot of CFP-STIM1 IP products closely resemble those seen by the anti-STIM1 blot of the same sample. Likewise, the bands present in the anti-Myc blot of STIM1-Myc IP products are quite similar to the anti-STIM1 blot of the same sample. Together, these results provide strong evidence for STIM1 existing minimally as a dimer in resting cells, which can be stabilized by disulfide bonds or by the sulfhydryl-reactive BMH crosslinking reagent once cells are lysed. Our Blue NativePAGE studies further indicate that STIM1is present in higher order oligomers that do not require stabilization by disulfide bonds in intact cells.

Discussion:

Understanding the process of intracellular Ca^{2+} trafficking is integral to regulating a wide variety of cell functions (Berridge et al. 2003). Of particular importance is understanding the mechanism by which Ca^{2+} depletion from intracellular stores leads to Ca^{2+} influx from the extracellular matrix in a process known as SOCE. While the two key proteins required for SOCE, STIM1 (Roos et al. 2005, Liou et al. 2005, Zhang et al. 2005) and Orai1 (Yeromin et al.

2006, Vig et al. 2006a, Vig et al. 2006b, Prakriya et al. 2006) have been identified, many questions still remain unanswered as to how these proteins facilitate this process.

Our study focused on investigating the STIM1 protein and the mechanisms that underlie its capacity to oligomerize and translocate to the plasma membrane. Using a series of IP experiments, summarized in Table 2.1, we find evidence to suggest that STIM1 exists in multiple forms in resting cells, including the monomeric 85 kDa STIM1 protein and two larger STIM1 complexes that appear in Western blots at 110 kDa and 260 kDa (Figure 2.1). The retention of multiple products in SDS/PAGE and Blue NativePAGE assays, encompassing both monomeric and oligomeric forms of STIM1, points to the complexity of STIM1 interactions and provides better understanding for why no consensus has been reached about the oligomeric state of STIM1 in resting cells. Some argue for the monomeric existence of STIM1 (Stathopulos et al. 2006) while others claim that STIM1 is present as small oligomers (Williams et al. 2002, Baba et al. 2006, Penna et al. 2008, Covington et al. 2010). Our SDS/PAGE results, shown in Figure 2.1, are consistent with both possibilities – STIM1 may simultaneously exist as both monomers and oligomers. Due to the denaturing conditions of SDS/PAGE, we hypothesize that the retention of monomers results from the assay conditions and that intact cells likely contain oligomeric STIM1 complexes at rest. Retention requires stabilization by bonds forming between proximal cysteines, and oligomeric complexes lacking a completely connecting set of these bonds would not be completely retained.

We directly investigated STIM1 IP products to determine how they are formed. Addition of the reducing agent βME (Figure 2.1) and/or addition of sulfhydryl reactive NEM (Figure 2.2) causes the disappearance of higher molecular weight STIM1 IP products at 110 kDa and 260 kDa. These results clearly show that disulfide bond interactions stabilize higher molecular

Table 2.1: Summary of STIM1 IP parameters and immunoblotting results. Results are representative of 3-20 individual experiments, depending on condition, and indicate the abundance and/or presence of the STIM1 disulfide-bonded complexes: strong, distinct band (✓); faint band (weak); or no band present (--).

Immunoprecipitation Condition	85 kDa band	110 kDa band	260 kDa band	85 kDa band	110 kDa band	260 kDa band
	Non-reduced			*Reduced*		
---	✓	✓	✓	✓	--	--
1 mM NEM During	✓	weak	weak	✓	--	--
1 mM NEM Before	✓	weak	weak	✓	--	--
0.5 μg/mL TG	✓	✓	✓	✓	--	--
C437A-STIM1	✓	--	✓	✓	--	--
100 μM – 1 mM BMH	✓	✓	✓	✓	weak	✓
BMH (250 μM) :						
0.5 μg/mL TG				✓	weak	✓
1 mM NEM During				✓	weak	✓
Pre-quench (5 mM GSH)				✓	--	--
C437A-STIM1				✓	--	✓
BMH (250 μM) + TG (0.5 μg/mL):						
1 mM NEM During				✓	weak	✓
Pre-quench (5 mM GSH)				✓	--	--
C437A-STIM1				✓	--	✓

weight STIM1 species that associate non-covalently prior to cell lysis. By adding NEM both before cell lysis and during cell lysis, high molecular weight STIM1 IP products disappear (Figure 2.2). Sulfhydryl reactive NEM binds free –SH groups present on the cysteine residues of STIM1, preventing any further binding interactions from taking place (Figure 2.2A). In the absence of NEM, these free –SH groups bind to other nearby –SH groups during cell lysis, either with STIM1 or other protein(s), producing strong disulfide bonds that allow for retention of high molecular weight STIM1 IP products. The high abundance of the 110 kDa and 260 kDa bands also indicates that these oligomeric products form specifically between certain proteins and not by random association.

Upon stimulation with TG and consequent activation of SOCE, no significant changes were seen in STIM1 IP products, indicating that the formation of these is not sensitive to any changes in conformation or state of aggregation. Previous studies have shown that STIM1 aggregates and redistributes to form puncta near the plasma membrane in response to TG stimulation (Liou et al. 2005, Wu et al. 2006, Calloway et al. 2009). Luik et al. (2008) further established that this aggregation of STIM1 was due to the formation of higher order STIM1 oligomers. Thus, we expected that pre-stimulation of cells with TG and subsequent IP may lead to an increased quantity of oligomeric STIM1 IP products seen, or the formation of entirely new oligomeric species. However, as Figure 2.3 reveals, stimulation with TG did not significantly alter the disulfide-bonded IP products formed, neither in the presence of bands formed nor the abundance of the bands formed. Together, this information suggests several key characteristics about STIM1 oligomerization as it relates to SOCE. First, we confirm that similar low-order STIM1 IP oligomers can be isolated from both resting cells and TG-stimulated cells. This information suggests that the IP products identified are basic building components of any higher

order STIM1 oligomers formed. We also establish that higher order oligomers that result from TG stimulation are not retained via IP, likely because covalent bonds do not form to stabilize the structures and also because SDS/PAGE denaturing conditions will not capture macromolecular complexes unless they are covalently linked.

Using a series of IP experiments involving sulfhydryl-reactive crosslinker, BMH, we established that the identified STIM1 oligomeric products are present in resting cells prior to lysis (Figures 2.4-2.8). This reinforces the results of NEM experiments wherein it was determined that addition of NEM prior to cell lysis prevented disulfide bonds and thereby higher molecular weight IP products (Figure 2.2). Our results with BMH show that the cysteine residues within the 260 kDa and 110 kDa IP products must be within ~ 13 Å, the width of the crosslinker, in resting cells to allow for successful bridging. In the absence of BMH, disulfide bonds form during cell lysis and thereby increase the stability of STIM1 complexes/oligomers that are already present. We also note that under reducing conditions (Figures 2.4-2.5), the 110 kDa band is less abundant than the 260 kDa band, implying that it is less affected by the addition of crosslinker. One possibility is that the 260 kDa product has more free –SH groups available for crosslinking than the 110 kDa product and/or that it is sterically more difficult for BMH to bind and to stabilize the 110 kDa product than the 260 kDa product. It is also possible that BMH tends to bind monovalently at the site(s) required for disulfide bond stabilization for the 110 kDa product, thereby preventing crosslinking bridges from forming.

We also repeated IP experiments with TG-stimulated cells in the presence of crosslinker to determine whether higher order STIM1 oligomers could be stabilized with BMH following store depletion. Our results show no significant differences between IP products from unstimulated cells and TG stimulated cells (Figure 2.6), indicating that no new large, oligomeric

STIM1 products are covalently bonded allowing for isolation. More likely, these aggregates are held together via non-covalent interactions or associate with other proteins to form large, stable oligomeric complexes that are not retained after cell lysis and subsequent separations by IP and SDS/PAGE.

Western blotting IP products, under denaturing conditions using SDS, are useful for isolating and identifying proteins, but the use of denaturing reagents does not allow for retention of the native structure of macromolecular complexes. Thus, STIM1 IP products were prepared using non-denaturing buffers and analyzed on Blue NativePAGE gels. The benefit of this technique is that all proteins in the sample are returned to a similar isoelectric point, pH ~ 7.5, prior to separation via electrophoresis, which allows for separation of the proteins and complexes to be based on their size and shape (Schägger 2001, Wittig et al. 2006). As shown by Figure 2.9A, at least two major STIM1 complexes can be identified from STIM1 IP products under non-denaturing conditions. The high molecular weights of these products, ~ 480 kDa and > 720 kDa respectively, provide a consistent result that STIM1 is part of macromolecular complexes in resting cells. The formation of DDM detergent micelles (~ 50 kDa) containing the IP products further suggests why the relative molecular weights of the native IP products are much larger than their SDS/PAGE counterparts. We postulate that the native STIM1 IP products at and below 480 kDa are actually complexes consisting of the 260 kDa oligomeric SDS/PAGE STIM1 IP product and at least two micelles. The larger native IP product above 720 kDa is approximately twice the size of the < 480 kDa species, suggesting that this larger product is actually a dimer of the smaller complex. The Blue NativePAGE samples are prepared under non-denaturing conditions, and they notably showed no smaller (< 200 kDa) STIM1 IP products. Rather, this absence of smaller STIM1 IP products further supports our hypothesis that STIM1

exists as small oligomers, possibly dimers and tetramers, of STIM1 in intact cells and partially reduces to a monomeric form during IPs under denaturing conditions.

When cells are pre-treated with TG prior to cell lysis and immunoprecipitated under non-denaturing (native) conditions (Figure 2.9A), we see a noticeable shift in both IP products to slightly higher molecular weights, suggesting a conformational change in the complexes rather than the formation of larger oligomers. In addition, treatment of the samples with βME substantially reduced sample yield but did not reduce the overall macromolecular complexes that formed (Figure 2.9B), indicating that disulfide bonds provide stabilization but are not required for formation of STIM1 complexes in intact cells. Overall, our data indicate that non-covalent interactions are sufficient for the formation of low order oligomeric STIM1 products in resting cells and further suggests that higher order STIM1 oligomers formed following store depletion are similarly non-covalent.

In an effort to determine the composition of the 110 kDa and 260 kDa STIM1 species, protein bands of interest were excised from gels and submitted for MS protein identification on several separate occasions (Figure 2.10). In each case, STIM1 protein was identified as the most prevalent protein located within the sample, both for the 260 kDa and 110 kDa IP products. In addition, co-IP experiments did not positively identify any extra proteins present in STIM1 complexes (data not shown). Together, these data suggest that the STIM1 IP products formed may be composed solely of STIM1, as homo-oligomer(s), or as a complex between STIM1 protein and yet to be identified peptide(s) in the case of the 110 kDa product. Based on the approximate molecular weights of the oligomeric IP products, we hypothesize that the 110 kDa IP species is formed via a disulfide bond between STIM1 and a 20-25 kDa peptide. The dominant presence of STIM1 in our mass spectrometry data suggests that this 20-25 kDa peptide

is actually a fragment of STIM1 that contains a cysteine residue, though we cannot rule out the possibility that the 20-25 kDa peptide is a novel protein/peptide. We have further shown that the 260 kDa complex corresponds to a STIM1 homo-oligomer or a STIM1 containing complex.

While we were unable to identify the specific binding partner of STIM1 in the formation of the 110 kDa IP product, we have successfully isolated the site of interaction between STIM1 and a 20-25 kDa peptide. Williams et al. (2002) first noted that the cytosolic domain of STIM1 was sufficient to promote oligomerization of the protein in resting cells. Following the discovery of CAD (residues 342-448) as the minimal portion of STIM1 required to bind Orai1 and to activate SOCE (Park et al. 2009), Covington et al. (2010) further showed that this CAD region is also important to the oligomerization of STIM1 required for SOCE initiation. Considering the role of disulfide bonds in STIM1 oligomerization, we mutated the only cysteine residue present in the cytosolic region of STIM1, Cys-437. By transfecting C437A-STIM1 into cells and immunoblotting for a reporter tag present on the cDNA, we obtained clear evidence that mutation of the Cys-437 residue abolishes stabilization of the 110 kDa STIM1 IP product during cell lysis (Figures 2.12-2.14). Both the identity of this STIM1 binding partner and the function of this interaction remain to be determined.

We also determined the oligomeric state of STIM1 in the 260 kDa species. Using co-transfection of two separately labeled STIM1 constructs, the resulting IP products allowed for separation of the 260 kDa species into multiple, distinct bands (Figure 2.15). Based on the formation of three distinct bands in the region of 260 kDa (Figure 2.16), we conclude that the 260 kDa STIM1 IP product represents a dimer of STIM1. This result is somewhat surprising based on the large molecular weight of the 260 kDa oligomer formed, as a STIM1 dimer would have been expected closer to 170 kDa. Why such a large discrepancy? While no concrete

conclusions can be made from the immunoblotting data, these results suggest that the covalently bonded STIM1 dimer may take on a conformation that is large and bulky, and which may electrophorese more slowly than expected depending on shape. An alternative hypothesis is that additional, unidentified proteins are present in complex with the STIM1 dimer, adding mass to the overall complex. While we cannot exclude the possibility of a STIM1 dimer-containing complex present in resting cells, we also cannot confirm the existence or identity of any complex binding partners at this time. However, this study does reveal some information about the formation of the 260 kDa oligomeric STIM1 species. We have shown repeatedly that the 260 kDa STIM1 dimer exists and is stabilized via disulfide bond interactions following cell lysis. In addition, our experiments involving IP products of C437A-STIM1 transfected cells reveal that stabilization of the 260 kDa STIM1 oligomeric species does not depend on disulfide bonds formed within CAD, but instead relies on disulfide bonds formed from luminal and/or transmembrane cysteine residues.

The results of this study, together with previous data, suggest that the oligomeric state of STIM1 in resting cells is complicated. Here, we provide biochemical evidence for the presence of oligomeric STIM1 species from intact resting cells, including a STIM1 dimer species and a previously unidentified 110 kDa STIM1-containing oligomer. Notably, these oligomers represent the minimal species captured under denatured conditions, each of which is stabilized by the formation of disulfide bonds. Under non-denaturing conditions, we show evidence of even larger STIM1 species in intact cells, possibly tetramers, which are not dependent on the stabilization of disulfide bonds. In intact cells, these larger oligomers are held together via non-covalent interactions; however, upon cell lysis and under denaturing conditions, the macromolecular STIM1 complexes are unstable and disassemble. Disulfide bond formation

stabilizes these minimal oligomers, the 260 kDa dimer and 110 kDa species, in solution, which allows for identification via SDS/PAGE. While we are unable to identify any other components of the 110 kDa and 260 kDa species aside from STIM1 at this time, we have determined that the interaction between a 20-25 kDa peptide and the Cys-437 residue of STIM1 is necessary for covalent bonding of the 110 kDa species. Both identification of this polypeptide and elucidation of the function of the 110 kDa STIM1 complex are important questions that require further investigation. Additionally, questions remain as to the composition of the 260 kDa oligomeric species. Further investigation is required to determine whether this species represents a STIM1 homo-dimer or rather a STIM1 dimer-containing complex with other proteins. Our mass spectrometry data do not provide strong evidence for other polypeptides, consistent with its identification as a homo-dimer.

REFERENCES

Baba Y, Hayashi K, Fujii Y, Mizushima A, Watarai H, Wakamori M, Numaga T, Mori Y, Iino M, Hikida M, and Kurosaki T (2006). Coupling of STIM1 to store-operated Ca^{2+} entry through its constitutive and inducible movement in the endoplasmic reticulum. Proc Natl Acad Sci USA, 103: 16704-16709.

Barsumian EL, Isersky C, Petrino MG, and Siraganian RP (1981). IgE–induced histamine release from rat basophilic leukemia cell lines: Isolation of releasing and nonreleasing clones. Eur J Immunol, 11: 317-323.

Berridge MJ, Bootman MD, and Roderick HL (2003). Calcium signalling: Dynamics, homeostasis and remodelling. Nat Rev Mol Cell Biol, 4: 517-529.

Bishop AL, and Hall A (2000). Rho GTPases and their effector proteins. Biochem J, 348: 241-255.

Calloway N, Vig M, Kinet JP, Holowka D, and Baird B (2009). Molecular clustering of STIM1 with Orai1/CRACM1 at the plasma membrane depends dynamically on depletion of Ca^{2+} stores and on electrostatic interactions. Mol Biol Cell, 20: 389-399.

Calloway N, Holowka D, and Baird B (2010). A basic sequence in STIM1 promotes Ca^{2+} influx by interacting with the C-terminal acidic coiled-coil of Orai1. Biochemistry, 49: 1067-1071.

Calloway N, Owens T, Corwith K, Rodgers W, Holowka D, and Baird B (2011). Stimulated association of STIM1 and Orai1 is regulated by the balance of PtdIns(4,5)P_2 between distinct membrane pools. J Cell Sci, 124: 2602-2610.

Covington E, Wu MM, and Lewis RS (2010). Essential role for the CRAC activation domain in store-dependent oligomerization of STIM1. Molec Biol Cell, 21: 1897-1907.

Dziadek MA, and Johnstone LS (2007). Biochemical properties and cellular localization of STIM proteins. Cell Calcium, 42: 123-132.

Felgner PL, Gadek TR, Holm M, Roman R, Chan HW, Wenz M, Northrop JP, Ringold GM, and Danielsen M (1987). Lipofection: A highly efficient, lipid-mediated DNA-transfection procedure. Proc Natl Acad Sci USA, 84: 7413-7417.

Grigoriev I, Gouveia SM, van der Vaart B, Demmers J, Smyth JT, Honnappa S, Splinter D, Steinmetz MO, Putney JW Jr., Hoogenraad CC, and Akhmanova A (2008). STIM1 is a MT-plus-end-tracking protein involved in remodeling of the ER. Curr Biol, 18: 177-182.

He J, Yu T, Pan J, and Li H (2012). Visualization and identification of the interaction between STIM1s in resting cells. PLoS One, 7: e33377.

Hong-Geller E, and Cerione RA (2000). Cdc42 and Rac stimulate exocytosis of secretory granules by activating the IP_3/calcium pathway in RBL-2H3 mast cells. J Cell Biol, 148: 481-494.

Hoover PJ, and Lewis RS (2011). Stoichiometric requirements for trapping and gating of Ca^{2+} release-activated Ca^{2+} (CRAC) channels by stromal interaction molecule 1 (STIM1). Proc Natl Acad Sci USA, 108: 13299-13304.

James P, Quadroni M, Carafoli E, and Gonnet G (1993). Protein identification by mass profile fingerprinting. Biochem Biophys Res Commun, 195: 58-64.

Jermy A (2008). STIM1 tracks growing microtubule ends. Nat Cell Biol, 10: 384.

Kerppola TK (2008). Bimolecular fluorescence complementation (BiFC) analysis as a probe of protein interactions in living cells. Annu Rev Biophys, 37: 465-487.

Li Z, Liu L, Deng Y, Ji W, Du W, Xu P, Chen L, and Xu T (2011). Graded activation of CRAC channel by binding of different numbers of STIM1 to Orai1 subunits. Cell Res, 21: 305-315.

Liou J, Kim ML, Heo WD, Jones JT, Myers JW, Ferrell JE Jr., and Meyer T (2005). STIM is a Ca^{2+} sensor essential for Ca^{2+}-store-depletion-triggered Ca^{2+} influx. Curr Biol, 15: 1235-1241.

Liou J, Fivaz M, Inoue T, and Meyer T (2007). Live-cell imaging reveals sequential oligomerization and local plasma membrane targeting of stromal interaction molecule 1 after Ca^{2+} store depletion. Proc Natl Acad Sci USA, 104: 9301-9306.

Lis A, Peinelt C, Beck A, Parvez S, Monteilh-Zoller M, Fleig A, and Penner R (2007). CRACM1, CRACM2, and CRACM3 are store-operated Ca^{2+} channels with distinct functional properties. Curr Biol, 17: 794-800.

Luik RM, Wang B, Prakriya M, Wu MM, and Lewis RS (2008). Oligomerization of STIM1 couples ER calcium depletion to CRAC channel activation. Nature, 454: 538-542.

Manjarrés IM, Rodríguez-García A, Alonso MT, and García-Sancho J (2010). The sarco/endoplasmic reticulum Ca^{2+} ATPase (SERCA) is the third element in capacitative calcium entry. Cell Calcium, 47: 412-418.

Mercer JC, DeHaven WI, Smyth JT, Wedel B, Boyles RR, Bird GS, and Putney JW Jr. (2006). Large store-operated calcium selective currents due to co-expression of Orai1 or Orai2 with the intracellular calcium sensor, Stim1. J Biol Chem, 281: 24979-24990.

Park CY, Hoover PJ, Mullins FM, Bachhawat P, Covington ED, Raunser S, Walz T, Garcia KC, Dolmetsch RE, and Lewis RS (2009). STIM1 clusters and activates CRAC channels via direct binding of a cytosolic domain to Orai1. Cell, 136: 876-890.

Penna A, Demuro A, Yeromin AV, Zhang SL, Safrina O, Parker I, and Cahalan MD (2008). The CRAC channel consists of a tetramer formed by STIM-induced dimerization of Orai dimers. Nature, 456: 116-120.

Pierini L, Holowka D, and Baird B (1996). FcεRI-mediated association of 6 μm beads with RBL-2H3 mast cells results in exclusion of signaling proteins from the forming phagosome and abrogation of normal downstream signaling. J Cell Biol, 134: 1427-1439.

Prakriya M, Feske S, Gwack Y, Srikanth S, Rao A, and Hogan PG (2006). Orai1 is an essential pore subunit of the CRAC channel. Nature, 443: 230-233.

Price LS, Langeslag M, ten Klooster JP, Hordijk PL, Jalink K, and Collard JG (2003). Calcium signaling regulates translocation and activation of Rac. J Biol Chem, 278: 39413-39421.

Putney JW Jr. (1986). A model for receptor-regulated calcium entry. Cell Calcium, 7: 1-12.

Roos, J, DiGregorio PJ, Yeromin AV, Ohlsen K, Lioudyno M, Zhang S, Safrina O, Kozak JA, Wagner SL, Cahalan MD, Veliçelebi G, and Stauderman KA (2005). STIM1, an essential and conserved component of store-operated Ca^{2+} channel function. J Cell Biol, 169: 435-445.

Rosado JA, and Sage SO (2000). The actin cytoskeleton in store-mediated calcium entry. J Physiol, 526: 221-229.

Sampieri A, Zepeda A, Asanov A, and Vaca L (2009). Visualizing the store-operated channel complex assembly in real time: Identification of SERCA2 as a new member. Cell Calcium, 45: 439-446.

Schägger H (2001). Blue-Native gels to isolate protein complexes from mitochondria. Methods Cell Biol, 65: 231-244.

Stathopulos PB, Li GY, Plevin MJ, Ames JF, and Ikura M (2006). Stored Ca^{2+} depletion-induced oligomerization of stromal interaction molecule 1 (STIM1) via the EF-SAM region: An initiation mechanism for capacitive Ca^{2+} entry. J Biol Chem, 281: 35855-35862.

Thastrup O, Cullen PJ, Drøbak BK, Hanley MR, and Dawson AP (1990). Thapsigargin, a tumor promoter; discharges intracellular Ca^{2+} stores by specific inhibition of the endoplasmic reticulum $Ca^{2(+)}$-ATPase. Proc Natl Acad Sci USA, 87: 2466-2470.

Varnai P, Toth B, Toth DJ, Hunyady L, and Balla T (2007). Visualization and manipulation of plasma membrane-endoplasmic reticulum contact sites indicates the presence of additional molecular components within the STIM1-Orai1 complex. J Biol Chem, 282: 29678-29690.

Vig M, Peinelt C, Beck A, Koomoa DL, Rabah D, Koblan-Huberson M, Kraft S, Turner H, Fleig A, Penner R, and Kinet JP (2006a). CRACM1 is a plasma membrane protein essential for store-operated Ca^{2+} entry. Science, 312: 1220-1223.

Vig M, Beck A, Billingsley JM, Lis A, Parvez S, Peinelt C, Koomoa DL, Soboloff J, Gill DL, Fleig A, Kinet JP, and Penner R (2006b). CRAC multimers form the ion-selective pore of the CRAC channel. Curr Biol, 16: 2073–2079.

Williams RT, Senior PV, Van Stekelenburg LV, Layton JE, Smith PJ, and Dziadek MA (2002). Stromal interaction molecule 1 (STIM1), a transmembrane protein with growth suppressor activity, contains an extracellular SAM domain modified by N-linked glycosylation. Biochim Biophys Acta, 1596: 131-137.

Wittig I, Braun H-P, and Schägger H (2006). Blue native PAGE. Nat Protoc, 1: 418-428.

Wu MM, Buchanan J, Luik RM, and Lewis RS (2006). Ca^{2+} store depletion causes STIM1 to accumulate in ER regions closely associated with the plasma membrane. J Cell Biol, 174: 803-813.

Yeromin AV, Zhang SL, Jiang W, Yu Y, Safrina O, and Cahalan MD (2006). Molecular identification of the CRAC channel by altered ion selectivity in a mutant of Orai. Nature, 443: 226-229.

Zhang SL, Yu Y, Roos J, Kozak JA, Deerinck TJ, Ellisman MH, Stauderman KA, and Cahalan MD (2005). STIM1 is a Ca^{2+} sensor that activates CRAC channels and migrates from the Ca^{2+} store to the plasma membrane. Nature, 437: 902-905.

CHAPTER THREE

The Importance of Cys-437 in STIM1 Interactions and Store-Operated Calcium Entry

Introduction:

Ca^{2+} release-activated Ca^{2+} (CRAC) channels serve a critical role in mediating extracellular Ca^{2+} influx following depletion of Ca^{2+} from intracellular stores. Activation of CRAC channels is accomplished by successful coupling of the endoplasmic reticulum (ER)-transmembrane protein stromal interaction molecule 1 (STIM1) to Orai1 proteins located at the plasma membrane (PM) (Liou et al. 2005, Zhang et al. 2005, Vig et al. 2006). Before coupling and activation of the channel occurs, STIM1 first aggregates into higher order oligomers and diffuses along the ER to junctions with the PM (Luik et al. 2008). Once at the PM-ER junctions, STIM1 oligomers recruit two dimers of Orai1, forming a tetrameric Orai1 pore (Penna et al. 2008). Coupling between basic residues inside the CRAC activation domain (CAD) region of STIM1 (Park et al. 2009) and acidic residues on the C-terminus of Orai1 (Calloway et al. 2010) lead to activation of the fully formed CRAC channel and Ca^{2+} influx.

Much research over the past several years has focused on better understanding the interactions and functional importance of CAD and its regulation of store-operated Ca^{2+} entry (SOCE). In 2009, laboratories simultaneously identified the ~100 amino acid CAD region (approximately residues 342-448) in the cytoplasmic portion of STIM1 and established it as the minimal segment of STIM1 required for both interaction with Orai1 and activation of the fully formed CRAC channel (Park et al. 2009, Yuan et al. 2009, Muik et al. 2009). Soon after, CAD was found to directly associate with Orai1 (Zhou et al. 2010) via interactions between a short

basic residue sequence within CAD (res. 382-387) and several acidic residues located on the C-terminus of Orai1 (Calloway et al. 2010). It should be noted that while mutation of these basic residues in CAD together with the critical acidic residues in Orai1 result in stimulated FRET, no Ca^{2+} influx was detected (Calloway et al. 2010). In addition to the noted basic residue sequence, residues 391-448 of the CAD segment, in conjunction with the neighboring coiled-coil (CC) domain of STIM1, were shown to be crucial for higher order oligomerization of STIM1 following store depletion (Covington et al. 2010), which is a prerequisite for SOCE initiation. Together, this work supports a dual functional role for CAD: enabling higher order STIM1 oligomerization and activating Orai1 to allow SOCE.

Although many studies focus on the enabling roles that CAD plays in SOCE, others point out that the regulation of activation by this domain is equally important. When intracellular Ca^{2+} stores are full, STIM1 is held in an inactive state via intramolecular shielding of the CAD region, though the exact interactions are not well understood (Yu et al. 2011). Additionally, several studies have examined the inhibitory roles of residues C-terminal to CAD (residues 450-485) and their effects on oligomerization and SOCE (Muik et al. 2009, Derler et al. 2009, Lee et al. 2009, Mullins et al. 2009). While the STIM1 homomerization domain (SHD, residues 450-474) was found to be critical to STIM1 oligomerization (Muik et al. 2009), the C-terminal region adjacent to it (approximately residues 475-490) contains a Ca^{2+}-dependent inhibitory (CDI) domain (Derler et al. 2009, Lee et al. 2009, Mullins et al. 2009). This CRAC modulatory domain (CMD) contains several acidic residues that promote inactivation of the CRAC channel by interfering with STIM1-Orai1 interactions in a Ca^{2+} dependent manner (Derler et al. 2009). In addition to the region C-terminal to CAD, Korzeniowski et al. (2010) have identified a series of acidic residues within the first CC of STIM1 that may act as an autoinhibitory domain and retain

STIM1 in its inactive state when Ca^{2+} stores are full. They further propose that this acidic region binds electrostatically to the key basic residues of CAD identified previously (Calloway et al. 2010). Based on these findings, current models depict STIM1 as containing an intramolecular switch (Korzeniowski et al. 2010, Soboloff et al. 2011). In the resting, ER store-replete state, Ca^{2+} bound STIM1 is held inactive via electrostatic interactions and intramolecular shielding of the CAD region. Upon store depletion, the loss of luminal Ca^{2+} leads to conformational changes in the cytoplasmic region of STIM1 and removes autoinhibitory folding, leaving CAD open to interactions for both homo-oligomerization and activation of Orai1 (Korzeniowski et al. 2010, Soboloff et al. 2011, Yu et al. 2011).

In 2009, Park et al. introduced evidence supporting a functional role for Cys-437 in regulating the Ca^{2+} influx rate of the CRAC channel. In our current study, we provide evidence for a role for Cys-437 in both stimulated STIM1 oligomerization and regulation of SOCE. Our previous studies using RBL mast cells show evidence for full-length STIM1 oligomers in resting cells, including a previously unidentified 110 kDa hetero-dimer (Chapter 2). Using mutational analysis, this oligomer was found to be stabilized by a disulfide bond between Cys-437 of STIM1, present in the CAD region, and a yet to be identified 20-25 kDa peptide, which may be a proteolytic fragment of STIM1 (Chapter 2). As described in this chapter, cells expressing C437A mutant STIM1 show no significant change in stimulated STIM1-Orai1 association as measured by FRET, compared to wild type STIM1. However, cells expressing C437A mutant STIM1 show a substantial (2 min) delay in Ca^{2+} entry. Together, these results suggest possible functional roles for Cys-437 and the 110 kDa oligomer in gating the CRAC channel but not for translocation of STIM1 to the plasma membrane. Thus, interaction of the 20-25 kDa peptide

with STIM1 may serve an important role in the initiation of functional coupling between STIM1 and Orai1 and activation of SOCE.

Materials & Methods:

Materials:

Anti-STIM1 (S6197, C-terminal) antibody (rabbit, polyclonal, 1mg/mL), N-ethylmaleimide (NEM), Thapsigargin (TG), phorbol-12,13-dibutyrate (PDB), and sulfinpyrazone were purchased from Sigma Aldrich (St. Louis, MO). The anti-Myc antibody (mouse, monoclonal, 1 mg/mL) was purchased from Upstate Biotechnology (Lake Placid, NY). Anti-STIM1 antibody (mouse, monoclonal, 250 μg/mL) came from BD Biosciences (San Jose, CA). The secondary antibody Biotin-(SP) conjugated $F(ab')_2$ fragment goat anti-mouse IgG (H + L) was purchased from Jackson Immunoresearch Labs (West Grove, PA), while detection was provided by NeutrAvidin Horseradish Peroxidase (HRP) (1 mg/mL) from Thermo Fisher Scientific (Rockford, IL). Fluo-4-AM indicator dye was purchased from Invitrogen (Carlsbad, CA).

Cell culture

Rat basophilic leukemia (RBL-2H3) cells (Barsumian et al. 1981) were maintained in a monolayer culture in Minimum Essential Medium (MEM) from Invitrogen (Carlsbad, CA) supplemented with 20 % (v/v) fetal bovine serum (FBS), purchased from Atlanta Biologicals (Lawrenceville, GA). Similarly, Cos7 cells were maintained in a monolayer culture in

Dulbecco's Modified Eagle Medium (DMEM, Invitrogen, Carlsbad, CA), supplemented with 10 % (v/v) FBS as described by Felgner et al. (1987). Growth medium for both cell types was further supplemented with 10 μg/mL gentamicin sulfate (Invitrogen, Carlsbad, CA) to prevent bacterial growth. Cells were harvested with trypsin-ethylenediaminetetraacetic acid (trypsin-EDTA, Invitrogen, Carlsbad, CA) three to five days after passage (Pierini et al. 1996).

For IP experiments involving transfection of DNA constructs into RBL cells, plasmids containing wild type (wt)-STIM1 and/or C437A-STIM1 were electroporated using 32 μg of plasmid for ~ 5 x 10^6 cells (Exponential Decay pulse, 280 V, 950 μF). RBL cells were harvested 24 hours post-transfection. Similarly, Cos7 cells used for IP assays were transfected with wt-STIM1 or C437A-STIM1constructs via electroporation (Exponential Decay pulse, 220 V, 950 μF) using 32 μg of plasmid for ~ 1.5 x 10^6 cells. Cos7 cells were harvested 18-24 hours post-transfection.

For microscopy experiments involving the transfection of DNA constructs into RBL cells, cells were plated at ~ 0.5 x 10^6 cells into 35 mm MatTek dishes (MatTek Corporation, Ashland, MA). Cells were transiently transfected with AcGFP-Orai1 and either wildtype (wt)-STIM1-mRFP or C437A-STIM1-mRFP. The constructs were co-transfected using ~ 1 μg of each appropriate cDNA and Fugene HD (Roche Diagnostics, Indianapolis, IN). Cells were then incubated with the Fugene-DNA complexes for ~ 1 hour at 37 ^oC in Opti-MEM (Invitrogen, Carlsbad, CA). To promote DNA uptake, 0.1 M phorbol-12,13-dibutyrate (PDB) in Opti-MEM was added and cells were incubated for an additional 4-6 hours, as previously described (Gosse et al. 2005). Cells were rinsed to remove PDB and cultured overnight at 37 ^oC. Experiments were performed on live cells 20-24 hours post-transfection.

For microscopy experiments involving the transfection of DNA constructs into Cos7 cells, cells were plated at ~ 0.25 x 10^6 cells into 35 mm MatTek dishes. Cells were transfected with Orai1-FLAG and either wt-STIM1-mRFP or C437A-STIM1-mRFP. The constructs were co-transfected using ~ 1 μg of each appropriate cDNA and Fugene HD prepared in Opti-MEM. The Fugene-DNA-Opti-MEM complexes were added directly to the culture medium. Cells were incubated overnight at 37 ^oC. Experiments were performed on live cells 20-24 hours post-transfection.

DNA constructs:

Wildtype (wt)-STIM1 and Orai1-FLAG cDNA constructs, both encoded in pcDNA4 vectors, were gifts from Dr. Jean-Pierre Kinet at Harvard University Medical School (Vig et al. 2006). The generation of wt-STIM1-mRFP and AcGFP-Orai1 constructs were previously described (Calloway et al. 2009). Both C437A-STIM1 and C437A-STIM1-mRFP were generated by the Cys to Ala mutation at residue 437 using the sense primer 5'-GCA ACA GAT CGA GAT CCT CGC TGG CTT CCA GAT TGT CAA CAA CC-3' and the antisense primer 5'-GGT TGT TGA CAA TCT GGA AGC CAG CGA GGA TCT CGA TCT GTT GC -3' (Integrated DNA Technologies, Coralville, IA) in collaboration with Dr. Alice Wagenknecht-Wiesner (Cornell University).

Immunoprecipitations and immunoblotting:

Immunoprecipitations (IPs) were performed as described in Chapter 2. Briefly, RBL-2H3 cells were harvested and lysed with cold 2x Lysis Buffer (20 mM Tris, 100 mM NaCl, 2 mM sodium orthovanadate, 60 mM sodium pyrophosphate-10H_2O, 20 mM sodium β-glycerophosphate, 0.04 units/mL aprotinin, and 0.02 % sodium azide) further supplemented with 1 % (v/v) TritonX-100 (TX-100), 4 mM 4-(2-Aminoethyl) benzenesulfonyl fluoride hydrochloride (AEBSF), and a 1/2000 dilution of protease cocktail inhibitor (Sigma Aldrich, St. Louis, MO). Cell lysates were immunoprecipitated using Protein A beads (Thermo Fisher Scientific, Rockford, IL) and anti-STIM1 (C-terminal) antibody. Western Blot samples were prepared by boiling the IP products in 1x SDS Sample Buffer (10 % (w/v) glycerol, 1 % (w/v) sodium dodecyl sulfate (SDS), 0.02 % (w/v) bromophenol blue in 50 mM Tris, pH 6.8) to separate proteins from the beads.

Other variations on IP experiments included addition of 1 mM N-ethylmaleimide (NEM), either before or during cell lysis and transfection of DNA constructs via electroporation as described in Chapter 2. Briefly, 1 mM NEM was added to RBL cells in suspension before lysis or 2 mM NEM was included directly with the 2x Lysis Buffer. Lysates were immunoprecipitated, separated via SDS/PAGE, and Western blotted as described in Chapter 2. In some experiments, RBL cells and Cos7 cells were transfected via electroporation with wt-STIM1 or C437A-STIM1 prior to cell lysis and IP with anti-STIM1 (C-terminal) antibody as described above. In these instances, the starting cell concentration per sample was reduced to ~ 7 x 10^6 cells for RBL cells and ~ 2-3 x 10^6 cells for Cos7 cells. Aside from lower starting cell concentrations, the transfected cells were immunoprecipitated identically to untransfected RBL cells.

Western Blotting samples were prepared from IP products as described above. In some experiments, samples were re-boiled for 5 min in the presence of 1 % (v/v) β-mercaptoethanol (βME) to reduce disulfide bonds. Samples were then electrophoresed, transferred onto polyvinylidene fluoride (PVDF) membrane (EMD Millipore, Billerica, MA), and labeled with antibodies as described in Chapter 2. The anti-STIM1 (mouse, polyclonal) antibody was used at 1:250 dilution and anti-Myc at 1:1000. Primary antibody labeling was followed with washes of goat-anti-mouse biotin conjugated antibody (1:4000 dilution) and NeutrAvidin HRP (1:1400 dilution). All solutions were prepared in Tris-buffered saline Tween (TBST, 50 mM Tris, pH 7.6, 150 mM NaCl, and 0.1 % (v/v) Tween 20) supplemented with 10 mg/mL BSA and 1 % (v/v) fish gelatin (Sigma Aldrich, St. Louis, MO).

Live-cell imaging:

Immediately prior to imaging, RBL cells were rinsed repeatedly with buffered saline solution (BSS, 135 mM NaCl, 5 mM KCl, 1.8 mM $CaCl_2$, 1 mM $MgCl_2$, 5.6 mM glucose, 20 mM HEPES, pH 7.4) supplemented with 1 mg/mL BSA and incubated for ~ 5 min at 37 ^{o}C. Images were taken with a Leica TCS SP2 microscope using a Leica APO 63x dipping objective lens (0.9 NA). Cells were excited at 488 nm and 543 nm while fluorescence emission was monitored at 495-540 nm and 555-675 nm respectively. Both laser intensity and phototube sensitivity were adjusted to maximize the signal-to-noise ratio. Live-cell imaging was performed at 37 ^{o}C. Cells were imaged for 5 min (31 frames, 10 sec/frame) prior to stimulation. Stimulation was initiated by the addition of 0.5 mL BSS containing thapsigargin (TG, 150 nM final concentration) directly to the MatTek dish. Image acquisition was resumed within 10-15

sec following TG addition, and the same cells were imaged for 15 min (91 frames, 10 sec/frame). Images were acquired using Leica Confocal Software and processed into micrographs using ImageJ.

Ca^{2+} measurements:

Immediately prior to experiments, Cos7 cells were rinsed with BSS containing 1 mg/mL BSA. Cells were then incubated with 0.9 μM Fluo-4-AM dye for 10 min at 37 ^{o}C in BSS containing 1 mg/mL BSA and 0.5 mM sulfinpyrazone. Cells were rinsed to remove excess Fluo-4-AM and resuspended in BSS with 0.5 mM sulfinpyrazone. Stimulation was initiated by addition of 0.5 mL BSS containing TG (150 nM final concentration). Fields of cells were imaged before and during TG stimulation with the same microscope and conditions as described for live-cell imaging. Pre-stimulated cells were imaged for < 300 sec (11 frames, 15 sec/frame), while stimulated cells were imaged for 10 min (41 frames, 15 sec/frame). All experiments were performed at 37 ^{o}C. Following acquisition with Leica Confocal Software, ImageJ software was used to quantify the changes in Fluo-4-AM (green) fluorescence in regions of interest (ROIs) within the cell body. The ROIs were selected so as to maximize the amount of cell body being measured without encompassing the nucleus, whose excited fluorescence intensity can cause bleedthrough to the red channel. A sample ROI can be seen in Figure 3.5 (white circle).

FRET imaging:

RBL-2H3 cells were imaged for FRET analysis using the same microscope and cell preparation described above for live-cell imaging. The FRET imaging technique used was developed by Calloway et al. (2009) as previously described. Briefly, equatorial images of cells containing AcGFP-Orai1 and STIM1-mRFP constructs were monitored for fluorescence emission at 495-540 nm (for AcGFP) and 575-700 nm (for mRFP), using an excitation wavelength of 476 nm. This excitation wavelength was found to sufficiently excite AcGFP fluorophores while negligibly exciting the mRFP acceptor fluorophores. The Förster distance, i.e. the distance corresponding to 50 % FRET efficiency for the chosen fluorophores, was estimated to be ~ 5 nm (Erickson et al. 2003). All experiments were performed at 37 ^{o}C. Cells were stimulated with 150 nM TG and imaged using the same time series as described for live-cell imaging.

FRET calculations:

FRET calculations and analysis were performed using the same MatLab script described by Calloway et al. (2009). Briefly, the script uses the green channel images of cells at every time point and creates a mask of the pixels to determine the donor fluorescence intensity at each time point, which is then integrated over the background to generate a value. Red pixel values prior to stimulation are measured and are considered to be bleedthrough from the donor fluorophore. Together, these red and green integrated intensities are used to calculate the coefficient of bleedthrough (β) value, which are subtracted from the measured red acceptor intensity. Lastly, the corrected ratio between red acceptor and green donor integrated intensities are calculated at

each time point as a determination of relative FRET, according to Equation 1 (van Rheenen et al. 2004):

$$FRET = \frac{M_A - \beta M_D}{M_D} \quad \text{(Eq. 1)}$$

where M_D = measured donor fluorescence and M_A = measured acceptor fluorescence at each time point. Both values are corrected by subtracting background pixel gray values. Data shown is an average of 16-18 cells for each condition.

Results:

STIM1 forms disulfide-bonded IP products during cell lysis

Chapter 2 described a series of IP experiments to investigate the interactions of STIM1 proteins in resting cells. RBL cells were lysed with TX-100 and immunoprecipitated using anti-STIM1 (C-terminal) antibody. Western Blotting analysis of these IP products revealed that STIM1 exists in three major forms in living cells at rest: an 85 kDa monomer, a 110 kDa species, and a 260 kDa dimer species (Figure 3.1A). When the same samples were reduced with βME and blotted (Figure 3.1B), the high molecular weight products at 110 kDa and 260 kDa disappeared. These results indicated the importance of disulfide bonds for stabilizing the larger oligomeric products. To further understand when these STIM1 complexes form, N-ethylmaleimide (NEM), a sulfhydryl, alkylating reagent, was added to the samples either before cell lysis or during cell lysis prior to IP. The results are shown in Figure 3.1A. Under non-reducing conditions, addition of 1 mM NEM either before or during IP prevents the stabilization

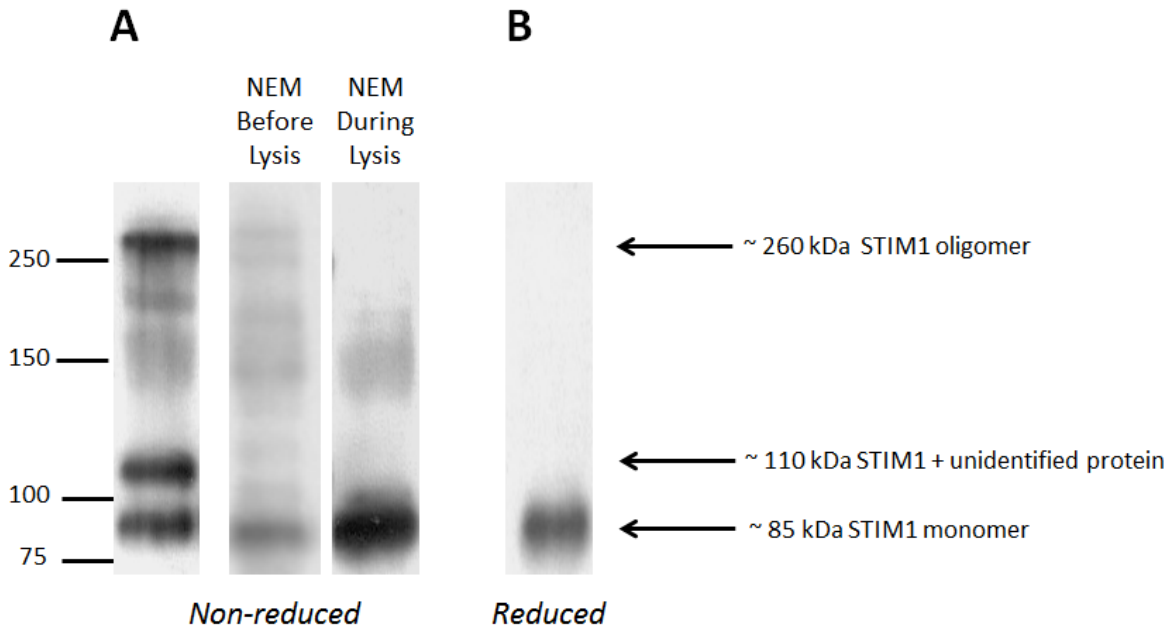

Figure 3.1: STIM1 forms multiple disulfide-bonded complexes during cell lysis. RBL-2H3 cells were lysed with detergent and immunoprecipitated with anti-STIM1 antibody. 1 mM N-ethylmaleimide (NEM) was added before or during lysis to alkylate free sulfhydryl groups that may be present. Samples were prepared under **(A)** non-reduced conditions or **(B)** reduced with 1% (v/v) βME prior to SDS/PAGE and Western blotting. Blots are representative of more than 5-20 individual experiments.

of most high molecular weight STIM1 IP products. As shown, the presence of 110 kDa and 260 kDa bands is quite faint in both NEM-containing lanes as compared to the control STIM1 lane (far left). In fact, the banding patterns seen in the NEM-containing lanes more closely resembles that of the reduced lane (Figure 3.1B), where disulfide bonds have been reduced. This suggests that NEM is alkylating free sulfhydryl groups present on cysteine residues within STIM1 and preventing stabilization of the larger IP products. Together, these results imply that STIM1 forms oligomeric, disulfide-bonded IP products from resting cells and that the disulfide bonds form during cell lysis. Additional experiments showed that these large STIM1 IP products exist natively inside cells and are held together via non-covalent interactions (Chapter 2).

The 110 kDa product is stabilized by a disulfide bond between STIM1 Cys-437 and an unidentified 20-25 kDa peptide

IP experiments described in Chapter 2 showed clear evidence that expression of C437A mutant STIM1 (Figure 3.2) in RBL and Cos7 cells prevents formation of the 110 kDa STIM1 IP product as compared to cells expressing wt-STIM1 (Figures 2.12 & 2.14). These results indicate that the Cys-437 residue of STIM1 is the site of disulfide bond formation between STIM1 and an unidentified 20-25 kDa polypeptide to stabilize the 110 kDa complex. In addition, we showed that the Cys-437 residue is not required for stabilization and retention of the 260 kDa STIM1 complex (Figures 2.12 & 2.14).

Figure 3.2: Full-length STIM1 and Orai1 and generated DNA constructs. (A) Full-length STIM1 and generated DNA constructs denoting putative functional regions, the location of all cysteine residues, and reporter labels. **(B)** Full-length Orai1denoting and generated DNA constructs highlighting putative functional regions and reporter labels. SAM (sterile α-motif), TM (transmembrane domain), CC (coiled-coil region), CAD (CRAC activation domain), S/P Rich (serine/proline rich region)

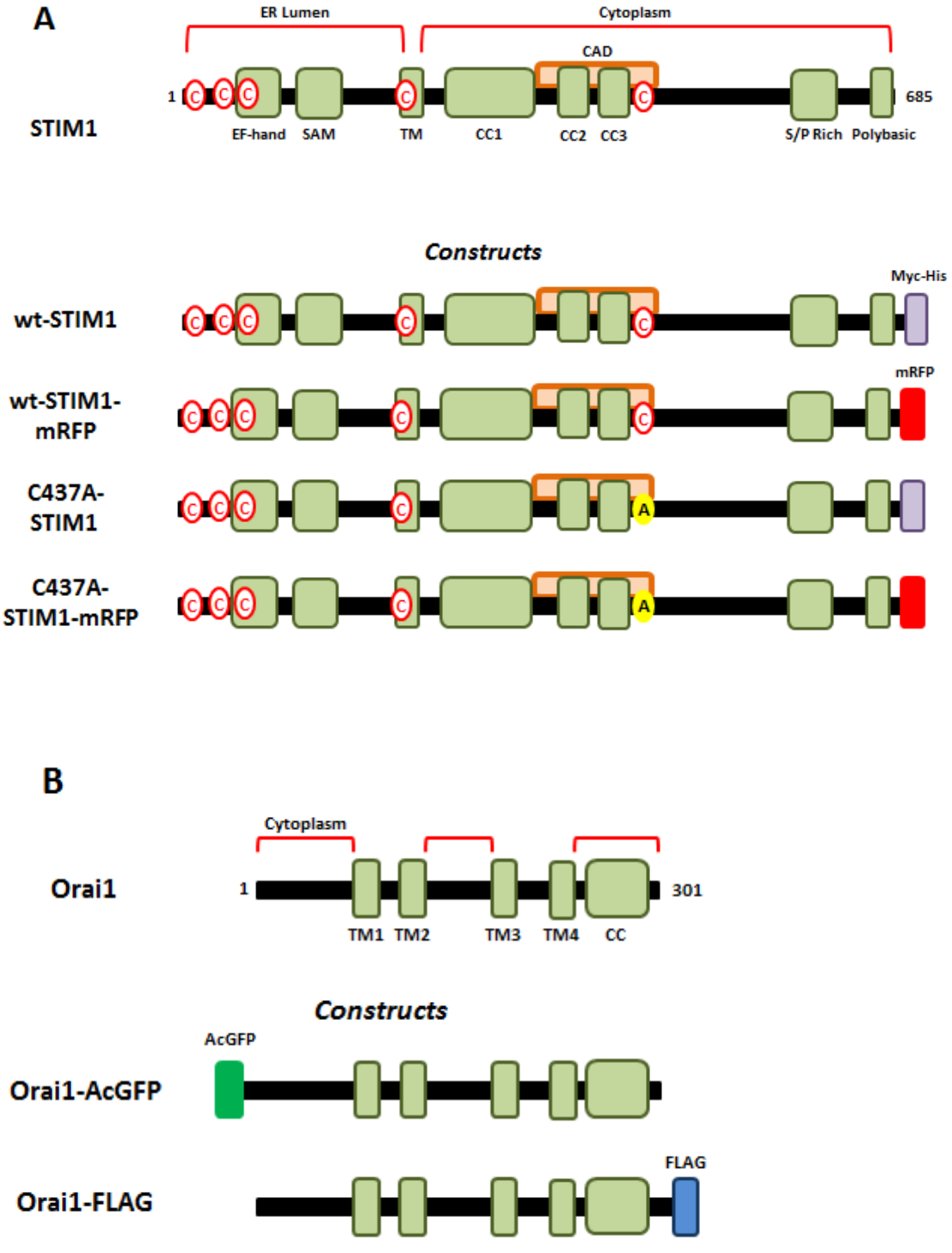
A
ER Lumen
Cytoplasm
CAD
STIM1
1
685
EF-hand
SAM
TM
CC1
CC2
CC3
S/P Rich
Polybasic
Constructs
Myc-His
wt-STIM1
mRFP
wt-STIM1-mRFP
C437A-STIM1
C437A-STIM1-mRFP
B
Cytoplasm
Orai1
1
301
TM1
TM2
TM3
TM4
CC
Constructs
AcGFP
Orai1-AcGFP
FLAG
Orai1-FLAG

C437A does not significantly alter the ability of STIM1 to translocate to the PM

With a specific STIM1 interaction site identified at Cys-437, we next sought to determine the functional role of the 110 kDa species. In the same paper that first described the STIM1 CAD region, Park et al. (2009) showed that their C437G-STIM1 mutant forms puncta with Orai1 similarly to wt-STIM1 following store depletion in confocal microscope images. In their experiment, HEK293 cells were co-transfected with C437G-STIM1 and Orai1 and imaged when cells were at rest in a low-[Ca^{2+}] containing buffer or 10 min post TG stimulation in Ca^{2+}-free buffer. In a similar experiment using confocal microscopy, we show equatorial images of RBL cells co-transfected with AcGFP-Orai1 and wt-STIM1-mRFP or C437A-STIM1-mRFP (Figures 3.2-3.3). Cells were maintained in BSS containing Ca^{2+} at all times. Images were acquired both before and after 10 min stimulation with TG at 37 ^{o}C. As shown by Figure 3.3, both STIM1 constructs (red channel) are present in the ER prior to stimulation, while Orai1 (green channel) is visible in the PM. Following the addition of 150 nM TG, both wt-STIM1 and C437A-STIM1 translocate to a region juxtaposed to the PM wherein the STIM1 constructs co-localize with Orai1 and form puncta, as shown by the formation of yellow regions in the merged images (Figure 3.3). These results confirm the findings originally shown by Park et al. (2009) and suggest that the C437A mutation does not significantly alter the capacity of STIM1 to translocate to the PM.

While these experiments reveal translocation of STIM1 mutants to the PM within 10 min after store depletion, they reveal very little about the kinetics of the translocation process. To assess whether our C437A-STIM1 mutation causes any significant changes to the translocation mechanism of STIM1, we monitored changes in Förster resonance energy transfer (FRET) between STIM1 and Orai1 at the PM. During traditional FRET measurement, an excited donor

Figure 3.3: Wt-STIM1 and C437A-STIM1 co-localize with Orai1 at the plasma membrane following stimulation with TG. Cells were transfected with AcGFP-Orai1 (green channel) and either (top) wt-STIM1-mRFP or (bottom) C437A-STIM1-mRFP (red channel). Images were taken before (unstimulated) and 10 min after stimulation with 150 nM TG. Images are representative of 8-12 individual experiments. Scale bars indicate 5 μm.

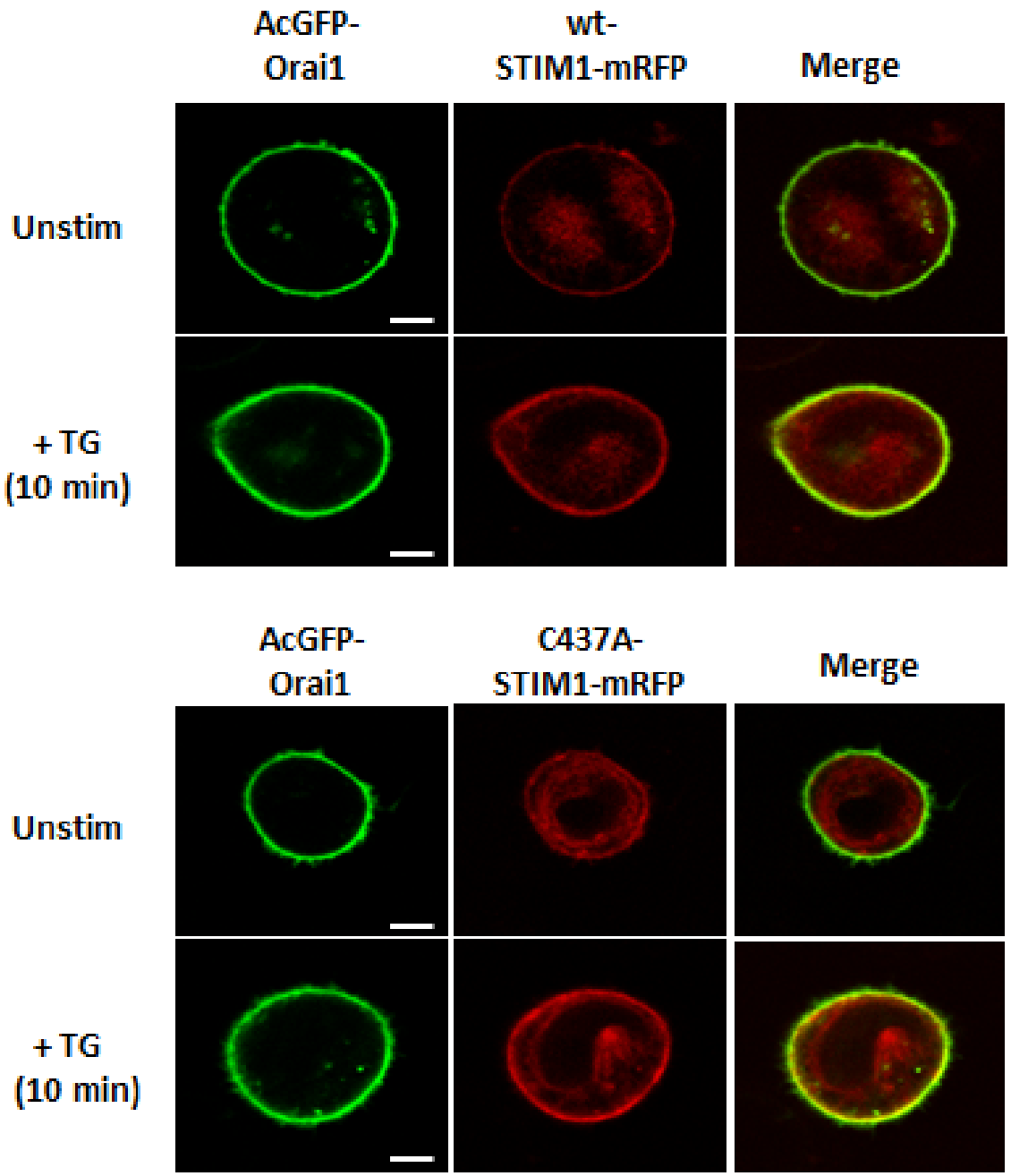
AcGFP-
Orai1
wt-
STIM1-mRFP
Merge
Unstim
+ TG
(10 min)
AcGFP-
Orai1
C437A-
STIM1-mRFP
Merge
Unstim
+ TG
(10 min)

fluorophore transfers some of its resonant energy to an acceptor fluorophore if those fluorophores are in close proximity with one another, in the range of the Förster distance (< 10 nm) (Padilla-Parra & Tramier 2012, Pietraszewska-Bogiel & Gadella 2011). Thus, when energy transfer occurs, the donor fluorescence decreases while acceptor fluorescence increases. The efficiency of the energy transfer is then monitored as the fraction of excited state energy transferred per donor excitation. These FRET values are reported as ratios of sensitized acceptor fluorescence emission, less any bleedthrough attributed to the donor fluorophore, and divided by the donor fluorescence intensity (Equation 1; van Rheenen et al. 2004, Calloway et al. 2009). Here, we monitored changes in FRET from the donor AcGFP-Orai1 to the acceptor wt-STIM1-mRFP or STIM1-C437A-mRFP in response to TG stimulation.

Using a confocal microscopy FRET-based technique developed previously in our laboratory (Calloway et al. 2009), we evaluate equatorial images of RBL cells before and up to 10 min after stimulation by TG to monitor changes in FRET between the proteins of interest. The results, expressed as a ratio of the corrected red (acceptor) fluorescence to the green (donor) fluorescence, are based on an average of 16-18 cells (Figure 3.4). As shown in Figure 3.4, both wt-STIM1 and C437A-STIM1 exhibit similar FRET values and on the same relative time scale in response to TG stimulation. We observe no significant delay in the time required for FRET to occur with C437A-STIM1, indicating that the mutation does not detectably alter the mechanism by which STIM1 translocates to the PM. Thus, the disulfide bond at Cys-437 that stabilizes the 110 kDa STIM1 IP complex is apparently not required for STIM1 translocation or association with Orai1 at the PM.

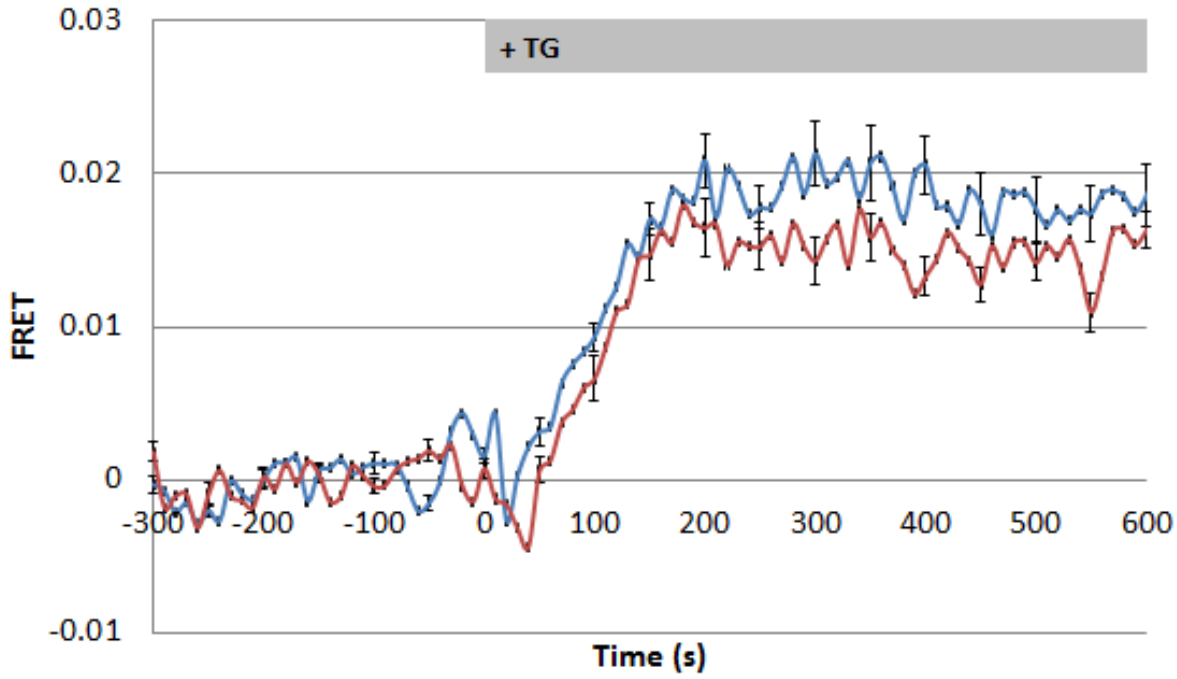

Figure 3.4: Wt-STIM1 and C437A-STIM1 exhibit similar TG-stimulated FRET response with Orai1. RBL-2H3 cells were co-transfected with AcGFP-Orai1 and either wt-STIM1-mRFP (blue) or C437A-STIM1-mRFP (red) and monitored for FRET after addition of 150 nM TG (indicated by bar). FRET results are expressed as a ratio of the corrected acceptor (STIM1) fluorescence to the donor (Orai1) fluorescence (Equation 1) and are based on an average of 16-18 cells. Error bars denote SEM.

C437A-STIM1 causes a significant delay in SOCE

While C437A-STIM1 does not inhibit association of STIM1 with its SOCE partner, Orai1, a key question remained as to whether this mutation has any functional effect on SOCE activation. To address this question, we monitored changes in the Ca^{2+} response to TG in Cos7 cells transiently expressing Orai1-FLAG and either wt-STIM1-mRFP or C437A-STIM1-mRFP. Cos7 cells contain only a limited pool of endogenous STIM1 and Orai1, and SOCE is quite small as compared to the Ca^{2+} response in Cos7 cells overexpressing both proteins (Varnai et al. 2007). Here, we evaluate regions of interest (ROIs) within equatorial images of Cos7 cells before and up to 10 min after TG stimulation to monitor changes in the Ca^{2+} levels present inside the cells. Fluo-4-AM dye is added to the cells just prior to imaging to serve as the Ca^{2+} indicator. Thus, as Ca^{2+} levels increase inside the cell, the fluorescence intensity of Fluo-4 increases linearly. As shown in Figure 3.5, Cos7 cells co-transfected with Orai1-FLAG and STIM1-mRFP constructs (red channel) and incubated with Fluo-4 (green channel) show enhanced fluorescence of Fluo-4 following stimulation with 150 nM TG.

The plots in Figure 3.6 show the average Ca^{2+} response of 34-36 Cos7 cells, co-expressing STIM1 and Orai1, before and after stimulation with TG. As shown, both wt-STIM1 (blue) and C437A-STIM1 (red) transfected cells elicit an immediate Ca^{2+} response to stimulation by TG. This response is brief, typically occurring within the first 30 sec of stimulation (purple box), and can be attributed to the release of Ca^{2+} from ER stores. In addition, untransfected cells (green, n = 12) incubated with Fluo-4-AM dye show a substantial increase in Ca^{2+} levels immediately following stimulation. These values match closely with those obtained using transfected cells and provide further evidence that the immediate Ca^{2+} response represents Ca^{2+}

Figure 3.5: TG stimulated SOCE in Cos7 cells co-transfected with STIM1 and Orai1. Cos7 cells were co-transfected with Orai1-FLAG and (top) wt-STIM1-mRFP or (bottom) C437A-STIM1-mRFP, and monitored for Ca^{2+} response (labeled with Fluo-4 dye, green) to addition of 150 nM TG. An increase of Fluo-4 fluorescence indicates an increase in Ca^{2+} concentration. It should be noted, however, that Fluo4 bleedthrough is contributing to the mRFP images shown in both TG stimulated conditions, as indicated by labeling of the nucleus in the red channel. Images are representative of 7-11 individual experiments. White circle indicates a sample region of interest (ROI) used to calculate Ca^{2+} response. Scale bars indicate 10 μm.

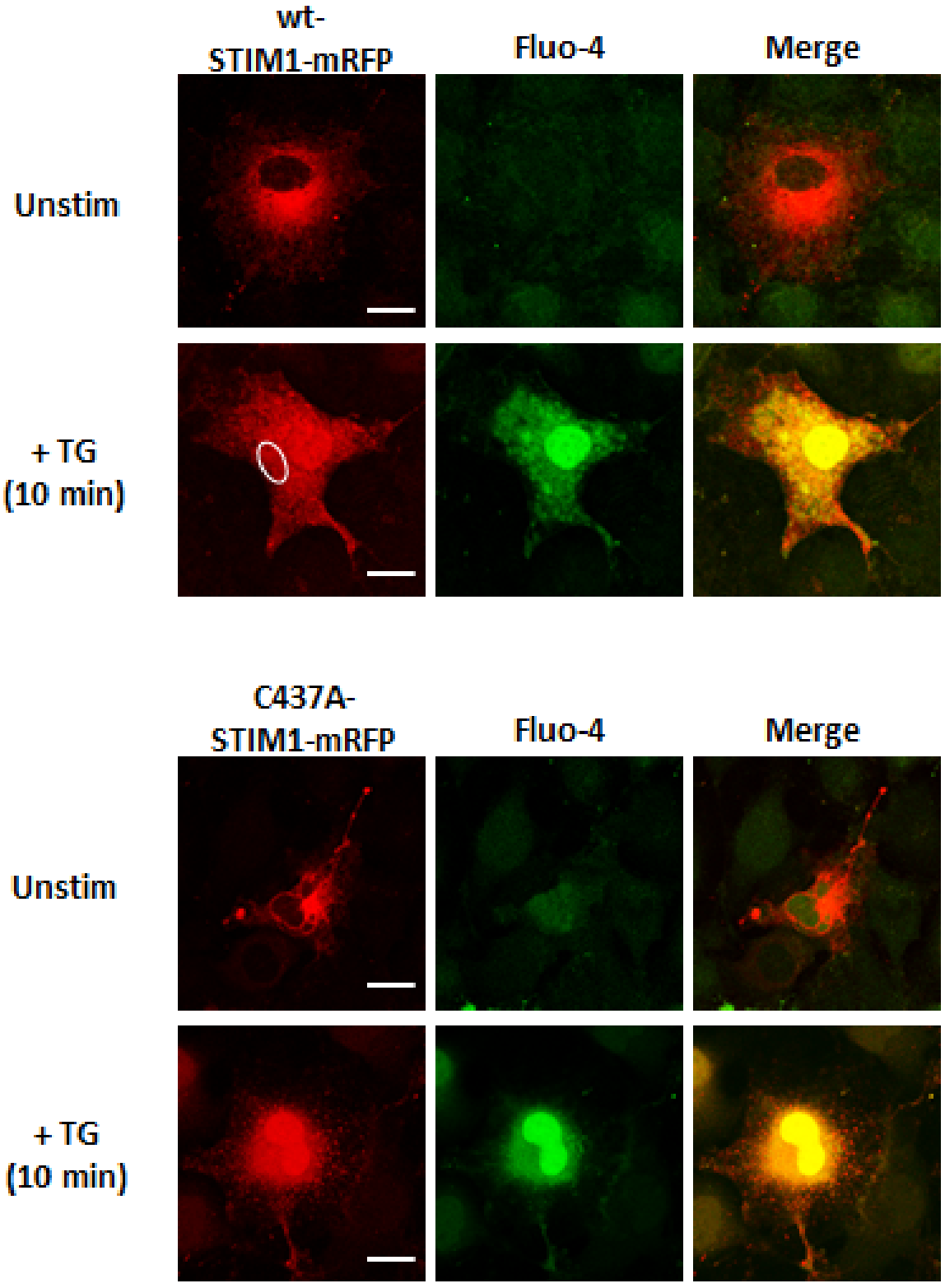
wt-
STIM1-mRFP
Fluo-4
Merge
Unstim
+ TG
(10 min)
C437A-
STIM1-mRFP
Fluo-4
Merge
Unstim
+ TG
(10 min)

Figure 3.6: C437A-STIM1 causes a significant delay in TG-stimulated SOCE. Cos7 cells, either untransfected (green) or co-transfected with Orai1 and wt-STIM1 (blue) or C437A-STIM1 (red), were monitored for Ca^{2+} response (labeled with Fluo-4) upon addition of 150 nM TG. All values were normalized by dividing by the average Fluo-4 fluorescence intensity value of untransfected, unstimulated cells from individual experiments. Values represent an average of 34-36 cells transfected cells and 12 untransfected cells. Purple box indicates the first ~ 30 sec of Ca^{2+} response following TG stimulation when cells undergo Ca^{2+} store depletion from the ER stores. Orange box indicates SOCE following TG stimulation. Error bars show SEM.

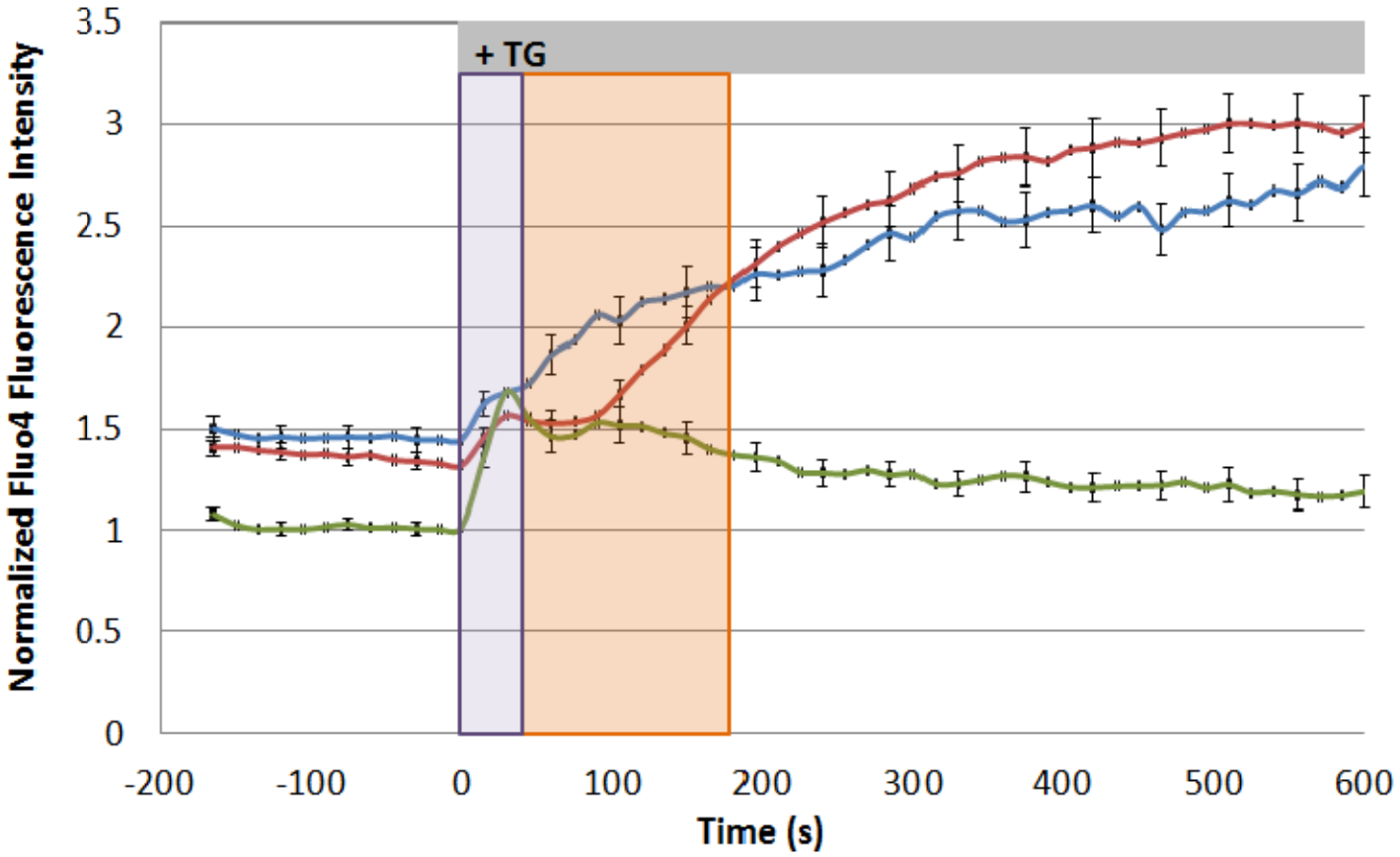
+ TG
Normalized Fluo4 Fluorescence Intensity
3.5
3
2.5
2
1.5
1
0.5
0
-200
-100
0
100
200
300
400
500
600
Time (s)

released from intracellular stores, as untransfected Cos7 cells lack large endogenous pools of SOCE machinery required for Ca^{2+} influx.

Following this initial Ca^{2+} release from stores phase, Ca^{2+} responses vary significantly depending on the STIM1 construct being expressed (Figure 3.6, orange box). For cells that have been transfected with wt-STIM1 construct, release of Ca^{2+} from stores is followed almost immediately by a larger Ca^{2+} response, which appears to be due to Ca^{2+} influx via SOCE. In contrast to this immediate response, cells transfected with C437A-STIM1 construct reveal a significant delay of approximately 2 min before Ca^{2+} influx is initiated. While Park et al. (2009) noted that C437G-STIM1 resulted in an approximate 75 % reduction in Ca^{2+} influx rate as compared to wt-STIM1, our findings with C437A-STIM1 suggest that this may reflect a difference in the timing of Ca^{2+} influx rather than the rate. Cells transfected with C437A-STIM1 gave rise to slightly larger overall Ca^{2+} levels following TG-stimulated SOCE than cells transfected with wt-STIM1. The substantial delay in Ca^{2+} influx suggests a significant gating role for the Cys-437 residue of STIM1 and potentially the 110 kDa product. While a mutation at Cys-437 may not directly affect the capacity of STIM1 to associate with Orai1 at the PM, it apparently affects the opening of CRAC channels and thus delays Ca^{2+} influx. The capacity of the cells to successfully open CRAC channels following this delay and in a manner that surpasses even wt-STIM1 Ca^{2+} response further suggests that a secondary SOCE mechanism exists and can be implemented when the wildtype pathway is impaired.

Discussion:

In Chapter 2, we identified disulfide bond formation at cysteine residues as stabilizing STIM1 oligomeric IP products from whole cell lysates. These disulfide bonds are not normally

present in resting cells, but form during cell lysis. Furthermore, mutational analysis revealed that the previously unidentified 110 kDa STIM1 IP product is stabilized via a disulfide bond with the STIM1 Cys-437 residue and an unidentified 20-25 kDa peptide. Based on mass spectrometry data, we postulate that the 20-25 kDa peptide is actually a fragment of STIM1 that contains a cysteine residue, though we cannot rule out the possibility that the peptide represents a novel protein. We focused our attention on determining the functional role of Cys-437.

Previously, Park et al. (2009) identified the CAD region and provided supporting evidence for the role of CAD in initiating Ca^{2+} influx. Their initial report also suggested the importance of Cys-437 within the CAD region. Using their C437G point mutation, Park et al. (2009) showed that STIM1-C437G forms puncta with Orai1 similar to wt-STIM1 following TG stimulation. These findings match closely with our own confocal images in Figures 3.3 and 3.5, which show the capacity of C473A-STIM1 to translocate to the PM (Figure 3.3) and form puncta (Figure 3.5) in a manner similar to wt-STIM1. While both studies reveal that Cys-mutated STIM1 translocates to the PM within 10 min of ER store depletion, the images do not provide temporal resolution of this movement.

To determine whether C437A-STIM1 translocates to the PM on the same time scale as wt-STIM1, we used FRET to monitor the presence of STIM1 at the PM. In resting cells, the majority of STIM1 is located in the ER (Figure 3.3). Following stimulation, wt-STIM1 translocates to the PM where it interacts with and activates Orai1 (Figure 3.3). Using a FRET technique developed by Calloway et al. (2009), we show FRET interactions between fluorescently labeled STIM1 and Orai1 proteins following stimulation with TG. By monitoring the FRET response between Orai1 and STIM1 every 10 sec over the course of 15 min, we provide temporal resolution of STIM1's translocation, both with wt-STIM1 and C437A-STIM1

(Figure 3.4). As shown by Figure 3.4, mutation of Cys-437 to Ala does not significantly alter the capacity of STIM1 to translocate to the PM and associate with Orai1. Both wt-STIM1 and C437A-STIM1 produce FRET responses with Orai1 at similar values and on similar time scales. This data suggests that the complex represented by the 110 kDa STIM1 IP product, stabilized as a result of a disulfide bond at Cys-437, is not responsible for the translocation process.

After revealing the absence of a functional role for Cys-437 in STIM1 translocation by microscopy and FRET analysis, we investigated the role of Cys-437 in SOCE. In their previous work, Park et al. (2009) noted that STIM1-C437G showed a dramatic reduction (~ 75 %) of Ca^{2+} influx rate as compared to wt-STIM1 in HEK cells. However, these experiments were performed via whole-cell patch clamp analysis (Prakriya & Lewis 2001), wherein cells begin in low-[Ca^{2+}] containing buffer and SOCE stimulation occurs via addition of a high-[Ca^{2+}] containing buffer. The cells are then monitored for an unspecified amount of time to determine Ca^{2+} influx rate. Our data monitoring the Ca^{2+} response of Cos7 cells following stimulation show a kinetic difference that is not apparent in the patch clamp measurements. In Figure 3.6, we show that, following TG stimulation, cells expressing C437A-STIM1 exhibit a significant 2 min delay in SOCE as compared to cells expressing wt-STIM1. This may explain the low Ca^{2+} influx rate of Park et al. (2009) cells expressing C437G mutant STIM1 if the rate was monitored for less than 150 sec following stimulation. Our data further show that once SOCE begins in C437A-STIM1 transfected cells, the rate of influx is faster than wt-STIM1 expressing cells and leads to slightly higher overall Ca^{2+} plateau concentrations. These results contrast the Ca^{2+} measurements obtained via Park et al. (2009) which show HEK cells expressing C437G-STIM1 as having a significantly reduced SOCE response, approximately half to one-third, as compared to that of wt-STIM1. Both results reinforce the functional importance of the Cys-437 residue in

gating SOCE. Our results further substantiate the functional significance of the disulfide bond at Cys-437, as STIM1 is still able to translocate to the PM and exhibit activation of SOCE, albeit in a delayed in manner.

While some variations between the Park et al. (2009) data and our own can be attributed to differences in cell type, these differences in Ca^{2+} response suggest that more complex interactions may be taking place. In designing our STIM1 mutant construct, we decided to maintain as much of the steric shape and bulk of the amino acid –R group as possible while neutralizing the residue; thus, an Ala residue was replaced for Cys. Park et al. (2009) chose the neutralizing Cys to Gly mutation, which by virtue of its smaller size, may have altered the folding structure of the protein slightly as compared to its wt form. A further point of discrepancy between our experimental design and that of Park et al. (2009) is the incubation of cells in buffer in the absence or presence of Ca^{2+}. While SOCE should occur via interactions of the same proteins in both instances, we cannot exclude the possibility that the state of the extracellular environment may elicit some variations in response.

The results of this study, together with data from Chapter 2, reinforce the notion of the functional duality of the CAD segment as an integral part of STIM1 oligomerization and SOCE activation. In Chapter 2, we provided clear evidence that the Cys-437 residue, present in the CAD region, is required for stabilization of the low-order 110 kDa STIM1 oligomer created via a disulfide bond between STIM1 and an unidentified 20-25 kDa peptide. Using microscopy and FRET analysis, we confirm that this disulfide bond is not required for the translocation of STIM1 to the PM following store depletion, consistent with previous results (Park et al. 2009). By monitoring the Ca^{2+} response following stimulation, we further show that mutation of the Cys-437 residue leads to a substantial delay in SOCE, suggesting a significant CRAC channel gating

function for the Cys-437 residue. While the cell circumvents the effects of the mutation and allows eventual Ca^{2+} influx, it remains unclear whether the delay is caused by the absence of the protein represented by the 20-25 kDa peptide and/or the removal of a cysteine residue interaction site in the CAD region. Thus, identification of the unknown 20-25 kDa peptide remains a key objective to understanding both the oligomeric interactions of STIM1 at rest and the regulation of SOCE activation.

REFERENCES

Barsumian EL, Isersky C, Petrino MG, and Siraganian RP (1981). IgE-induced histamine release from rat basophilic leukemia cell lines: Isolation of releasing and nonreleasing clones. Eur J Immunol, 11: 317-323.

Calloway N, Vig M, Kinet JP, Holowka D, and Baird B (2009) Molecular clustering of STIM1 with Orai1/CRACM1 at the plasma membrane depends dynamically on depletion of Ca^{2+} stores and on electrostatic interactions. Mol Biol Cell, 20: 389-399.

Calloway N, Holowka D, and Baird B (2010). A basic sequence in STIM1 promotes Ca^{2+} influx by interacting with the C-terminal acidic coiled coil of Orai1. Biochemistry, 49: 1067-1071.

Covington ED, Wu MM, and Lewis RS (2010). Essential role for the CRAC activation domain in store-dependent oligomerization of STIM1. Molec Biol Cell, 21: 1897-1907.

Derler I, Fahrner M, Muik M, Lackner B, Schindl R, Groschner K, and Romanin C (2009). A Ca^{2+} release-activated Ca^{2+} (CRAC) modulatory domain (CMD) within STIM1 mediates fast Ca^{2+}-dependent inactivation of Orai1 channels. J Biol Chem, 284: 24933-24938.

Erickson MG, Moon DL, and Yue DT (2003). DsRed as a potential FRET partner with CFP and GFP. Biophys J, 85: 599-611.

Gosse JA, Wagenknecht-Wiesner A, Holowka D, and Baird B (2005). Transmembrane sequences are determinants of immunoreceptor signaling. J Immunol, 175: 2123-2131.

Felgner PL, Gadek TR, Holm M, Roman R, Chan HW, Wenz M, Northrop JP, Ringold GM, and Danielsen M (1987). Lipofection: A highly efficient, lipid-mediated DNA-transfection procedure. Proc Natl Acad Sci USA, 84: 7413-7417.

Korzeniowski MK, Manjarrés IM, Varnai P, and Balla T (2010). Activation of STIM1-Orai1 involves an intramolecular switching mechanism. Sci Signal, 3: ra82.

Lee KP, Yuan JP, Zeng W, So I, Worley PF, and Muallem S (2009). Molecular determinants of fast Ca^{2+}-dependent inactivation and gating of the Orai1 channels. Proc Natl Acad Sci USA, 106: 14687-14692.

Liou J, Kim ML, Heo WD, Jones JT, Myers JW, Ferrell JE Jr., and Meyer T (2005). STIM is a Ca^{2+} sensor essential for Ca^{2+}-store depletion-triggered Ca^{2+} influx. Curr Biol, 15: 1235-1241.

Luik RM, Wang B, Prakriya M, Wu MM, and Lewis RS (2008). Oligomerization of STIM1 couples ER calcium depletion to CRAC channel activation. Nature, 454: 538-542.

Muik M, Fahrner M, Derler I, Schindl R, Bergsmann J, Frischauf I, Groschner K, and Romanin C (2009). A cytosolic homomerization and a modulatory domain within STIM1 C-terminus determines coupling to Orai1 channels. J Biol Chem, 284: 8421-8426.

Mullins FM, Park CY, Dolmetsch RE, and Lewis RS (2009). STIM1 and calmodulin interact with Orai1 to induce Ca^{2+}-dependent inactivation of CRAC channels. Proc Natl Acad Sci USA, 106: 15495-15500.

Padilla-Parra S, and Tramier M (2012). FRET microscopy in the living cell: Different approaches, strengths, and weaknesses. Bioessays, 34: 369-376.

Park CY, Hoover PJ, Mullins FM, Bachhawat P, Covington ED, Raunser S, Walz T, Garcia KC, Dolmetsch RE, and Lewis RS (2009). STIM1clusters and activates CRAC channels via direct binding of a cytosolic domain to Orai1. Cell, 136: 876-890.

Penna A, Demuro A, Yeromin AV, Zhang SL, Safrina O, Parker I, and Cahalan MD (2008). The CRAC channel consists of a tetramer formed by STIM-induced dimerization of Orai dimers. Nature, 456: 116-120.

Pierini L, Holowka D, and Baird B (1996). FcεRI-mediated association of 6 μm beads with RBL-2H3 mast cells results in exclusion of signaling proteins from the forming phagosome and abrogation of normal downstream signaling. J Cell Biol, 134: 1427-1439.

Pietraszewska-Bogiel A, and Gadella TWJ (2011). FRET microscopy: From principle to routine technology in cell biology. J Microscopy, 241: 111-118.

Prakriya M, and Lewis RS (2001). Potentiation and inhibition of Ca^{2+} release-activated Ca^{2+} channels by 2-aminoethyldiphenyl borate (2-APB) occurs independently of IP_3 receptors. J Physiol, 536: 3-19.

Soboloff J, Madesh M, and Gill DL (2011). Sensing cellular stress through STIM proteins. Nat Chem Biol, 7: 488-492.

Van Rheenen J, Langeslag M, and Jalink K (2004). Correcting confocal acquisition to optimize imaging of fluorescence resonance energy transfer by sensitized emission. Biophys J, 86: 2517–2529.

Varnai P, Toth B, Toth DJ, Hunyady L, and Balla T (2007). Visualization and manipulation of plasma membrane-endoplasmic reticulum contact sites indicates the presence of additional molecular components within the STIM1-Orai1 complex. J Biol Chem, 282: 29678-29690.

Vig M, Peinelt C, Beck A, Koomoa DL, Rabah D, Koblan-Huberson M, Kraft S, Turner H, Fleig A, Penner R, and Kinet JP (2006). CRACM1 is a plasma membrane protein essential for store-operated Ca^{2+} entry. Science, 312: 1220-1223.

Yu F, Sun L, Courjaret R, and Machaca K (2011). Role of the STIM1 C-terminal domain in STIM1 clustering. J Biol Chem, 286: 8375-8384.

Yuan JP, Zeng W, Dorwart MR, Choi Y-J, Worley PF, and Muallem S (2009). SOAR and the polybasic STIM1 domains gate and regulate Orai channels. Nat Cell Biol, 11, 337-343.

Zhang SL, Yu Y, Roos J, Kozak JA, Deerinck TJ, Ellisman MH, Stauderman KA, and Cahalan MD (2005). STIM1 is a Ca^{2+} sensor that activates CRAC channels and migrates from the Ca^{2+} store to the plasma membrane. Nature, 437: 902-905.

Zhou Y, Meraner P, Kwon HT, Machnes D, Oh-hora, M, Zimmer J, Huang Y, Stura A, Rao A, and Hogan PG (2010). STIM1 gates the store-operated calcium channel Orai1 in vitro. Nat Struct Mol Biol, 17, 112-116.

CHAPTER FOUR

Orthogonal Patterning of Multiple Biomolecules Using an Organic Fluorinated Resist and Imprint Lithography*

Summary:

The ability to spatially deposit multiple biomolecules onto a single surface with high-resolution while retaining biomolecule stability and integrity is critical to the development of micro- and nanoscale bio-devices. While conventional lithographic patterning methods are attractive for this application, they typically require the use of UV exposure and/or harsh solvents and imaging materials, which may be damaging to fragile biomolecules. Here, we report the development of a new patterning process based on a fluorinated patterning material that is soluble in hydrofluoroether solvents, which we show to be benign to biomolecules, including proteins and DNA. We demonstrate the implementation of these materials into an orthogonal processing system for patterning multi-biomolecule arrays by imprint lithography at room temperature. We further showcase this method's capacity for fabricating patterns of receptor-specific ligands for fundamental cell studies.

* This work was performed in collaboration with Dr. Priscilla Taylor, Carol Newby, and Dr. Jin-Kyun Lee in the laboratory of Prof. Christopher Ober of the Department of Materials Science Engineering at Cornell University. Additionally, some experiments were performed by Dr. Margarita Chatzichristidi of the Department of Chemistry at the University of Athens – Greece and Dr. Panagiota S. Petrou and Dr. Sotiris E. Kakabakos of the Institute of Radioisotopes & Radiodiagnostic Products (NCSR "Demokritos") in Athens, Greece. Experimental contributions are specified at the end of the chapter.

Introduction:

Tremendous advances have recently been made in the field of bioelectronics. Biosensors, biological microelectromechanical systems (bio-MEMs), and microfluidic devices are revolutionizing biological and medical research (Katz 2006, Berggren & Richter-Dahlfor 2007, James et al. 2008, Bashir 2004, Domachuk et al. 2010, Svennersten et al. 2011). Similarly, the development of biomolecular arrays and regenerative therapies are enabling unprecedented studies in fundamental biology and applications in tissue engineering, respectively (Joos & Bachmann 2009, Wolf-Yadlin et al. 2009, Atala 2009, Bettinger 2009, Arrabito & Pignataro 2012). The ability to spatially deposit multiple biomolecules with high-resolution onto a single surface is integral to the development of these bio-devices (Blawas & Reichert 1998, Kane et al. 1999).

Consequently, multi-component patterning of biomolecules has become an active area of research. Patterning techniques for single components have been extensively developed (Blawas & Reichert 1998, Christman et al. 2006). However, multi-component patterning introduces unique challenges, which have yet to be satisfactorily addressed. Importantly, multi-component protein patterning requires depositing distinct regions of biomolecules onto a single substrate while retaining biomolecule integrity and avoiding nonspecific binding (Arrabito & Pignataro 2012).

Techniques using photolithography (Pritchard et al. 1995, Sundberg et al. 1995), soft-lithography (Delamarche et al. 1997), dip-pen lithography (Piner et al. 1999, Wu et al. 2011), electron beam lithography (Kolodziej & Maynard 2011), stereomask lithography (Zhao et al. 2011), and spot-arraying (Mosbach et al. 2001) have all been explored and represent the

principal advances in the field of multi-component protein patterning. Photolithography is a mature patterning technique that is promising for biomolecule applications (Douvas et al. 2002, Petrou et al. 2007), as it allows for high-resolution, precise alignment, and is a high-throughput process. The greatest disadvantage of photolithography is that it traditionally requires harsh photoresists and developers as well as applications of heat, which often lead to denaturation of delicate biomolecules. Many clever strategies have been developed to circumvent these requirements (Doh & Irvine 2004, Holden & Cremer 2003, Ilic & Craighead 2000, Orth et al. 2003, Shiu & Chen 2007, Goudar et al. 2012); however, these strategies are necessarily specialized and lack universal applicability. Soft-lithography is an inexpensive and parallel patterning process, which also has the capacity to produce three-dimensional structures. Yet, due to the elastomeric nature of the stamps, mechanical deformation necessarily occurs, which can also result in pattern deformation. Furthermore, soft-lithography is limited by a lack of registration capabilities (Eichinger et al. 2012). Dip-pen lithography can precisely place nanoscale arrays of proteins; though, by nature, this technique can also be prohibitively time-consuming (Pimpin & Srituravanich 2011). Similarly, electron beam lithography can produce patterns with high-resolution; however, this method is extremely expensive and difficult to scale up (Kolodziej & Maynard 2011). Stereomask lithography, while relatively new, is hindered by low resolution and high production costs as well (Zhao et al. 2011). Though spot-arraying techniques, including ink-jet printing, can be cost-effective, the resolution is too low to be practical for many applications (Eichinger et al. 2012).

Recently, we published our synthesis of both fluorinated resists and light-emitting materials, which are processable in fluorinated hydrofluoroether (HFE) solvents, for application to organic electronic device patterning (Lee et al. 2008, Taylor et al. 2009, Lee et al. 2010).

Similar to biomolecule patterning, organic electronic materials can also be damaged by the harsh photoresists and solvents required by photolithography. We showed that these highly-fluorinated solvents and resist materials are completely benign to organic electronic materials such that they can be used for photolithographic patterning of these delicate materials (Zakhidov et al. 2008). HFEs have been shown to be environmentally-friendly, non-flammable, and non-toxic, and they have been used previously in protein research (Sarkari et al. 2003). Furthermore, as process solvents, HFEs are recyclable to enable a sustainable processing system.

Here, we show that HFE solvents, along with a resist that we have developed, are benign to biomolecules and can serve in a processing system for patterning biomolecules by lithography. We show that proteins and DNA may be directly patterned by this benign lithography technique. In this way, high-resolution and high-throughput biomolecule patterning can be accomplished with precise alignment capabilities in a reproducible lithographic process.

We have selected imprint lithography to demonstrate the lithographic patterning properties of this biocompatible processing system. Imprint lithography has recently received significant attention as a patterning technique with the potential to assume a key role in the manufacture of nanoscale structures for electronic, optical, biological, and energy applications (Balla et al. 2008, Stuart & Chen 2009). Because of its capacity to produce patterns as small as 10 nm over large areas, with high-reproducibility and high-throughput capacity, imprint lithography has also found applications in protein patterning (Hoff et al. 2004). One particular advantage of this approach is that the proteins are not exposed to the denaturing effects of UV radiation as found with most photolithography. However, similar to photolithography, imprint lithography also commonly requires harsh resists and resist removal steps. We replace the traditional harsh processing system with a biocompatible one and demonstrate the lithographic

patterning of DNA and multi-protein arrays. In addition, we show that this resist and patterning technique can be used to pattern protein arrays for fundamental studies with cells.

Materials & Methods:

Materials:

Benzotrifluoride (TFT); 3,3,4,4,5,5,6,6,7,7,8,8,9,9,10,10,10-heptadecafluorodecyl methacrylate; 3-aminopropyl (trimethoxysilane) (APTMS); and 3-aminopropyl (triethoxysilane) (APTES) were purchased from Sigma Aldrich (St. Louis, MO). Azobisisobutyronitrile (AIBN) was purchased from Sigma Aldrich and recrystalized from $CHCl_3$. 3M™ Novec™ Engineered Fluid Hydrofluoroether (HFE) 7200 and HFE 7500 were purchased from 3M™ USA (St. Paul, MN).

Bovine serum albumin (BSA), biotin-BSA, and streptavidin labeled with horseradish peroxidase (streptavidin-HRP) were purchased from Sigma Aldrich. DNP-BSA was prepared from BSA conjugated to 2,4-dinitrophenyl (DNP), (Invitrogen, Carlsbad, CA), with approximately 20 DNP per BSA. Cy3 and Cy5 fluorescent dyes were purchased from GE Healthcare Life Sciences (Piscataway, NJ) and conjugated to DNP-BSA, with a stoichiometry of 2-3 molecules of each dye per DNP-BSA. Mouse monoclonal anti-DNP Immunoglobulin E (IgE) was purified as described by Subramanian et al. (1996). The IgE was then modified with AlexaFluor 488 (A488), purchased from Invitrogen, according to the labeling kit instructions. Streptavidin-AlexaFluor 568 (streptavidin-A568) and streptavidin-AlexaFluor 546 (streptavidin-A546) were purchased from Invitrogen and used as received. The 20 mer DNA probe 5'-CTGAACGGTAGCATCTTGGA-3' construct with biotin at its 5'-terminus and the 20-mer

target DNA 5'-TCCAAGATGCTACCGTTCAG-3' construct with A488 at its 5'-terminus were purchased from Integrated DNA Technologies (San Diego, CA). Immunopure streptavidin and 2,2'-azino-bis(3-ethylbenzthiazoline-6-sulfonic acid) (ABTS) peroxidase substrate were purchased from Pierce (Rockford, IL). Mouse monoclonal antibodies (Mab clones AP003S and BP005S) against prostate specific antigen (PSA) were purchased from Scripps Laboratories (San Diego, CA). Free-PSA calibrators in human serum were obtained from CIS Bio-International (Bagnols-sur-Cèze, France). Mouse monoclonal anti-PSA antibody (clone BP005S) conjugated to biotin was prepared according to a published method (Niotis et al. 2010). MaxiSorp polystyrene 96 well-plates were purchased from Nunc (Roskilde, Denmark).

Synthesis and Characterization of Imprint Resist (ImR):

To a 25 cm^3 Schlenk tube, 7.00 g (13.15 mmol) of 3,3,4,4,5,5,6,6,7,7,8,8,9,9,10,10,10-heptadecafluorodecyl methacrylate was added followed by 0.07 g (0.43 mmol) AIBN and 7 mL TFT. The tube was then sealed and degassed by three freeze-thaw cycles in liquid N_2 under reduced pressure. The reaction was stirred at 75 ^oC for 12 h under a N_2 atmosphere. The solution was then precipitated in hexanes and dried under reduced pressure to give a colorless solid, yielding 6.5 g (93 % of theoretical yield). Characterization of ImR: IR: ν = 1732, 1194, 114, 704, 655, 559 cm^{-1}; ^1H NMR (400 MHz, $CDCl_3$:$CFCl_3$ (v/v)): δ = 4.25 (br s, 2 H, CH_2CF_2), 2.49 (m, 2H, C$H_2CH_2CF_2$), 1.67-0.80 ppm (m, 5 H); T_d (TGA) = 168.92 ^oC; M_n = 611,000; M_w/M_n = 1.2.

Lithographic Evaluation:

The lithographic properties of ImR, using silicon wafers, were investigated using a Nanonex NX-2500 nanoimprint lithography tool. The resist films were spun-cast from a solution of polymer (0.05 g) in HFE-7500 (1.0 g) at 2000 rpm. The resulting films had a thickness of *ca.* 200 nm. Before imprint, the film was exposed to a 5 sec oxygen plasma clean to improve the adhesion to the template. Films were imprinted at 300 psi and 25 ^{o}C for 3 min using a fused silica stencil with *ca.* 600 nm feature relief. The imprint stencil was prepared through standard photolithographic technique (Willson & Colburn 2004) on a fused silica mask with feature sizes ranging from 1 μm to 100 μm.

Streptavidin-Biotin Binding Compatibility Assay:

The effect of ImR and HFE solvents on streptavidin-biotin interactions was investigated. Streptavidin solutions of final concentrations 1 μg/mL, 2 μg/mL, and 5 μg/mL were prepared in carbonate buffer (43 mM $NaHCO_3$, 7 mM Na_2CO_2, 0.05 % (w/v) NaN_3, pH 9.2). These solutions were deposited into three separate sets of microtitration wells and incubated for 1 h at room temperature (RT) for protein adsorption. Then the supernatants were decanted, and the wells were washed twice with a 10 mM Tris-HCl solution (washing solution, pH 8.25) before refilling with 100 mM $NaHCO_3$ (pH 8.5) supplemented with 10 mg/mL BSA for 1 h at RT to minimize nonspecific binding. Finally, wells were rinsed with washing solution (pH 8.25) and followed by two rinses with distilled water before adding test samples.

To one set of wells (Set 1), consisting of wells coated with 1 μg/mL, 2 μg/mL, and 5 μg/mL streptavidin concentrations, washing solution was added. To a second set of wells (Set 2), HFE 7200 solvent was added. To the third set of wells (Set 3), a 10 % (w/v) solution of ImR dissolved in HFE 7500 was added and incubated for 2 min at RT and then decanted. Set 3 wells were then baked for 5 min at 50 ^{o}C. To remove the resist, Set 3 wells were washed in HFE 7200 four times for 3 min each while shaking, which mimics the processing conditions of ImR removal after each patterning cycle. The wells of Sets 1 and 2 remained filled with buffer and HFE solvent, respectively, for the whole duration of processing Set 3. All wells in Sets 1, 2, and 3 were finally decanted and rinsed first with washing solution (pH 8.25) and then with distilled water before testing for biotin binding capacity.

To test the binding capacity of streptavidin immobilized in the wells, 100 μL of 100 ng/mL BSA multiply conjugated with biotin in phosphate buffer (16 mM Na_2HPO_4, 34 mM KH_2PO_4, pH 7.0) or 100 μL of blocking solution (phosphate buffer, pH 7.0, containing 10 mg/mL BSA) were added to the wells and incubated for 30 min at RT. Following streptavidin-biotin binding, wells were rinsed four times with TWEEN washing buffer (10 mM Tris-HCl, 150 mM NaCl, 0.05 % TWEEN20 (v/v)). To detect the bound biotin-BSA, a solution of 250 ng/mL streptavidin-HRP in blocking solution was added to all wells and incubated for 15 min at RT while shaking. Wells were washed as described above. The presence of streptavidin-HRP was determined via addition of ABTS peroxidase substrate solution and incubation for 30 min at RT while shaking. Absorption signals were measured at 405 nm on a Labsystems Multiskan RC microplate reader.

Antibody-Antigen Interaction Compatibility Assay:

To investigate the effect of ImR and HFE solvents on antibody-antigen binding, a solution of 5 μg/mL mouse monoclonal anti-prostate specific antigen (Mab-PSA) in carbonate buffer (pH 9.2) was deposited into three separate sets of microtitration wells and incubated overnight at RT to adsorb. Wells were then washed, blocked, and processed as described above for the streptavidin-biotin binding assay. To each set of wells, 20 μL of free-PSA calibrator solutions (0, 0.39, 0.95, 2.48, and 4.9 ng/mL) and 100 μL of 5 μg/mL biotinylated anti-PSA monoclonal antibody solution in Tris-HCl buffer (50 mM Tris-HCl, 150 mM NaCl, 5 mg/mL BSA, pH 8.25) were added and incubated for 1 h at RT while shaking. Wells were then washed four times with TWEEN washing buffer. PSA, bound to the immobilized antibodies, was detected via addition of streptavidin-HRP and ABTS peroxidase substrate solution in the sequence described above for the streptavidin-biotin binding assay. Absorption was measured at 405 nm as described above.

DNA Compatibility Assay:

For testing the effect of ImR and HFE solvents on the binding of complementary DNA strands, a 20-mer probe 5'-CTGAACGGTAGCATCTTGGA-3' was selected with its complementary target sequence 5'-CCAAGATGCTACCGTTCAG-3' (Dandy et al. 2007). The probe DNA contained biotin at its 5'-terminus while the target DNA was labeled with A488 at its 5'-terminus for fluorescence detection. Both constructs were purchased post-modification from Integrated DNA Technologies, Inc.

Silicon wafers were patterned with 1 μm or 5 μm features using the parylene lift-off method as previously described (Orth et al. 2003, Torres et al. 2008). The silicon wafer chips with patterned parylene layer were first incubated with streptavidin-A568 (25 μg/mL in phosphate buffer, pH 7.0) for 30-60 min at RT, which adsorbed to the substrate, and this was followed by rinsing with phosphate buffer (pH 7.0). Nonspecific binding was prevented by incubation with blocking solution for 15 min at RT and followed by rinsing again with phosphate buffer (pH 7.0). To assemble the ssDNA monolayer, these chips were incubated with 1 μM biotinylated DNA probe in phosphate buffer for 30-45 min at RT, followed by rinsing three times with phosphate buffer (pH 7.0). Separate chips were then incubated with a solution of phosphate buffer (pH 7.0), HFE 7200, or ImR for 5 min at RT. In the sample with ImR, the resist was baked for 5 min at 37 ^{o}C and then removed via three separate washes with HFE 7200. To test the capacity for binding complementary DNA strands, the sample chips were rinsed three times with phosphate buffer (pH 7.0) and incubated with 0.75 μM A488-labeled target DNA in phosphate buffer for 30 min at 37 ^{o}C followed by 15 min at RT to allow for DNA hybridization. The sample chips were then incubated with blocking solution and the parylene layer was peeled off. The remaining DNA patterned arrays were imaged using a x63 (NA of 1.4) oil immersion objective lens on a Zeiss 710 confocal microscope. A488-target DNA was excited using the 488 nm line of an argon laser. Streptavidin-A568 was excited using a 561 nm laser line. Acquired images were processed with ImageJ software.

Assay for Protein Stability over Repeated Cycles of Imprint Lithography:

This assay assessed the stability of immobilized proteins undergoing multiple cycles of resist application and removal with ImR and HFE solvents. Prior to immobilizing proteins, silicon wafers were first hydrophylized for 20 min in Piranha solution (1:1 v/v concentrated H_2SO_4 : 30 % H_2O_2) and then thoroughly washed with distilled water. *Caution: Piranha is a very strong oxidant and should be handled with care.* After drying the wafers under a stream of N_2, they were immersed in 2 % (v/v) aqueous APTES for 20 min at RT. Wafers were gently washed, dried with N_2, and baked for 20 min at 120 ^oC. Then, one wafer was incubated with phosphate buffer (pH 7.0) containing 25 μg/mL of a biotinylated-BSA for 1 h at RT, while a second wafer was incubated with 25 μg/mL BSA solution for blank measurements. After this step of protein adsorption, both wafers were washed with phosphate buffer (pH 7.0) and blocking solution for 1 h at RT. After rinsing with washing solution containing 150 mM NaCl (pH 8.25) and distilled water, the wafers were then dried and a piece of each was cleaved off to be kept as a control. The remaining wafers were spun-cast with ImR, baked for 5 min at 50 ^oC, and developed with HFE 7200 to remove the resist.

The resist application/removal cycle described above was repeated up to ten times. A piece was cut from each wafer following 1, 2, 4, 6, 8, and 10 cycles. All wafer pieces were then covered with 5 μg/mL streptavidin-A546 in blocking solution, and incubated for 30 min at RT. After washing with phosphate buffer (pH 7.0) containing 0.05 % (v/v) TWEEN20 and distilled water, the chips were dried with N_2 gas. The stability of the adsorbed protein to repeated resist application/removal cycles was evaluated by fluorescence intensity measurements on images (5 per sample) acquired via an Axioscope 2 Plus epifluorescence microscope facilitated with a Sony Cyber-Shot digital camera and processed with the ImagePro Plus software.

Fabrication of Protein Arrays:

Patterned arrays containing one or two different proteins were fabricated as follows. ImR was spun-cast from solution in HFE 7500 onto a silicon substrate to yield a *ca.* 200 nm polymer film. The film was imprinted at room temperature as described above (see Figure 4.5A). A layer of APTMS was then vapor deposited using an Applied Microstructures MVD100 vapor deposition tool. The self-assembling monolayer of APTMS is used to provide reactive (-NH) groups at the wafer surface for biomolecule adhesion. Protein solutions containing 25 μg/mL of either DNP-BSA or biotin-BSA in phosphate buffered saline (PBS, pH 7.4) were prepared. The first protein solution was incubated for 1h at RT on the wafer surface before being rinsed with additional PBS. Following deposition of the first protein, the resist was removed using washes with HFE 7200 while shaking. Onto the first patterned protein layer, another layer of ImR was spun-cast and patterns were then imprinted offset from the initial protein layer. APTMS was once again vapor deposited on the surface of the resist. The second protein solution was incubated for 1 h at RT on the wafer surface before being rinsed with PBS and removing the resist with HFE 7200.

After these two distinct steps of protein immobilization, photoresist was removed using 10 min washes with HFE 7200 while shaking. Then, to prevent nonspecific binding of fluorophores, wafer chips were incubated with PBS blocking solution (PBS, 10 mg/mL BSA, pH 7.4) for 15 min at RT followed by rinses with PBS. For detection of each protein, fluorescently labeled components (25 μg/mL in PBS) were added in separate incubations with the wafer chips for 30-45 min each at RT followed by rinsing with distilled water between each fluorophore addition. Biotin-BSA was detected with Streptavidin-A568 and DNP-BSA was detected with A488-IgE specific for DNP. Fluorescence microscopy was performed using a Zeiss 710

confocal microscope with the same lens and lasers described above for the DNA compatibility assay with A488 and A568 fluorophores. Acquired images were processed with ImageJ software.

Cell Culture:

Rat basophilic leukemia (RBL-2H3) cells (Barsumian et al. 1981) were maintained in a monolayer culture in Minimum Essential Medium (MEM) from Invitrogen (Carlsbad, CA) supplemented with 20 % Fetal bovine serum (FBS), purchased from Atlanta Biologicals (Lawrenceville, GA), and 10 μg/mL gentamicin sulfate, purchased from Invitrogen. Cells were harvested with trypsin-ethylenediaminetetraacetic acid (trypsin-EDTA, Invitrogen, Carlsbad, CA) three to five days after passage (Pierini et al. 1996).

Ligand-Mediated Cell Patterning:

A layer of ImR was imprinted atop a silicon substrate. A solution of 25 μg/mL of DNP-BSA, conjugated to cyanine fluorescent dyes (Cy3-Cy5), in PBS was deposited and incubated with the substrate for 1 h at RT for protein adsorption. The resist was removed, using washes in HFE 7200, leaving behind the patterned DNP-BSA Cy3-Cy5. RBL-2H3 cells were first sensitized by incubating for 40-60 min at 37 ^{o}C with 2-3 μg/mL A488-IgE, specific for DNP, then washed and re-suspended at a concentration of 1-2 x 10^6 cells per mL in buffered saline solution (BSS, 135 mM NaCl, 5 mM KCl, 1.8 mM $CaCl_2$, 1 mM $MgCl_2$, 5.6 mM glucose, 20 mM HEPES, pH 7.4) supplemented with 1 mg/mL BSA. Sensitized cells were added to the

protein patterned substrate in the center of a 35 mm Petri dish with coverglass bottom (0.16–0.19 mm; MatTek Corp., Ashland, MA), as described by Torres et al. (2008). After 30-60 min of incubation at 37 °C, cells were fixed with 4 % paraformaldehyde in PBS for 20 min followed by quenching with PBS blocking solution. After fixation, the substrates were imaged using a x63 (NA of 1.4) oil immersion objective lens on a Zeiss 710 confocal microscope. A488-IgE was excited using the 488 nm line of an argon laser and Cy3-Cy5 DNP-BSA using a 561 nm laser line. Acquired images were processed with ImageJ software.

Results:

Imprint resist (ImR) is patternable

Imprint resist (ImR) was synthesized by radical polymerization of 2,2,3,3,4,4,5,5,6,6,7,7,8,8,9,9,9-Heptadecafluorononyl methacrylate using AIBN as the radical initiator (Figure 4.1A). ImR was designed to be fluorinated enough to be processable in HFE solvents and also free of unnecessary functional groups that might react with biomolecules. The resulting polymer demonstrated sufficient solubility to be processable in both HFE 7200 and HFE 7500 solvents.

To demonstrate its capacity for patterning, ImR was tested using imprint lithography (Figures 4.1B-4.1F). During imprint lithography, a pattern is "stamped" into the resist using high pressure, rather than UV-exposure techniques required by traditional photolithography, which cause biomolecule damage. A solution of ImR in HFE 7500 was spun-cast onto a wafer surface, forming a thin film. Several parameters were varied and tested to identify the optimal set of imprint processing conditions, including temperature, pressure, imprint time, resist

Figure 4.1: **Preparation and patterning of ImR**. **(A)** Synthesis of ImR. ImR (shown in gray) patterned by imprint lithography leads to exposure of the underlying bare silicon wafer surface (white) with: **(B)** 100 μm features, **(C)** 50 μm features, **(D)** 10 μm features, **(E)** 5 μm features, **(F)** 2 μm features, and **(G)** 1 μm features.

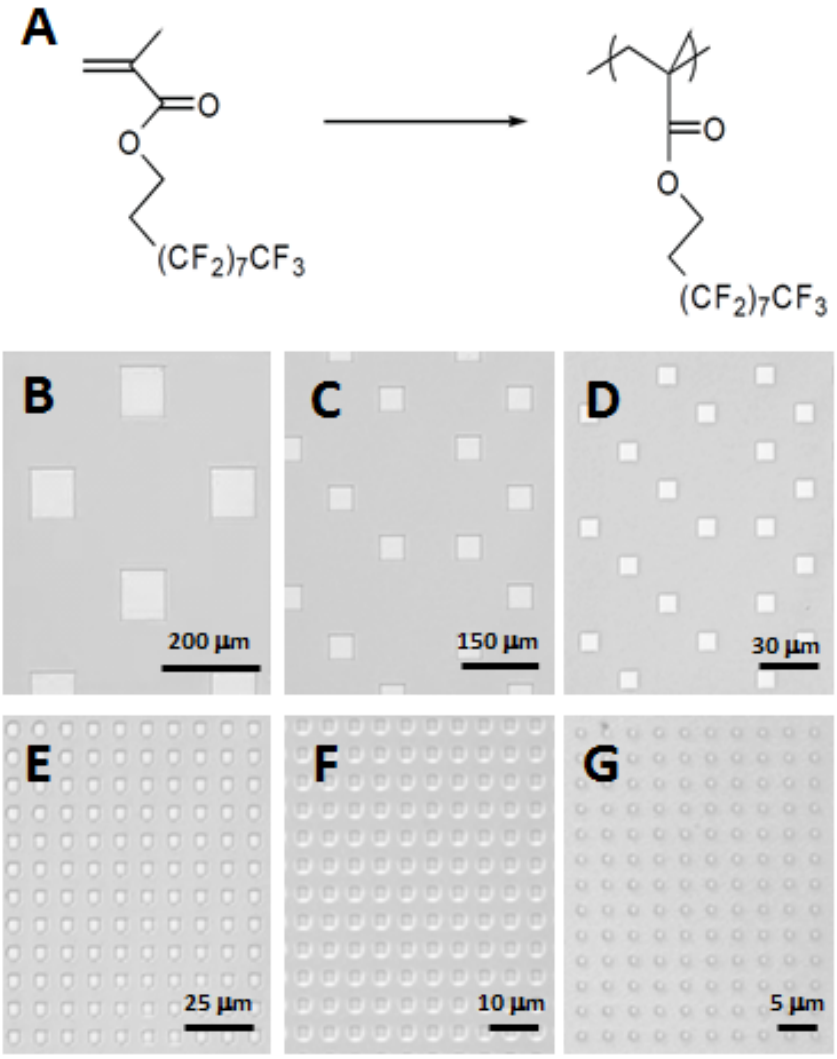
A
O
O
(CF2)7CF3
O
O
(CF2)7CF3
B
200 µm
C
150 µm
D
30 µm
E
25 µm
F
10 µm
G
5 µm

thickness, and surface treatments of both the stamp and substrate. Optimal results were achieved by imprinting at 25 ^{o}C and 300 psi for 3 min. Since this temperature is well below ImR's glass-transition temperature or melting temperature, the patterns are not formed by the traditional process of resist flowing to take the shape of the template's features. Rather, we hypothesize that patterns are formed by the resist adhering to the template more strongly than the substrate. The ImR is then pulled off with the template during imprinting. We suspect that this is facilitated by the formation of cracks in the resist at the edge of imprint features due to shear forces present between the imprinted, compressed regions and the non-imprinted regions. Square features ranging in size from 1 μm to 100 μm were obtained using a silica template with corresponding features and *ca.* 200 nm relief, as shown in Figures 4.1B-4.1F.

ImR is compatible with streptavidin patterning and with PSA monoclonal antibody patterning

We examined the capacity of ImR to pattern binding-active proteins. Specifically, a streptavidin-biotin assay was employed to determine the effect of ImR and HFE solvents on binding between immobilized streptavidin and a biotinylated ligand. For the assay, three sets of samples were evaluated (see Materials & Methods), and ImR and HFE solvents were deposited onto adsorbed streptavidin so as to mimic the processing steps required for imprint patterning. The capacity of streptavidin to bind biotin-BSA following exposure to HFE 7200 or ImR in HFE 7500 was tested and compared to a control set which received only buffer (Figure 4.2A). The amount of biotin bound in each well was detected using HRP-streptavidin conjugate and a chromogenic peroxidase substrate (H_2O_2/ABTS) to produce measurable signal.

Figure 4.2: Effect of HFE solvent and ImR application/removal onto the binding capacity of immobilized proteins. Wells coated with **(A)** streptavidin or **(B)** anti-PSA antibody were incubated with washing solution (control set; closed squares), with HFE 7200 (open circles), or were subjected to ImR application and removal (open triangles). **(A)** Streptavidin's capacity to bind its biotin ligand was then tested by applying a sandwich type assay for biotinylated-BSA as described in the Methods section. Concentrations of streptavidin solutions to coat wells are indicated. Blank values obtained using coated control wells, not incubated with biotinylated-BSA, are shown (closed circles). Data represents the mean of four separate trials. **(B)** Detection of free-PSA after application of a sandwich type assay, described in the Methods section, to the wells coated with anti-PSA antibody. Concentrations of free PSA incubated with the coated wells are indicated. Blank signal values have been subtracted from the values of all three treatment conditions. Data represents the mean of three separate trials. All error bars correspond to ± SD.

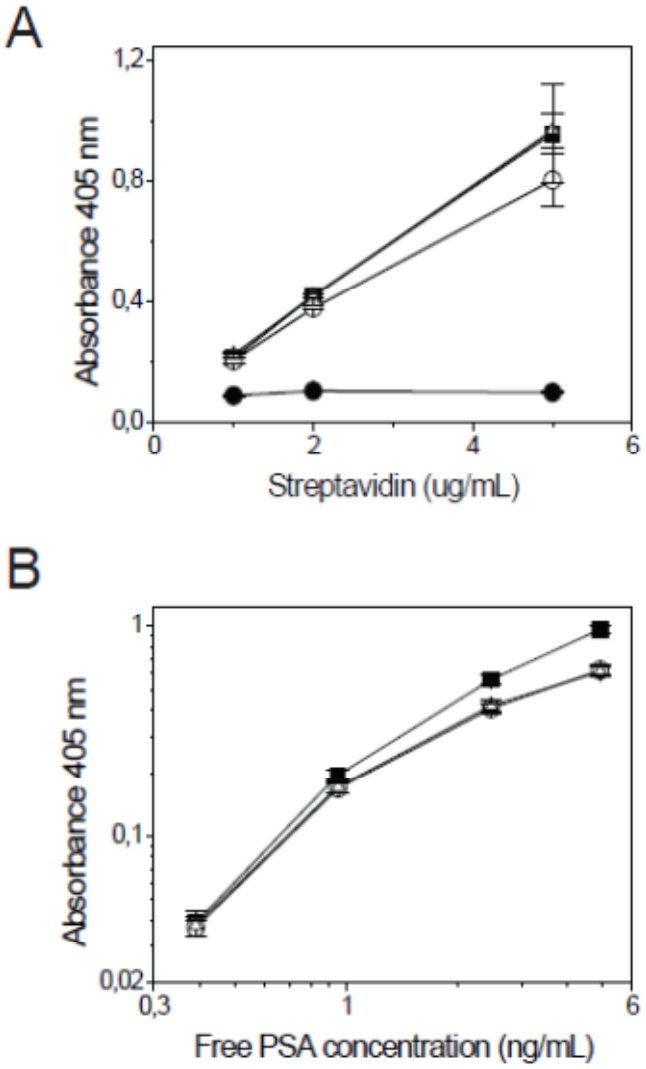
A
1,2
0,8
0,4
0,0
Absorbance 405 nm
0
2
4
6
Streptavidin (ug/mL)
B
1
0,1
0,02
Absorbance 405 nm
0,3
1
6
Free PSA concentration (ng/mL)

As shown in Figure 4.2A, the immobilized streptavidin was not affected by the resist application/removal procedure. At each streptavidin concentration, the optical density (OD) values for those samples treated by ImR application/removal (open triangles) are within standard deviation of the respective control samples treated only with washing solution (open squares), which suggests that the binding capacity, and thus the structure, of the immobilized streptavidin was not significantly altered by the addition and removal of ImR. However, it should be noted that samples treated solely with HFE solvent (open circles) produced a slight decrease (5-18 %) in the binding capacity of immobilized streptavidin. This effect could be ascribed to the fact that the solvent remained in contact with the streptavidin in Set 2 wells for the whole duration of the resist application, bake, and removal required for Set 3 wells (a total time of approximately 20 min). Whereas, in the case of ImR treated samples (Set 3 wells), this resist layer may have played a protective role against the solvent effect seen in the Set 2 wells. OD values from control wells incubated with non-biotinylated-BSA (blanks) are shown in Figure 4.2A as closed circles. In addition, separate blanks involving wells treated with HFE 7200 or ImR and non-biotinylated-BSA were tested (data not shown) and the OD values obtained from these trials were not statistically different from the blank values shown.

The capacity of PSA monoclonal antibody to bind PSA following exposure to HFE solvents and ImR was investigated. Similar to the streptavidin-biotin binding assay described above, HFE 7200 or ImR in HFE 7500 was placed onto immobilized anti-PSA antibody under conditions that mimic lithographic processing conditions. Following this, a sandwich type assay involving the addition of both PSA standards and biotinylated anti-PSA antibody was performed. The presence of biotinylated anti-PSA antibody was then determined using addition of streptavidin-HRP and incubation with ABTS peroxidase substrate. These results were compared

with those from the control samples, which did not receive HFE solvent and/or ImR applications (Figure 4.2B). At low PSA standard concentrations (< 1 ng/mL), the absorbance values for the control (open squares), HFE 7200 treated (open circles), and ImR treated (open triangles) samples are similar. However, at higher PSA standard concentrations (2.48 and 4.9 ng/mL), both the HFE 7200 and resist treated samples show a similar slight, yet significant, decrease in absorbance values as compared to samples incubated with washing solution only (control). In addition, blanks comprising wells treated with non-biotinylated anti-PSA antibody were tested and confirmed binding specificity for each experimental condition. These values were subtracted from their corresponding preparation condition – washing solution (control), HFE 7200, or ImR in Figure 4.2B. Thus the signals obtained from each experimental set are indeed due to the specific binding of biotin or PSA.

ImR is compatible with immobilized oligonucleotides

A DNA hybridization assay was performed to determine the effects of ImR and HFE solvents on patterned single-stranded DNA. A 20-mer DNA probe and its complementary target sequence were selected for this assay because they anneal stably at RT (Dandy et al. 2007). Additionally, the DNA probe was synthesized with biotin at the 5'-terminus to serve as a linker. For fluorescence detection, the target complementary DNA strand was labeled with A488 at the 5'-terminus.

Square arrays, formed using the parylene lift-off patterning method (Orth et al. 2003, Torres et al. 2008), were chosen to pattern the initial streptavidin protein layer. To confirm uniform adsorption of the protein to the silicon wafer surface, the streptavidin was conjugated to

A568 for visualization. The biotinylated DNA probe was incubated with the immobilized streptavidin. Samples then underwent treatment with control buffer, HFE solvent, or ImR application and removal so as to mimic lithographic processing techniques. Following treatment, the complementary ssDNA target-A488 was added to the biotin-DNA probe by first relaxing the DNA strands at 37 ^{o}C and then allowing them to hybridize at RT.

As visualized with fluorescence microscopy, neither treatment with HFE solvent nor ImR impeded the capacity of the target DNA-A488 strand to bind to the complementary DNA probe (Figure 4.3A). Expression of the DNA A488 target strand mirrors the expression of the underlying streptavidin-A568 with similar abundance whether treating with control buffer, HFE solvent, or ImR. This suggests that the ssDNA is not significantly degraded by the HFE solvent and ImR materials or by the treatment conditions, as DNA hybridization occurs readily. It should be noted, however, that the physical application and removal of ImR may partially remove the adsorbed streptavidin-ssDNA complex, as evidenced by the heterogeneous appearance of both probe and target DNAs in Figure 4.3A. Covalent binding between the surface and the initial streptavidin layer may prevent this loss of protein-ssDNA as we have observed in other experiments (data not shown). Additional controls were performed to confirm binding specificities and to rule out bleed through from green to red channels (Figures 4.3B-4.3E). In particular, when Cy3-Cy5 BSA was adsorbed to the wafer surface in place of streptavidin-A568, neither the biotin-DNA probe nor the complementary target DNA-A488 bound to the patterns (Figure 4.3E). Similarly, omission of the biotin-DNA probe prevented binding of the complementary target DNA-A488 to the adsorbed streptavidin proteins (Figure 4.3D).

Figure 4.3: Effect of HFE 7200 and ImR application/removal on the binding of complementary strands of DNA. A biotinylated DNA probe was immobilized onto the wafer surface by binding to adsorbed streptavidin-A568. To determine stability of the probe DNA, a complementary target DNA-A488 strand was then added and detected using fluorescence microscopy. **(A)** Prior to incubation with A488 target DNA strand, the surfaces were treated with control buffer (phosphate buffer, pH 7.0), with HFE solvent, or ImR application and removal. Control tests **(B-E)** were performed to determine the specificity of binding. For control tests, conditions were changed from the original assay as follows: **(B)** adsorbed streptavidin-A568 only on a patterned surface, **(C)** target DNA-A488 bound to a non-fluorescently labeled avidin protein and probe biotin-DNA, **(D)** omission of probe biotin-DNA, and **(E)** use of a non-avidin protein (Cy3 BSA) as the initial layer adsorbed onto the patterned surface. Scale bars represent 10 μm.

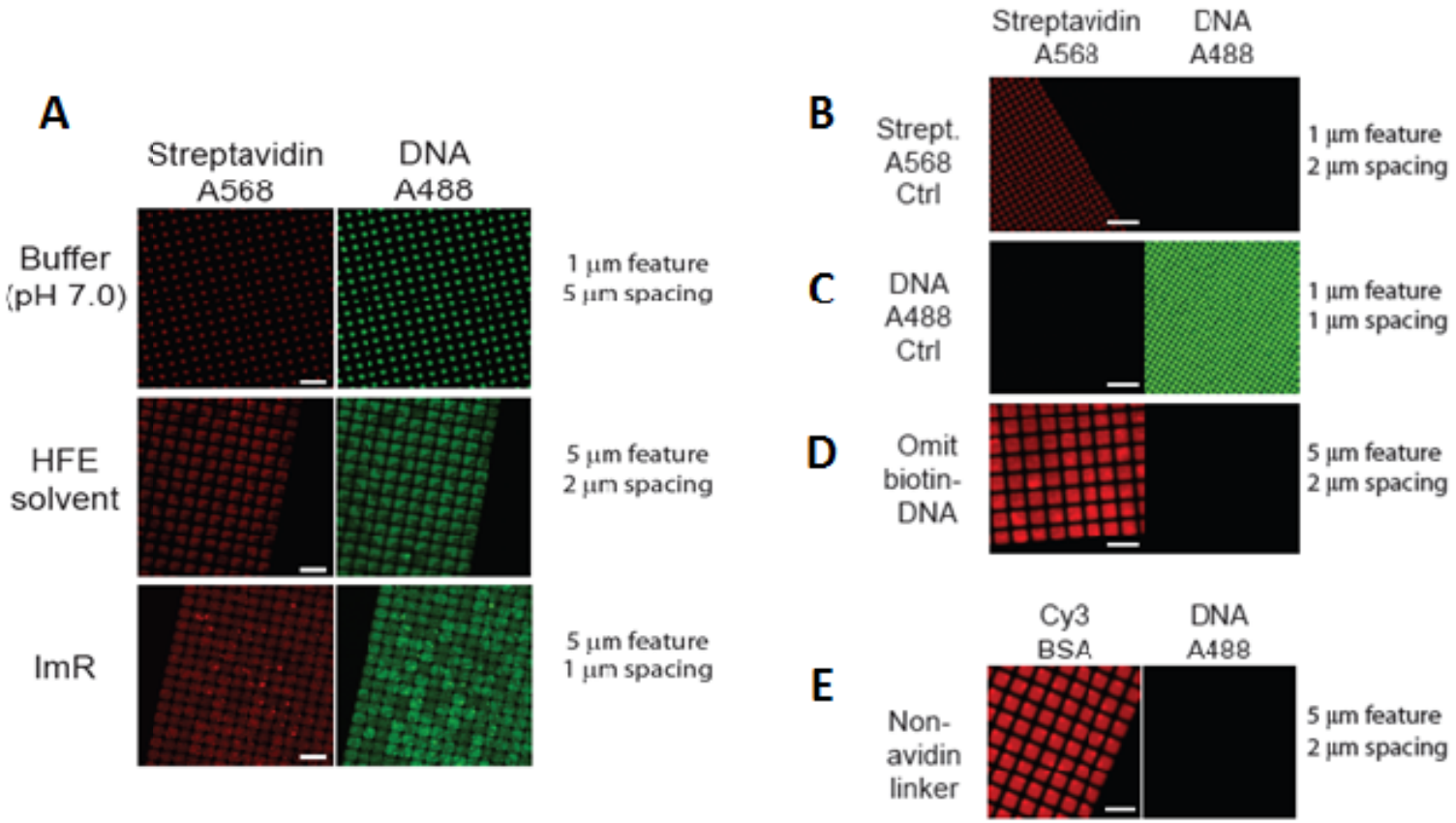
A
Streptavidin A568
DNA A488
Buffer (pH 7.0)
1 µm feature
5 µm spacing
HFE solvent
5 µm feature
2 µm spacing
ImR
5 µm feature
1 µm spacing
B
Streptavidin A568
DNA A488
Strept. A568 Ctrl
1 µm feature
2 µm spacing
C
DNA A488 Ctrl
1 µm feature
1 µm spacing
D
Omit biotin-DNA
5 µm feature
2 µm spacing
E
Cy3 BSA
DNA A488
Non-avidin linker
5 µm feature
2 µm spacing

Repeated imprint lithography cycles do not adversely affect previously deposited proteins

Further tests were performed to determine the potential of using ImR and imprint lithography for sequentially patterning multiple biomolecules. Biotin-BSA solution was adsorbed onto a clean, aminosilanized silicon wafer surface. ImR was then applied and removed with HFE solvents multiple times to mimic lithographic patterning techniques. A small piece was cut off from the wafer at 0, 1, 2, 4, 6, 8, and 10 cycles of resist addition and removal. These ten cycles serve to imitate the processing effects of imprinting ten subsequent resist layers onto the first biomolecule deposited. The chips were then incubated with streptavidin-A546 for detection of the protein remaining on the chip surface. The stability of protein adsorption after repeated resist application and removal cycles was evaluated by fluorescence intensity measurements. As shown in Figure 4.4, the relative fluorescence intensity of streptavidin-A546 bound to biotin-BSA (white columns) did not vary significantly over the course of ten resist application and removal cycles as compared to the original surfaces (at 0 cycles). A series of negative control wafer chips involving adsorption of non-biotinylated BSA (blank; black columns) in place of biotin-BSA was also performed and tested in parallel. These blank chips result in considerably lower signal values compared to those coated with biotin-BSA, further validating that the fluorescent signal measured was due to specific streptavidin-biotin binding.

ImR can be used for orthogonal patterning of multiple proteins

To demonstrate the potential of ImR and imprint lithography for multi-component biomolecule patterning, protein arrays containing one or two different proteins were fabricated (Figure 4.5). Clean silicon wafers coated with ImR were patterned using the imprint lithography

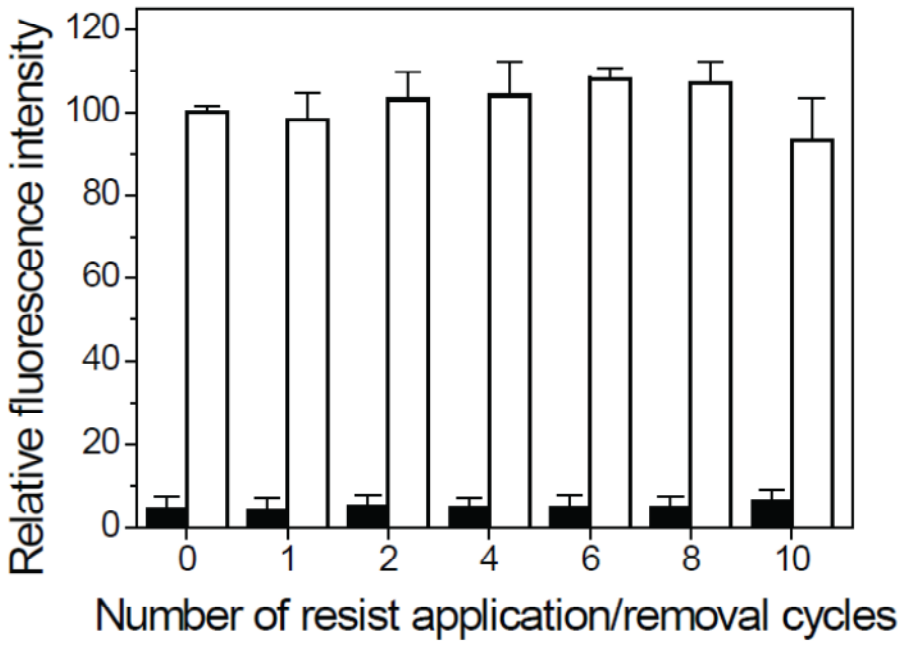

Figure 4.4: Effect of repeated lithography cycles on deposited protein. Fluorescence intensity values obtained from aminosilanized Si surfaces coated with BSA (black columns) or biotinylated-BSA (white columns) and subjected to repeated ImR application and removal cycles before being incubated with streptavidin-A546. The fluorescence values are expressed as percentages of the control sample value at 0 cycles. Data represents the mean of five separate experiments. Error bars denote SD.

Figure 4.5: Preparing multi-protein arrays. (A) Schematic for patterning a multi-protein array by imprint lithography using ImR and HFE solvent. **(B-E)** Fluorescence microscopy images of single and two-protein patterns prepared in this manner. **(B)** 100 μm square of patterned biotin-BSA labeled with streptavidin-A546. **(C)** 20 μm squares of patterned DNP-BSA labeled with (anti-DNP) A488-IgE. **(D)** A two-protein array of separate 20 μm squares and **(E)** a two-protein array with 10 μm square features within a 100 μm square feature. White arrows highlight spots of residual resist and/or formation of flaps along feature edges. For multi-protein arrays **(D & E)**, images of each fluorophore were taken on separate channels in the microscope and then merged to produce the images provided.

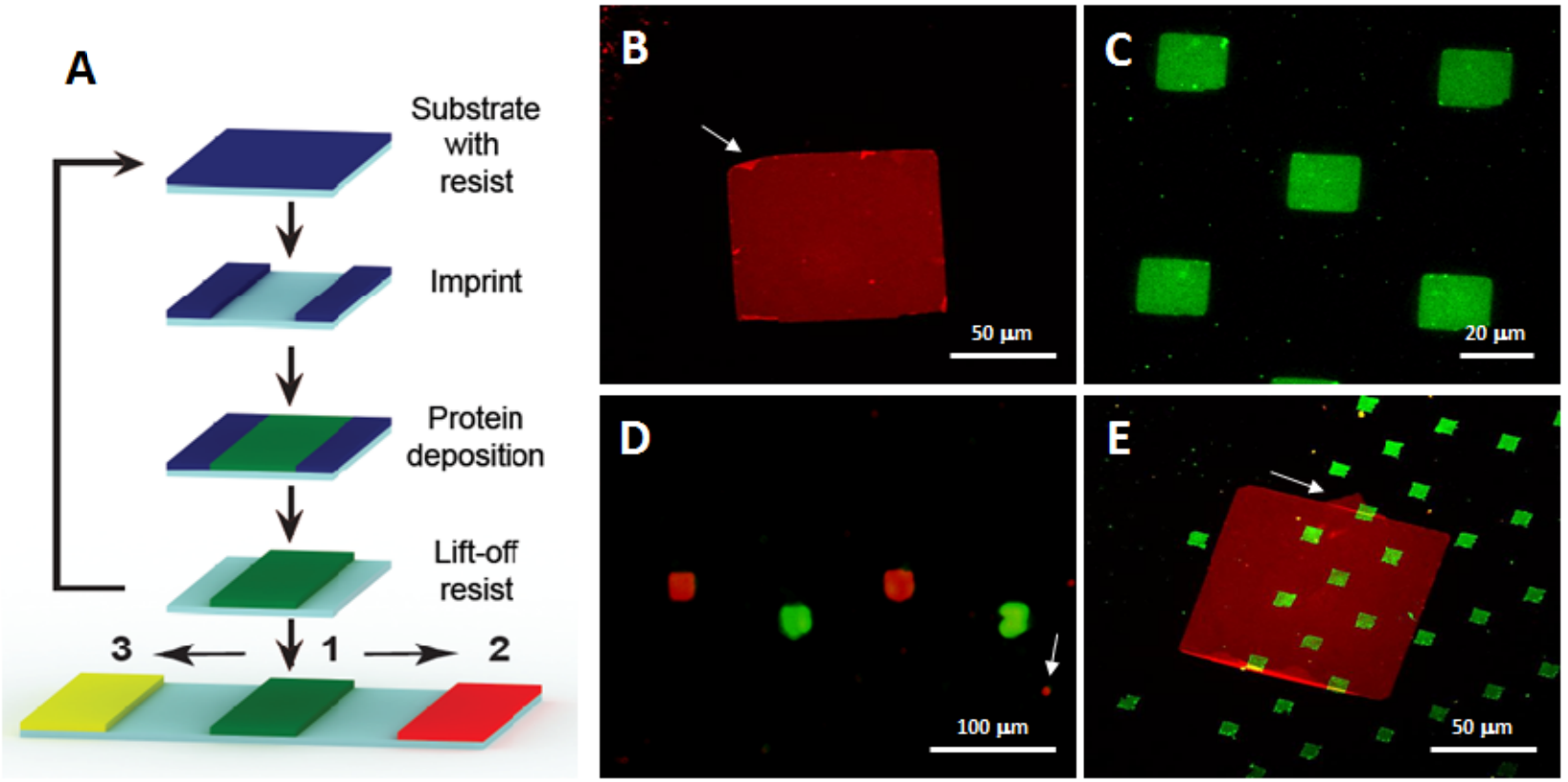
A
Substrate with resist
Imprint
Protein deposition
Lift-off resist
3
1
2
B
50 µm
C
20 µm
D
100 µm
E
50 µm

technique described in the Methods section and Figure 5A. Following aminosilanization of the patterned surface, the first protein solution was allowed to adsorb across the entire patterned area (Figures 4.5B & 4.5C). Lift-off was performed by washing the wafer repeatedly with HFE solvent, which allowed for removal of the resist while retaining the adsorbed patterned protein. For multi-protein patterning, a new layer of ImR was then applied to coat the entire wafer. New patterns were imprinted offset by 50-100 μm from the original protein patterned underneath. After deposition of a second protein sample, the resist was removed.

To demonstrate multi-protein patterning with ImR and HFE solvent, DNP-BSA and biotin-BSA proteins were patterned in sequential layers onto silicon wafer surfaces with feature sizes ranging from 1 μm to 100 μm. Following both rounds of protein deposition, separate solutions of fluorescently labeled (anti-DNP) IgE and streptavidin were added to bind specifically to their respective ligands. Patterns were then imaged with fluorescence microscopy. Example images of single protein patterns and two-protein arrays are depicted in Figures 4.5B-4.5E. It should be noted that small amounts of residual resist occasionally remained on the wafer following final resist removal, and this appeared as small spots between the features and/or flaps adjacent to feature edges. These spots typically occur on or close to the locations of our alignment marks on the imprint stencil, suggesting that repeated imprinting directly onto these closely spaced marks can sometimes make it difficult to remove all of the resist. Because our imprint technique does not rely on the traditional process of resist flowing around the template's features, we attribute the formation of flaps around the edges of some features to the development of cracks at the edge of the imprint feature causing formation of misshapen features. Additionally, the competition between shear forces both above and below the resist during imprint processing may cause adjacent regions of resist, such as flaps, to remain. As

marked by white arrows in Figures 4.5B-4.5E, some labeling fluorophores can bind nonspecifically to residual resist and appear as small spots (Figure 4.5D) and/or flaps on feature edges (Figures 4.5B & 4.5E) among the protein patterns.

Aside from traditional multi-protein patterns, where multiple proteins are deposited as arrays with distinct spacing between each feature (Figure 4.5D), our patterning technique also allows fabrication of multi-protein patterns with features of one protein located within features a different protein (Figure 4.5E). Previous multi-protein patterning efforts have focused on two-protein patterns wherein one protein is deposited with discrete features and the second protein is used to fill in the surrounding background (Doh & Irvine 2004). Our approach differs from this backfill technique by providing the ability to adhere new layers of proteins within already existing layers and in a spatially defined manner. While the second round of imprinting did remove deposited biotin-BSA proteins directly below template features to allow for deposition of DNP-BSA, the remaining biotin-BSA layer remains unaffected. Addition of fluorophores after all imprinting had taken place reveals the specificity of the second protein deposition to discrete features and further demonstrates that ImR successfully protects previously adhered protein layers. This technique makes possible the ability to deposit a large number of protein layers and thus fabricate much more complicated arrays.

ImR is compatible with ligand-mediated cell patterning

Further tests were performed to demonstrate the capabilities of this resist and patterning method with ligand-mediated cell patterning. Previous studies have shown that RBL cells sensitized with anti-DNP IgE display parallel clustering of receptor-bound IgE above patterns of

DNP ligands (Orth et al. 2003, Torres et al. 2008). We examined the capacity of ImR to pattern DNP-labeled proteins such that cells retain their capacity to interact with these proteins. A single protein array of Cy3-Cy5 labeled DNP-BSA was patterned onto an aminosilanized wafer surface with ImR as described in the Methods section. RBL-2H3 mast cells, sensitized with A488-IgE specific for DNP, were allowed to settle onto the wafer surface for several minutes before undergoing fixation and imaging. As shown by Figure 4.6, the A488-IgE-receptor complexes on these cells cluster over the patterned DNP-ligands, consistent with previous studies. These results indicate that any residual polymeric resist or HFE solvents left behind on the patterned silicon surface do not prevent cell adhesion or mobility of the cell's surface proteins. Thus, our processing conditions for imprint patterning are also biocompatible with ligand-mediated cell patterning, which points to its use in fabricating multi-protein patterns for fundamental studies of protein interactions on cells.

Discussion:

Previously, we synthesized fluorinated resists and light-emitting materials and showed that they can be processed in HFE solvent to fabricate organic electronic devices (Lee et al. 2008, Taylor et al. 2009, Lee et al. 2010, Zakhidov et al. 2008). Sarkari et al. (2003) also have shown these HFEs to be applicable to the patterning of proteins, whose delicate structures can easily be damaged with traditional lithography solvents and techniques. Based on the favorable results obtained in these previous studies, the idea of benign lithographic processing was extended more generally to biomolecule patterning. We chose a resist structure, which would be fluorinated enough to be processable in HFE solvents and which was also free of unnecessary

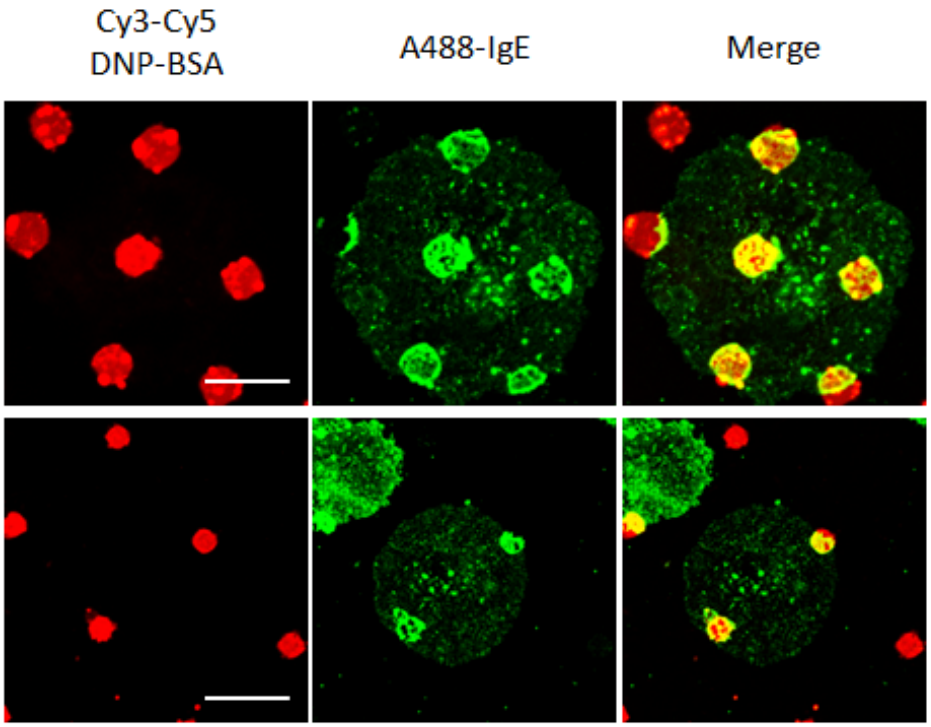

Figure 4.6: Cells interacting with an ImR patterned surface. Fluorescence microscopy images from different experiments performed under the same conditions in which RBL-2H3 were cells sensitized with A488-IgE (green) and incubated with patterned Cy3-Cy5 DNP-BSA (red). These proteins were patterned into 1-5 μm features using ImR and imprint lithography techniques. Images are representative of 4 individual experiments. Scale bars represent 10 μm.

functional groups that might interact with biomolecules. We synthesized ImR (Figure 4.1A) as a potential resist for this application. Upon further testing, ImR also proved to be soluble in HFEs.

We selected imprint lithography to demonstrate the lithographic patterning properties of this processing system, because of its capacity to create reproducible patterns of small features over a large area and its previous application to protein patterning (Hoff et al. 2004). While the use of UV radiation is not required for imprint lithography, this technique typically uses harsh resists and developers, much like photolithography methods, which can easily damage and denature biomolecules. Here, we replace the traditional harsh processing conditions with benign fluorinated ImR and with unreactive HFEs as processing solvents.

Traditional imprint lithography requires a moldable resist, such that it "flows" into the recesses of the imprint stamp during imprinting and releases from the stamp afterwards. Imprinting occurs through applied pressure of the stamp and simultaneous heating of the resist. Typically, samples are significantly heated to temperatures above the glass transition temperature (Tg) of the resist material. However, for biomolecule patterning applications, significant heating would damage and denature the proteins and DNA. Therefore, we developed an imprinting process that requires no heating and can be conducted in its entirety at room temperature. As this process does not rely on the flow of the resist, large features and small features can be formed with ease, both adjacent to and placed within one another.

Additionally, we investigated different surface treatments for both the stamp and substrate, including (1H,1H,2H,2H-perfluoroctyl)trichlorosilane (FOTS), oxygen plasma treatment, Piranha cleaning, and using untreated silicon with a native oxide. Traditionally, patterns are stamped into the imprint resist layer to give a degree of feature relief (Figure 4.5A).

The resist is then anisotropically etched to remove the remaining resist residue in the thinner regions to produce patterns, which are clean to the substrate. Our low-temperature process results in practically clean removal of the resist from the substrate without the need for an additional 'descum' etch. Samples of ImR post-imprinting and are shown in Figures 4.1B-G.

Both ImR and HFEs were demonstrated to be benign to biomolecules in that they did not significantly deteriorate protein and/or DNA binding capacities (Figures 4.2-4.3). Varying concentrations of streptavidin, a robust protein widely used for immobilization of biomolecules (Diamandis & Christopoulos 1991), were liberally exposed to ImR and HFE solvents under conditions which imitate lithographic processing. The capacity of streptavidin, post ImR exposure, to bind biotin was experimentally measured and found to be similar to that of streptavidin without any exposure to resist or solvent (Figure 4.2A). While longer time exposure to HFE solvent appeared to produce a small decrease in the binding capacity of the immobilized streptavidin, use of ImR and HFE solvents on streptavidin under our fabrication conditions did not significantly alter the capacity of the protein to bind to the biotin moiety. Similarly, we have shown the ability to hybridize complementary DNA strands following treatment with ImR and HFE solvents (Figure 4.3A), indicating that the probe DNA strand was not significantly altered by the treatment conditions. Together, these results show that both ImR and HFE solvents are compatible with biomolecule patterning.

As another sensitive test for binding capacity dependent on protein structure, a similar assay was performed wherein an anti-PSA antibody was exposed to HFE solvent and/or ImR (Figure 4.2B). At the higher PSA concentrations, both the solvent and resist treated samples produce a small decrease in absorbance values as compared to the buffer controls. These results indicate that the anti-PSA binding region is more vulnerable to resist application/removal

processing as compared to streptavidin, consistent with a more complicated and sensitive binding structure. While streptavidin binds biotin via non-covalent interactions deep within the β-barrel structure (Hendrickson et al. 1989), anti-PSA binding sites contact PSA epitopes at four to five individual segments of the protein structure (Stura et al. 2011). Thus, the binding site of streptavidin is both more protected and requires fewer interactions with tertiary protein structure as compared to anti-PSA antibodies.

A major advantage of our imprint patterning technique is its capacity for multi-component patterning. The ImR resist and HFE solvents are inherently benign to biomolecules, and we found that these imprinting materials can be applied at least 10 times without adversely affecting the underlying biotinylated protein layers to bind streptavidin (Figure 4.4). Thus, biomolecules deposited prior to resist application are not significantly damaged by undergoing additional rounds of patterning. We directly demonstrated our technique's capacity for fabricating multi-protein patterns (Figures 4.5B-4.5E). To detect for each distinct protein, we relied on bio-specific interactions: biotin binding to streptavidin and DNP binding to anti-DNP IgE. We further showed that patterns can be fabricated with multi-protein components in separate feature arrays or as features within other features. With this technique, it should be possible to fabricate much more complicated multi-component biomolecule arrays for a variety of applications.

One such application, the capacity to fabricate patterns biocompatible with cells, can be valuable for tissue engineering applications (Atala 2009) as well as fundamental cell studies. To this end, we investigated cellular interactions with imprinted surfaces. As demonstrated with RBL-2H3 mast cells and DNP-BSA protein, which was patterned using ImR and HFE solvents (Figure 4.6), we found that the cells showed no signs of abnormal morphology or cytotoxicity.

Furthermore, the cells exhibited the expected response of (anti-DNP) IgE-receptor clustering over the DNP patterns. These results point to the use of this ImR and patterning method in fabricating multi-protein patterns for investigations of more complicated cellular mechanisms, such as cellular responses to multiple, spatially defined stimuli.

Although our patterning technique advantageously addresses many of the challenges of biomolecule patterning with traditional lithography methods, including biocompatibility, high costs, and long production times, the full potential has not yet been reached. We were able to pattern features with dimensions as small as 1 μm, whereas tens of nanometers should be possible with available imprint lithography technology. Our current technique was limited both by the feature dimensions of our stencil and our characterization capability. In particular, the diffraction limit and the high reflectivity of silicon wafers can make it difficult to discern submicron features with fluorescence microscopy. However, fabrication of smaller features and on silicon and glass surfaces would allow for broader applications of this patterning method. We found that alignment marks, while necessary for multi-component patterning, allowed stray depositions: As more layers of ImR were applied and imprinted in the alignment areas, it became more difficult to remove completely the resist following each imprint cycle in these areas. Repeated imprinting on top of the same alignment marks may alter the shear forces of the silicon surface in those areas, providing a stronger bind between the silicon and the ImR. Further evidence of shear forces affecting our pattern resolution includes the formation of residual resist flaps and spots among the features. Additional improvements in this technique will focus on both higher resolution and higher fidelity multi-component patterns.

Conclusions:

We described an approach for multi-biomolecule patterning based on a highly-fluorinated polymer resist (ImR) that is processable in HFE solvents. We showed ImR to be patternable by imprint lithography at room temperature, producing feature sizes down to 1 μm. Both ImR and HFE solvents are largely benign to biomolecules, including proteins and DNA, and suitable for use in cell studies. We further used this methodology to pattern single-protein and two-protein arrays of DNP-BSA and biotin-BSA, demonstrating its potential for multi-component patterning. In addition, we showed that the surface immobilized biomolecules can undergo at least 10 cycles of lithographic processing with negligible effects. Thus, this versatile method makes possible the fabrication of arrays with multiple, spatially defined biomolecules, while avoiding many of the problems associated with more traditional lithographic approaches.

Specific Experimental Contributions:

PGT, CN, and J-KL carried out synthesis and characterization of ImR. Protein-ligand and antibody-antigen interaction compatibility, as well as protein stability over multiple cycles of imprint lithography, tests were performed by MC, PSP and SEK, while KMM determined DNA complementary strand compatibility. PGT, CN, and KMM fabricated protein arrays and examined this method's capacity for ligand-assisted cell patterning.

Acknowledgements:

The authors acknowledge support from the National Science Foundation FlexEBio IGERT Fellowship (Grant 0654112; PGT & KMM), the National Science Foundation (Materials World Network DMR-0908994; PGT & CN), and the National Institute of Health (Grant AI018306; KMM). This work was performed in part at the Cornell Nanoscale Facility (CNF), a member of the National Nanotechnology Infrastructure Network, which is supported by the National Science Foundation (Grant ECS-0335765). We further appreciate support from the Cornell Microscopy and Imaging Facility (MIF) and the Cornell Nanobiotechnology Center (NBTC) for the use of their fluorescence microscopes. Special thanks are also given to Dr. Alexander Zakhidov (Technische Universitat Dresden, Germany) for his help with lithographic patterning; to Dr. Yosuke Hoshi (Hitachi Chemical, Japan) for his help with fluorescence microscopy imaging; and to Dr. Amit Singhai (Cornell University, USA) for his preparation of parylene coated wafer chips, advice with ligand-mediated cell patterning, and guidance with fluorescence microscopy imaging.

REFERENCES

Arrabito G and Pignataro B (2012). Solution processed micro- and nano-bioarrays for multiplexed biosensing. Anal Chem, 84: 5450-5462.

Atala A (2009). Engineering organs. Curr Opin Biotechnol, 20: 575-592.

Balla T, Spearing SM, and Monk A (2008). An assessment of the process capabilities of nanoimprint lithography. J Phys D: Appl Phys, 41: 174001-174010.

Barsumian EL, Isersky C, Petrino MG, and Siraganian RP (1981). IgE-induced histamine release from rat basophilic leukemia cell lines: Isolation of releasing and non-releasing clones. Eur J Immunol, 11: 317-323.

Bashir R (2004). BioMEMS: State-of-the-art in detection, opportunities, and prospects. Adv Drug Deliv Rev, 56: 1565-1586.

Berggren M and Richter-Dahlfor A (2007). Organic bioelectronics. Adv Mater, 19: 3201-3213.

Bettinger CJ (2009). Synthesis and microfabrication of biomaterials for soft-tissue engineering. Pure Appl Chem, 81: 2183-2201.

Blawas AS and Reichert WM (1998). Protein patterning. Biomaterials, 19: 595-609.

Christman KL, Enriquez-Rios VD, and Maynard HD (2006). Nanopatterning proteins and peptides. Soft Matter, 2: 928-939.

Dandy DS, Wu P, and Grainger DW (2007). Array feature size influences nucleic acid surface capture in DNA microarrays. Proc Natl Acad Sci USA, 104: 8223-8228.

Delamarche E, Bernard A, Schmid H, Michel B, and Biebuyck H (1997). Patterned delivery of immunoglobulins to surfaces using microfluidic networks. Science, 276: 779-781.

Diamandis EP and Christopoulos TK (1991). The biotin-(strept)avidin system: Principles and applications in biotechnology. Clin Chem, 37: 625-636.

Doh J and Irvine DJ (2004). Photogenerated polyelectrolyte bilayers from an aqueous-processible photoresist for multicomponent protein patterning. J Am Chem Soc, 126: 9170-9171.

Domachuk P, Tsioris K, Omenetto FG, and Kaplan DL (2010). Bio-microfluidics: Biomaterials and biomimetic designs. Adv Mater, 22: 249-260.

Douvas AM, Argitis P, Misiakos K, Dimotikali D, Petrou PS, and Kakabakos SE (2002). Biocompatible photolithographic processing for the patterning of biomolecules. Biosens Bioelectron, 17: 261-278.

Eichinger CD, Hsiao TW, and Hlady V (2012). Multiprotein microcontact printing with micrometer resolution. Langmuir, 28: 2238-2243.

Goudar VS, Suran S, and Varma MM (2012). Photoresist functionalization method for high-density protein microarrays using photolithography. Micro Nano Letters, 7: 549-553.

Hendrickson WA, Pahler A, Smith JL, Satow Y, Meritt EA, and Phizackerley RP (1989). Crystal structure of core streptavidin determined from multiwavelength anomalous diffraction of synchrotron radiation. Proc Natl Acad Sci USA, 86: 2190-2194.

Hoff JD, Cheng L-J, Meyhöfer E, Guo LJ, and Hunt AJ (2004). Nanoscale protein patterning by imprint lithography. Nano Letters, 4: 853-857.

Holden MA and Cremer PS (2003). Light activated patterning of dye-labeled molecules on surfaces. J Am Chem Soc, 125: 8074-8075.

Ilic B and Craighead H (2000). Topographical patterning of chemically sensitive biological materials using a polymer-based dry lift off. Biomed Microdevices, 2: 317-322.

James T, Mannoor MS, and Ivanov DV (2008). BioMEMS -- Advancing the frontiers of medicine. Sensors, 8: 6077-6107.

Joos T and Bachmann J (2009). Protein microarrays: Potentials and limitations. Front Biosci, 14: 4376-4385.

Kane RS, Takayama S, Ostuni E, Ingber DE, and Whitesides GM (1999). Patterning proteins and cells using soft lithography. Biomaterials, 20: 2363-2376.

Katz E (2006). Bioelectronics. Electroanalysis, 18: 1855-1857.

Kolodziej CM and Maynard HD (2011). Electron beam lithography for patterning biomolecules at the micron and nanometer scale. Chem Mater, 24: 774-780.

Lee J-K, Chatzichristidi M, Zakhidov AA, Taylor PG, DeFranco JA, Hwang HS, Fong HH, Holmes AB, Malliaras GG, and Ober CK (2008). Acid-sensitive semiperfluoroalkyl resorcinarene: An imaging material for organic electronics. J Am Chem Soc, 130: 11564-11565.

Lee J-K, Fong HH, Zakhidov AA, McCluskey GE, Taylor PG, Santiago-Berrios M, Abruña HD, Holmes AB, Malliaras GG, and Ober CK (2010). Semiperfluoroalkyl polyfluorenes for orthogonal processing in fluorous solvents. Macromolecules, 43: 1195-1198.

Mosbach M, Zimmerman H, Laurell T, Nilsson J, Csoregi E, and Schuhmann W (2001). Picodroplet-deposition of enzymes on functionalized self-assembled monolayers as a basis for miniaturized multi-sensor structures. Biosens Bioelectron, 16: 827-837.

Niotis AE, Mastichiadis C, Petrou PS, Christofidis I, Kakabakos SE, Siafaka-Kapadai A, and Misiakos K (2010). Dual-cardiac marker capillary waveguide fluoroimmunosensor based on tyramide signal amplification. Anal Bioanal Chem, 396: 1187-1196.

Orth RN, Wu M, Holowka D, Craighead H, and Baird B (2003). Mast cell activation on patterned lipid bilayers of subcellular dimensions. Langmuir, 19: 1599-1605.

Petrou PS, Chatzichristidi M, Douvas AM, Argitis P, Misiakos K, and Kakabakos SE (2007). A biomolecule friendly photolithographic process for fabrication of protein microarrays on polymeric films coated on silicon chips. Biosens Bioelectron, 22: 1994-2002.

Pierini L, Holowka D, and Baird B (1996). FcεRI-mediated association of 6 μm beads with RBL-2H3 mast cells results in exclusion of signaling proteins from the forming phagosome and abrogation of normal downstream signaling. J Cell Biol, 134: 1427-1439.

Pimpin A and Srituravanich W (2011). Review on micro- and nano-lithography techniques and their applications. Engineering J, 16: 37-55.

Piner RD, Zhu J, Xu F, Hong S, and Mirkin CA (1999). Dip-pen nanolithography. Science, 283: 661-663.

Pritchard DJ, Morgan H, and Cooper JM (1995). Micron-scale patterning of biological molecules. Angew Chem Int Ed, 34: 91-93.

Sarkari M, Darrat I, and Knutson BL (2003). CO_2 and fluorinated solvent-based technologies for protein microparticle precipitation from aqueous solutions. Biotechnol Prog, 19: 448-454.

Shiu J-Y and Chen P (2007). Addressable protein patterning via switchable superhydrophobic microarrays. Adv Funct Mater, 17: 2680-2686.

Stuart C and Chen Y (2009). Roll in and roll out: A path to high-throughput nanoimprint lithography. ACS Nano, 3: 2062-2064.

Stura EA, Muller, BH, Bossus M, Michel S, Jolivet-Reynaud C, and Ducancel F (2011). Crystal structure of human prostate-specific antigen in a sandwich antibody complex. J Molec Biol, 414: 530-544.

Subramanian K, Holowka D, Baird B, and Goldstein B (1996). The Fc segment of IgE influences the kinetics of dissociation of a symmetrical bivalent ligand from cyclic dimeric complexes. Biochemistry, 35: 5518-5527.

Sundberg SA, Barrett RW, Pirrung M, Lu AL, Kiangsoontra B, and Holmes CP (1995). Spatially-addressable immobilization of macromolecules on solid supports. J Am Chem Soc, 117: 12050-12057.

Svennersten K, Larsson KC, Berggren M, and Richter-Dahlfors A (2011). Organic bioelectronics in nanomedicine. Biochim Biophys Acta, 1810: 276-285.

Taylor PG, Lee J-K, Zakhidov AA, Chatzichristidi M, Fong HH, DeFranco JA, Malliaras GG, and Ober CK (2009). Orthogonal patterning of PEDOT:PSS for organic electronics using hydrofluoroether solvents. Adv Mater, 21: 2314-2317.

Torres AJ, Vasudevan L, Holowka D, and Baird B (2008). Focal adhesion proteins connect IgE receptors to the cytoskeleton as revealed by micropatterned ligand arrays. Proc Natl Acad Sci USA, 105: 17238-17244.

Willson CG & Colburn ME (2004). *U.S. Patent No. 6,719,915.* Washington D.C.: U.S. Patent and Trademark Office.

Wolf-Yadlin A, Sevecka M, and MacBeath G (2009). Dissecting protein function and signaling using protein microarrays. Curr Opin Chem Biol, 13: 398-405.

Wu CC, Reinhoudt DN, Otto C, Subramaniam V, and Velders AH (2011). Strategies for patterning biomolecules with dip-pen nanolithography. Small, 7: 989-1002.

Zakhidov AA, Lee J-K, Fong HH, DeFranco JA, Chatzichristidi M, Taylor PG, Ober CK, and Malliaras GG (2008). Hydrofluoroethers as orthogonal solvents for the chemical processing of organic electronic materials. Adv Mater, 20: 3481-3484.

Zhao S, Chen A, Revzin A, and Pan T (2011). Stereomask lithography (SML): A universal multi-object micro-patterning technique for biological applications. Lab Chip, 11: 224-230.

CHAPTER FIVE

Summary and Conclusions

Oligomerization and interactions of STIM1 leading to SOCE:

Understanding the mechanisms by which processes occur at the cellular and molecular level is critical to determining the regulation of biological pathways. As an example, Ca^{2+} mobilization has been found to be critical to a number of short term and long term intracellular processes, including protein folding, secretion, transcription, migration, signaling, and apoptosis (Berridge et al. 2003, Berridge 2009, Baba & Kurosaki 2009, Fahrner et al. 2009). Of particular importance in immune cell research is the pathway of store-operated calcium entry (SOCE), wherein Ca^{2+} released from the endoplasmic reticulum (ER) stores leads to an influx of Ca^{2+} from the extracellular environment (Baba & Kurosaki 2009). While numerous research efforts have focused on understanding the interactions of STIM1 and Orai1 to elicit SOCE, much uncertainty remains about the inter- and intramolecular mechanisms by which stromal interaction molecule 1 (STIM1) initiates SOCE.

The oligomeric state of STIM1, both at rest and following activation, remains an unresolved question. While it is now generally acknowledged that STIM1 exists as small oligomers at rest (Baba et al. 2006, Penna et al. 2008, Covington et al. 2010, He et al. 2012), the exact stoichiometry of resting STIM1 has yet to be determined. Utilizing biochemical techniques, this thesis probed the interactions of STIM1 both at rest and during SOCE. With immunoprecipitation (IP) assays and denaturing SDS/PAGE blots, we show that STIM1 exists in oligomeric states in resting cells as represented by 110 kDa and 260 kDa complex species.

These complexes may be composed of STIM1 only or include other unidentified peptides. The 260 kDa product contains at least a dimer of STIM1. In addition, we found that these STIM1 IP products are stabilized after cell lysis by the formation of disulfide bonds, as shown by our experiments with reducing agent, N-ethylmaleimide, and a homo-bifunctional crosslinker, BMH. Under non-denaturing NativePAGE conditions, we establish that non-covalent bonds are sufficient to maintain STIM1 oligomeric species in lysed cells. We postulate that the smallest NativePAGE band retained (< 480 kDa) consists of the 260 kDa STIM1 oligomeric product and at least two detergent micelles retained under the non-denaturing conditions. The larger NativePAGE IP product above 720 kDa is approximately twice the size of the < 480 kDa species, suggesting that this larger product is a dimer of the smaller complex. Upon cell stimulation with thapsigargin (TG) and consequent sustained activation of SOCE, no significant changes were seen in the STIM1 IP products retained under denaturing conditions. Under non-denaturing, native conditions, a slight shift in molecular weight was observed, which suggests a change in the overall conformation of the STIM1 species; however, no new STIM1 species were stabilized and retained under either of these conditions. These results further suggest that higher order STIM1 oligomerization, initiated by Ca^{2+} store depletion, does not depend on covalent, disulfide bond interactions. Rather, formation may depend on non-covalent bonds and/or the aid of scaffold proteins.

We made repeated efforts to identify additional components of the 110 kDa and 260 kDa STIM1 complexes. While mass spectrometry analysis and co-IPs failed to positively identify components of the oligomeric species aside from STIM1, we made significant progress in understanding the intermolecular interactions needed to form these products. Using site-directed mutagenesis, we identified Cys-437 within the CRAC activation domain (CAD) region as the

binding site between STIM1 and an unidentified 20-25 kDa polypeptide to stabilize the 110 kDa STIM1 species. Failure of mass spectrometry fingerprinting to identify any potential binding partners with confidence leads us to postulate that the 20-25 kDa polypeptide may be a fragment of the cytosolic portion of STIM1 or a novel protein.

In addition, we showed that the 260 kDa STIM1 IP product represents a homo-dimer of STIM1. The apparent 260 kDa molecular weight of the complex, based on immunoblotting results, is larger than what would be expected from a dimer formed between two 85 kDa containing proteins, suggesting that the complex either takes on a bulky conformation or includes additional protein(s) that have not been identified. We further showed that the formation of the 260 kDa product does not depend on interactions at Cys-437, indicating that disulfide bonds between cysteines within the lumen and transmembrane region of STIM1 are important for stabilization of the 260 kDa product upon cell lysis.

Previously, Park et al. (2009) identified the CAD region of STIM1 and provided supporting evidence for the role of CAD in initiating Ca^{2+} influx, including the importance of Cys-437 in regulating the rate of Ca^{2+} influx in SOCE but not STIM1 association with Orai1. Using confocal microscopy and FRET-based analysis, we confirm that C437A mutant STIM1 translocates to the plasma membrane (PM) following store depletion at a rate similar to that of wildtype-STIM1. Both constructs exhibit stimulated energy transfer with Orai1 at the PM at similar values and on similar time scales, suggesting that the 110 kDa STIM1 product, stabilized by interaction with Cys-437, is not critical for the translocation process.

We next turned our attention to characterizing the role of Cys-437 in SOCE. In their previous work, using whole-cell patch clamp analysis, Park et al. (2009) noted that STIM1-

C437G showed a dramatic reduction (~ 75%) in Ca^{2+} influx rate as compared to wt-STIM1 in HEK cells. Using confocal microscopy to monitor the Ca^{2+} response of Cos7 cells following stimulation, our data reveal a kinetic difference that is not apparent in the patch clamp measurements. Following stimulation with TG, cells expressing C437A-STIM1 exhibit a significant (~ 2 min) delay in SOCE as compared to cells expressing wt-STIM1. Our data further shows that once SOCE begins in C437A-STIM1 transfected cells, the rate of Ca^{2+} influx is faster than wt-STIM1 expressing cells and leads to slightly higher overall Ca^{2+} plateau concentrations. Thus, both results reinforce the functional importance of the Cys-437 residue in gating SOCE and further substantiate the functional significance of the disulfide bond at Cys-437, as STIM1 retains the capacity to translocate to the PM and to activate SOCE, albeit in a delayed manner.

Together, this information provides new details into state of STIM1 leading to SOCE, as depicted by Figure 5.1. When cells are at rest, STIM1 exists in multiple low-order oligomer states throughout the ER, including 110 kDa hetero-dimer and 260 kDa homo-dimer complexes. Importantly, Figure 5.1 represents a minimal model for the resting state STIM1 oligomers. While our data reveals the isolation and stabilization of at least STIM1 dimers from unstimulated whole cell lysates, our NativePAGE results suggest that larger oligomeric species, bound non-covalently, also exist in resting cells. Following depletion from ER stores, the low-order STIM1 oligomers aggregate, forming higher order oligomers, and organize to form discrete puncta at ER-PM junctions. Based on previous work in our laboratory (Calloway et al. 2011), we propose that STIM1 puncta preferentially associate with ordered lipid regions of the PM following store depletion by TG. At the PM, STIM1 recruits Orai1 proteins, forming the Ca^{2+} release-activated Ca^{2+} (CRAC) channel and activates SOCE. It is important to note that the Cys-437 residue,

Figure 5.1: Interactions of STIM1 leading to store-operated Ca^{2+} entry (SOCE). At rest, STIM1 exists in low-order oligomeric states which, at minimum, include a homo-dimer and a hetero-dimer formed with a 20-25 kDa unidentified protein (shown in pink). Following store depletion, STIM1 aggregates into even higher order oligomers, which preferentially associate with lipid ordered domains juxtaposed to the plasma membrane. Here, STIM1 puncta recruit Orai1, forming the CRAC channel and initiating SOCE.

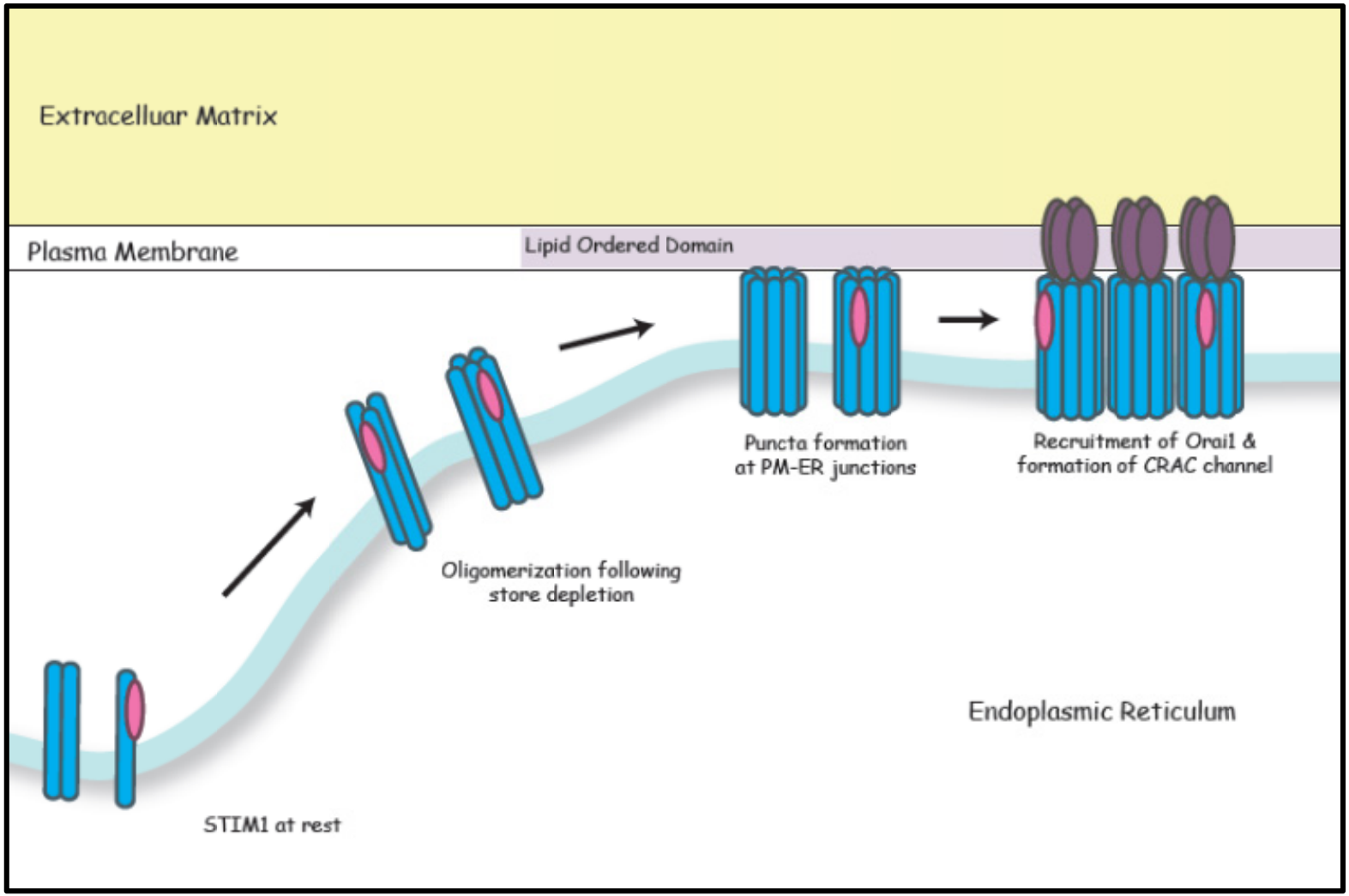
Extracelluar Matrix
Plasma Membrane
Lipid Ordered Domain
Puncta formation
at PM-ER junctions
Recruitment of Orai1 &
formation of CRAC channel
Oligomerization following
store depletion
Endoplasmic Reticulum
STIM1 at rest

required to stabilize the STIM1 complex represented by the 110 kDa species, is not required for higher order STIM1 oligomerization nor translocation to the PM. However, interactions with the Cys-437 residue appear to play a functional role in regulating wildtype SOCE.

Multi-biomolecule patterning using imprint lithography:

Recent advances in micro- and nano-fabrication techniques have presented vast opportunities for applications in biology and medicine. As such, multi-component patterning of biomolecules has become an active area of research. While each patterning method offers certain advantages for fabricating multi-component arrays, each is limited by certain disadvantages as well. Herein, we described a new biocompatible, multi-component patterning method that is based on imprint lithography techniques.

Previously, our collaborators synthesized fluorinated resists and light-emitting materials, which are processable in fluorinated hydrofluoroether (HFE) solvents, for application to organic electronic device patterning (Lee et al. 2008, Taylor et al. 2009, Lee et al. 2010). In our continuing collaborative study, we showed that HFE solvents, along with a newly synthesized highly fluorinated resist, can serve as a processing system for patterning via imprint lithography, producing feature sizes down to 1 μm. Using low temperature and pressure, we further showed the capacity of this system for biomolecule patterning and proved its compatibility with proteins, DNA, and mammalian mast cells. One of the greatest advantages of this patterning method is its capacity for multi-component patterning. As proof of this, we showed that these imaging materials may be applied at least 10 times without adversely affecting the underlying biomolecule layers. In addition, we showed application for this technique in fabricating complex

multi-protein arrays with spatially assigned protein deposition, both as individual, discrete features and as patterning features within features. While various two-protein arrays are the most complex arrangements shown, the goal of this method is to make possible the fabrication of a biomolecule array with as many patterned proteins as desired. More importantly, the success of this patterning method demonstrates a new model for multi-component biomolecule patterning that avoids many of the problems associated with more traditional lithographic techniques – thus allowing fabrication of multi-biomolecule patterns in a low cost, high throughput capacity for academic research settings. This technique now makes possible the ability to generate complex patterns for experiments ranging from multi-component biosensors, such as protein and DNA arrays, to ligand-mediated cell studies with multiple stimuli.

Future directions:

While the studies encompassed by this thesis provide new details into the oligomerization states and interactions of STIM1 leading to SOCE, many questions remain unanswered about the role of this protein in SOCE. Hence, future research is needed to determine the exact interactions between STIM1 and Orai1 necessary for activation and regulation of the CRAC channel. In particular, our studies with the Cys-437 residue illustrate a functional role for this residue in the proper gating of the CRAC channel. While mutation of Cys-437 results in a significant delay of SOCE, what remains to be determined is whether this delay is due to the loss of a cysteine residue and disulfide-binding site and/or the loss of the protein, represented by the 20-25 kDa polypeptide, that may bind to that site. In addition, identification of the 20-25 kDa protein that forms the 110 kDa STIM1 hetero-oligomer will remain key to understanding higher

order STIM1 oligomer formation and SOCE regulation. The identification and characterization of this polypeptide may further help to identify other proteins that interact with STIM1and aid in STIM1 oligomer formation. Based on negative results from our mass spectrometry data, we postulate that the 20-25 kDa peptide is a fragment of STIM1 protein. The generation of new antibodies specific to a small region of STIM1, including the Cys-437 residue, may aid in determining whether this hypothesis holds true, as our previous immunoblotting was accomplished with a STIM1 antibody specific to the C-terminal residues of STIM1. By preparing STIM1 IP products in the presence of reducing agent and immunoblotting with the newly generated STIM1 antibodies, the appearance of bands near 20-25 kDa and 85 kDa could confirm the identity of the 20-25 kDa peptide as a fragment of STIM1.

More recent advances in microscopy techniques may also aid in our ability to study the oligomerization of STIM1 as it occurs. While our own biochemical techniques were unable to retain higher order oligomers of STIM1 activated by depletion of Ca^{2+} stores, the emerging field of super-resolution microscopy provides the capacity to monitor single molecule motility in live cells. Both stochastic optical reconstruction microscopy (STORM) and photoactivated localization microscopy (PALM) are super-resolution imaging techniques that have shown great promise in studying biological samples (Fernández-Suárez & Ting 2008). By monitoring the mobilization of STIM1 species following Ca^{2+} store depletion in live cells, both techniques have the capacity to capture STIM1 oligomerization and puncta formation as it is occurring. Furthermore, these techniques may provide new details about the state(s) of STIM1 in terms of kinetics, stoichiometry, and localization at the single molecule level.

The capacity to fabricate complex, multi-protein patterned arrays offers exciting new applications for fundamental cell studies. By fabricating multi-protein arrays with proteins and

moieties known to stimulate or inhibit cells, we now have the ability to monitor cell and intracellular protein responses to simultaneous stimuli. Similarly, the capacity to fabricate features within features offers the ability to design even more complex patterns for more complicated cell studies, such as understanding the formation of T cell receptor (TCR) complexes and their bullseye and ring arrangements using multi-ligand stimuli and patterning features within features.

This biomolecule patterning may also offer a new venue for STIM1 studies. Previous research by Calloway et al. (2011) proposed that following store depletion by TG, STIM1 preferentially associates with ordered lipid regions of the plasma membrane, which may help facilitate the recruitment of Orai1. Using patterned lipid bilayers and patterned protein arrays, our laboratory has performed extensive research studying the FcεRI receptor pathway (Orth et al. 2003, Wu et al. 2004, Torres et al. 2008a, Torres et al. 2008b), which co-localizes to ordered lipid regions and/or immobilized proteins upon stimulation. Thus, a reasonable step would be to apply similar patterning techniques to studying STIM1 puncta formation near the PM following TG stimulation. For example, using patterned DNP-bound ligands (lipids or proteins), we can spatially define the clustering of IgE-bound FcεRI receptors on cell surfaces and thus the formation of lipid ordered domains, as the binding of IgE to DNP initiates crosslinking of IgE-bound receptors into ordered lipid regions on the cell surface and activates intracellular downstream signaling cascades including SOCE. It is then possible to monitor STIM1 and Orai1 recruitment to the lipid ordered domains as well as investigate other proteins that may be co-localizing to the CRAC channel during SOCE. Thus, expanding our toolbox to include a broader range of biophysical techniques, such as lipid bilayer- and protein-patterned surfaces, should increase our understanding of the role of STIM1 in SOCE.

REFERENCES

Baba Y, Hayashi K, Fujii Y, Mizushima A, Watarai H, Wakamori M, Numaga T, Mori Y, Iino M, Hikida M, and Kurosaki T (2006). Coupling of STIM1 to store-operated Ca^{2+} entry through its constitutive and inducible movement in the endoplasmic reticulum. Proc Natl Acad Sci USA, 103: 16704-16709.

Baba Y and Kurosaki T (2009). Physiological function and molecular basis of STIM1-mediated calcium entry in immune cells. Immunol Rev, 231: 174-188.

Berridge MJ, Bootman MD, and Roderick HL (2003). Calcium signaling: Dynamics, homeostasis and remodelling. Nat Rev Mol Cell Biol, 4: 517-529.

Berridge MJ (2009). Inositol trisphosphate and calcium signalling mechanisms. Biochim Biophys Acta, 1793: 933-940.

Calloway N, Owens T, Corwith K, Rodgers W, Holowka D, and Baird B (2011). Stimulated association of STIM1 and Orai1 is regulated by the balance of PtdIns(4,5)P2 between distinct membrane pools. J Cell Sci, 124: 2602-2610.

Covington ED, Wu MM, and Lewis RS (2010). Essential role for the CRAC activation domain in store-dependent oligomerization of STIM1. Molec Biol Cell, 21: 1897-1907.

Fahrner M, Muik M, Derler I, Schindl R, Fritsch R, Frischauf I, and Romanin C (2009). Mechanistic view on domains mediating STIM1-Orai coupling. Immunol Rev, 231: 99-112.

Fernández-Suárez M & Ting AY (2008). Fluorescent probes for super-resolution imaging in live cells. Nat Rev Mol Cell Biol, 9: 929-943.

He J, Yu T, Pan J, and Li H (2012). Visualization and identification of the interaction between STIM1s in resting cells. PLoS One, 7: e33377.

Lee J-K, Chatzichristidi M, Zakhidov AA, Taylor PG, DeFranco JA, Hwang HS, Fong HH, Holmes AB, Malliaras GG, and Ober CK (2008). Acid-sensitive semiperfluoroalkyl resorcinarene: An imaging material for organic electronics. J Am Chem Soc, 130: 11564-11565.

Lee J-K, Fong HH, Zakhidov AA, McCluskey GE, Taylor PG, Santiago-Berrios M, Abruña HD, Holmes AB, Malliaras GG, and Ober CK (2010). Semiperfluoroalkyl polyfluorenes for orthogonal processing in fluorous solvents. Macromolecules, 43: 1195-1198.

Orth RN, Wu M, Holowka D, Craighead H, and Baird B (2003). Mast cell activation on patterned lipid bilayers of subcellular dimensions. Langmuir, 19: 1599-1605.

Park CY, Hoover PJ, Mullins FM, Bachhawat P, Covington ED, Raunser S, Walz T, Garcia KC, Dolmetsch RE, and Lewis RS (2009). STIM1clusters and activates CRAC channels via direct binding of a cytosolic domain to Orai1. Cell, 136: 876-890.

Penna A, Demuro A, Yeromin AV, Zhang SL, Safrina O, Parker I, and Cahalan MD (2008). The CRAC channel consists of a tetramer formed by STIM-induced dimerization of Orai dimers. Nature, 456: 116-120.

Taylor PG, Lee J-K, Zakhidov AA, Chatzichristidi M, Fong HH, DeFranco JA, Malliaras GG, and Ober CK (2009). Orthogonal patterning of PEDOT:PSS for organic electronics using hydrofluoroether solvents. Adv Mater, 21: 2314-2317.

Torres AJ, Vasudevan L, Holowka D, and Baird B (2008a). Focal adhesion proteins connect IgE receptors to the cytoskeleton as revealed by micropatterned ligand arrays. Proc Natl Acad Sci USA, 105: 17238-17244.

Torres AJ, Wu M, Holowka D, and Baird B (2008b). Nanobiotechnology and cell biology: Micro- and nanofabricated surfaces to investigate receptor-mediated signaling. Annu Rev Biophys, 37: 265-288.

Wu M, Holowka D, Craighead HG, and Baird B (2004). Visualization of plasma membrane compartmentalization with patterned lipid bilayers. Proc Natl Acad Sci USA, 101: 13798-13803.